universität wien

MASTERARBEIT / MASTER'S THESIS

Titel der Masterarbeit / Title of the Master's Thesis

„ Mass spectrometry-based proteome, oxylipin and fatty acid mapping of ovine tissue “

verfasst von / submitted by

Hanna Troiss, BSc

angestrebter akademischer Grad / in partial fulfilment of the requirements for the degree of

Master of Science (MSc)

Wien, 2023

Studienkennzahl lt. Studienblatt / degree programme code as it appears on the student record sheet:	UA 066 862
Studienrichtung lt. Studienblatt / degree programme as it appears on the student record sheet:	Masterstudium Chemie
Betreut von / Supervisor:	Univ.-Prof. Dr. Christopher Gerner

Acknowledgement

My first major thanks I would like to address to Univ.-Prof. Dr. Christopher Gerner for giving me the opportunity to write my master's thesis on such an interesting and exciting topic in this dedicated and cordial research group. I would like to speak my gratitude, especially for Iris Gerner and Prof. Florien Jenner from the Veterinary University of Vienna, for providing the samples for setting up the protein and eicosanoid atlas and for or all the members of this group for their help during my master's thesis. My highest acknowledgements are addressed to Thomas Mohr, whose expertise in biochemical mechanisms and bioinformatics was one of the determining factors for the evaluation and presentation of the data in a scientifically high-quality manner. Many thanks for the help in the biochemical interpretation and the well-explained guidance through the complex results and plots. Further, I would like to express my gratitude to Gerhard Hagn, not only for introducing me to the main concepts of eicosanoid sample preparation, analysis and evaluation, but also for the help with the interpretation of the eicosadomics data. I would also like to speak a special thanks to Patricia Bortel, Lukas Skos, Yasmin Borutzki, Andrea Bileck, Andrea Hilbert, Günter Plessl-Walder and Johanna Mader for their kind help during my practical work. Moreover, I cannot forget to express my biggest thanks to my family, especially my mom and dad, whose mental, financial and personal support are one of the determining factors I was able to be at this stage of my scientific journey, where I am today. Lastly, this short chapter would be incomplete without expressing my deepest gratitude to my boyfriend, Dino, for his love and support during this time.

Table of Contents

List of Figures

List of Tables

List of Equations

Abbreviations

AA Arachidonic acid

AABG Advanced Active Beam Guide

ACOX Acyl-CoA oxidase

ADP Adenosine diphosphate

ALA α-Linolenic acid

APCI Atmospheric pressure chemical ionization

APPI Atmospheric pressure ionization

AQT Advanced quadrupole technology

ARF ADP-ribosylation-factor

BMBWF Bundesministerium für Bildung, Wissenschaft und Forschung (engl.: Federal Ministry of Education, Science and Research)

BSA Bovine serum albumin

BSEP Bile salt export pump

CASQ Calsequestrin

COX Cyclooxygenase

COX-ASA Cyclooxygenase modified with acetylsalicylic acid

CCS Collision cross section

CYP Cytochrome P450

DGLA Dihomo-gamma-linolenic Acid

DHA Docosahexaenoic Acid

DiHETE Dihydroxyeicosatetraenoic acid

DTT Dithiothreitol

EET Epoxyeicosatetraenoic acid

EI electron ionization

EMA European Medicines Agency

EPA Eicosapentaenoic Acid

ESI Electrospray ionization

FA Formic acid

FAO Fatty acid beta oxidation

FLAP 5-Lipoxygenase activating protein

GABA Gamma-Aminobutyric acid

GABA-A-R Gamma-Aminobutyric acid type A receptor

GFAP Glial fibrillary acidic protein

GPCR G-protein coupled receptor

HCTT High-capacity transfer tube

HESI Heated electrospray ionisation

HETE Hydroxyeicosatetraenoic acid

hGPR31 human 12-(S)-hydroxy5,8,10,14-eicosatetraenoic acid-receptor

HHATL Hedgehog Acyltransferase Like

HPA Human protein atlas

HPLC High-performance liquid chromatography

IAA Iodoacetamide

IMMS Ion mobility mass spectrometry

ISSCR International Society for Stem Cell Research

K Ion mobility

K0 Reduced mobility

LA Linoleic acid

LB Lysis buffer

LC Liquid chromatography

LDB LIM-domain binding

LFQ Label-free quantification

LOX Lipoxygenase

LT Leukotriene

m/z Mass-to-charge ratio

MAPK Mitogen-activated protein kinase

MATE Multidrug and toxin extrusion proteins

MRP multidrug resistance-associated protein

MS Mass Spectrometry

NADH Nicotinamide adenine dinucleotide

NIH National Institute of Health

OAT Organic anion transporters

OCT Organic cation transporters

OXER1 Oxoeicosanoid receptor 1

PASEF Parallel accumulation serial fragmentation

PG Prostaglandin

pLA2 Phospholipase A2

POR NADPH-cytochrome P450 oxidoreductase

PUFAs Polyunsaturated fatty acids

R Mass resolution

SLC Solute carriers

SNARE Soluble N-ethylmaleimide-sensitive factor attachment protein receptor

SPE Solid phase extraction

SUCNR1 Succinate receptor 1

TIMS Trapped ion mobility mass spectrometry

TOF Time of flight

TX Thromboxane

UHPLC Ultra-high-performance liquid chromatography

UHR-TOF Ultra-high-resolution TOF

WGS Whole genomic sequencing

1.0. Introduction

Small rodent animals are widely used models in a broad spectrum of research fields. However, in the last few years, the results of drug experiments undertaken on small animals, like rats and mice, do not show a sufficient and reliable prediction of the effects in the human body. This is owed to the differences in the metabolism between rodent animals and humans. Therefore, the use of larger mammalian animal models, like sheep and pig, was suggested to show a higher reliability in their power to predict human drug responses. When looking at the sheep, the protein abundances across individual ovine tissues is poorly researched, showing a profound lack in the understanding of the animal model. In cooperation with the Veterinary University of Vienna, this work provides insight into protein abundances and eicosanoid distributions in 13 different ovine tissues. To do so, the tissue samples were lysed with an ultrasonic stick and measured with the TIMS-TOF Pro MS device (proteomics part) or the Q Exactive HF MS device (eicosadomics part). For the evaluation and visualization of the results of both parts, diverse bioinformatic workflows were used, for example the z-transformed abundance-values in a heatmap or GO-term enrichment analysis. The sample preparation-, analysis- and evaluation workflow is shown in Figure 1.

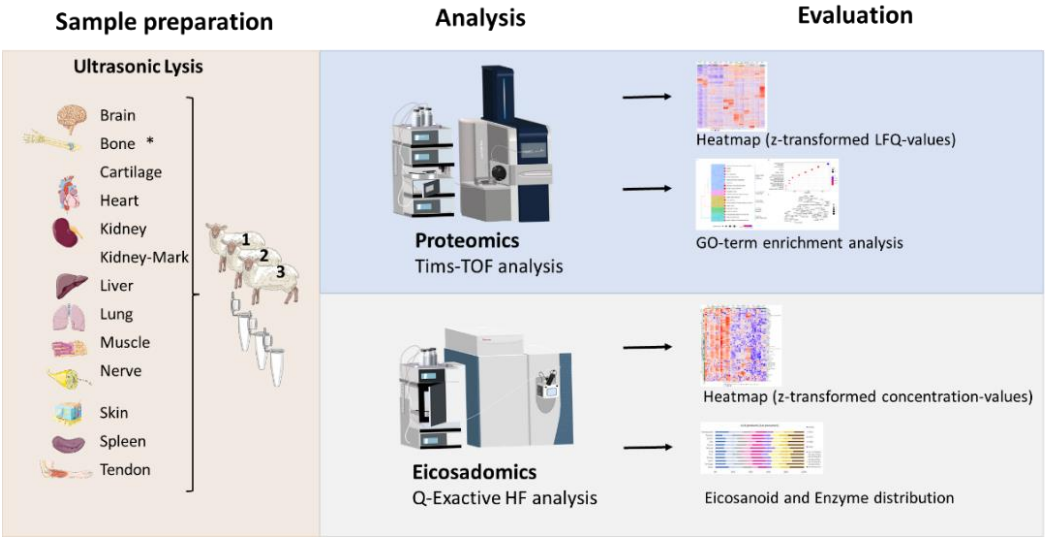

Figure 1: Overview of the sample preparation process of the 13 proteomics tissue samples (brain, bone, cartilage, heart, kidney, kidney mark, liver, lung, muscle, nerve, skin, spleen and tendon) and the 12 eicosadomics tissue samples (the same tissues without bone (noted with a "" in the Figure), the analysis via a TIMS-TOF (proteomics) and Q Exactive HF (eicosadomics) MS device and the evaluation with z-transformed LFQ-values presented in a heatmap, GO-term enrichment analysis and bar plots showing the differences in the eicosanoid, enzyme and Omega-3/Omega-6 distribution in the tissue samples analysed. Illustrations of organs, sheep and lab equipment used from ref.* [1].

The tissue-specificity of the proteins found in this study shows a good base for further research in the field of biochemistry, for example biomarkers. Eicosanoids are known mediators in inflammatory events and other biochemical reactions. These oxylipins can be assigned to a specific precursor molecule and enzymatic pathway. *Via* the analysis of the distribution of these oxidized fatty acid mediators, high informative value can be gained, like the extent of eicosanoids derived by one specific enzymatic pathway across the tissue sample, which shows insight into the activity of those enzymes. These results also provide a good base for further research in this field.

2.0. Theoretical Background

2.1. Mass Spectrometry

Analysis *via* Mass spectrometry (MS) provides an outstanding amount of information. It can be used to solve an extensive range of analytical problems, ranging from general bioanalytical approaches, to the identification of biological and synthetic polymers [2] and drugs in medical applications [3].

Mass-to-charge ratios (m/z), identified *via* different mechanisms in the MS device, depending on the mass analyser, provide insight into the species in the sample analysed. The redirection of charged atoms, molecules or aggregates, *via* designed electrical fields in the gas phase, represents the basics behind mass spectrometry [4].

The internal setup of a mass spectrometer consists of the sample inlet, ion source, mass analyser and the detector, with differences in the operating pressure for the individual elements (Figure 2). The sample inlet is kept under atmospheric pressure (around 1 bar). The following elements are under high or ultrahigh vacuum, with decreasing operating pressure, starting from the ion source with 10^{-5} to 10^{-6} mbar to the mass analyser and detector with 10^{-9} mbar [5].

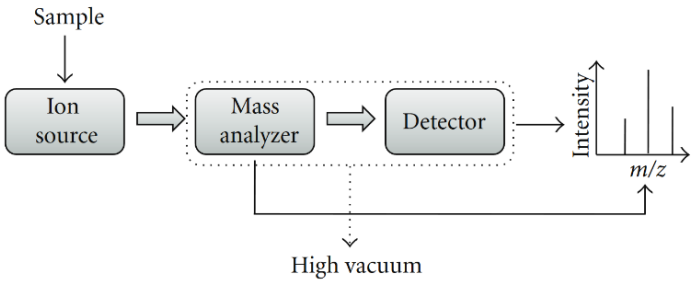

Figure 2: General setup of a mass spectrometer. 1) Ion source for the formation of charged analytes 2) mass analyser for the analysis of the m/z ratio of the compounds 3) detector [6].

The different commercially available MS devices can be characterized *via* a set of parameters like the resolving power, analysation speed, mass accuracy and precision. The mass resolution (R) of an MS device describes the ability to separate two adjacent peaks. For example, devices with ultrahigh resolving powers are capable of resolving isotopic fine structures and isotopologues. The influence of the mass resolution of an MS device on the obtained peak shapes in the mass spectrum can be seen in Figure 3. For example, Figure 3 clearly shows that the mass spectrum of one specific chemical compound can show profound differences in the number of obtained peaks, when measuring at different mass resolutions. For example, the isotopic pattern of the M+2 peak of Arg Vasopressin can be seen when measuring at high resolution (R = 1,000,000) compared to a low resolution (R = 50,000) [5].

A

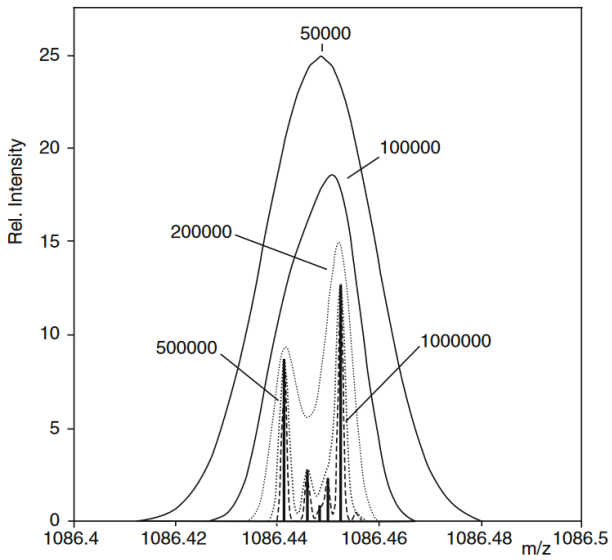

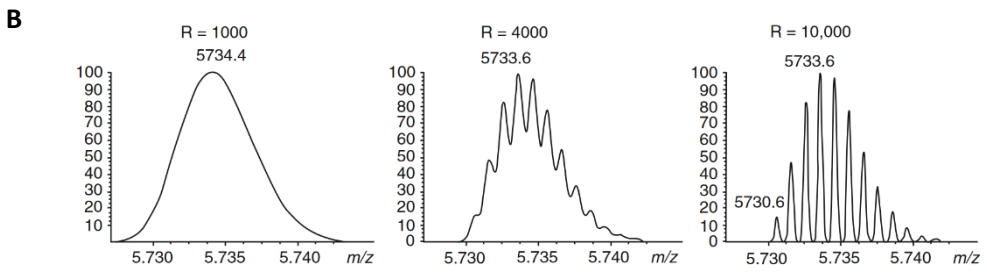

Figure 3: A) Illustration of the influence of the mass resolution (R= 50,000 to 1,000,000) of an MS device on the peak shape of the M+2 peak (m/z = 1086.4) in the mass spectrum of Arg Vasopressin. Higher resolution leads to the reveal of the isotopic pattern of the M+2 peak. B) Visual representation of different mass resolutions (R= 1,000, 4,000 and 10,000) influencing the calculated isotopic pattern for [M+H]+ for Bovine insulin [5].

Classic high-resolution mass spectrometry has the goal of achieving both, high mass resolution and mass accuracy. When defining the mass accuracy of an MS device, the difference in measured mass and the calculated exact mass, or true value, is analysed. Mass precision is defined by the deviation of measured masses among individual analysis runs. For a better demonstration of mass accuracy and precision, the true value of a measurement can be visualized as the centre of a target and the values measured are marked as dots on the surface of the target (Figure 4). The accuracy is defined by systematic errors and the precision by random errors. Highly accurate and precise measurements are located near the centre of the target with a narrow local distribution of the individual dots [5].

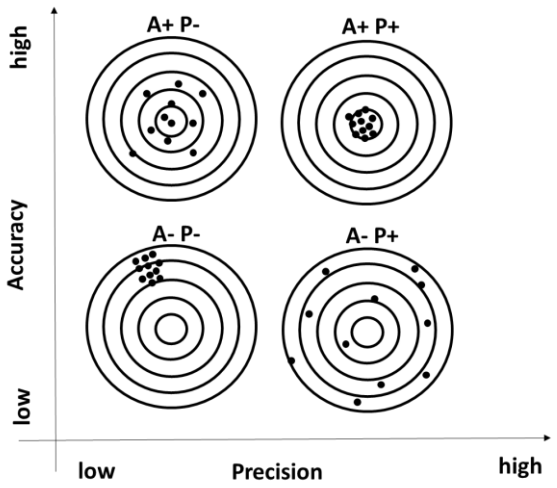

Figure 4: Mass accuracy and precision visually represented via a target with the true value of a measurement set at the centre of the target and the individual values of the analysis runs shown as black dots. Highly accurate and precise measurements are shortly annotated with A+ P+ (Accuracy good and precision good). Figure modified from ref. [5] *and* [7].

2.2. Liquid Chromatography

The basic idea behind liquid chromatography (LC) is the separation of a complex mixture based on different affinities of the individual compounds in a mobile phase with the interaction sites of the stationary phase. In the first stages of LC development, up to the 1970s, the mobile phase flow was induced *via* the gravitational force. Nowadays, high-performance liquid chromatography (HPLC), or ultra-high-performance liquid chromatography (UHPLC) are representing the most applied techniques in LC. The progress in speed, resolution and sensitivity, is owed to strong research over decades in column design, packing materials, especially particle size and size distribution and other parameters of the system [8].

The principle behind the separation in chromatographic columns is based on two simultaneously occurring processes, being the separation- and the dilution process. The dilution process is the main counteractor to the separation of components in the chromatographic column. The column itself can be described by various parameters, defining its quality in separation. One important parameter is the plate height H which can be described by three influencing factors, the Eddy diffusion A, the axial diffusion B, and the mass transfer resistance C. All these factors describe the band broadening process during an LC separation. The dependence of the individual influencing factors on the plate height of the column is described by the Van Deemter equation (Equation 1) [9].

$$H = A + \frac{B}{u} + Cu$$

Equation 1: Van Deemter equation describing the influence of the Eddy diffusion A, axial diffusion B, mass transfer resistance C and linear velocity u on the plate height H of a chromatographic column [9].

Band broadening *via* Eddy diffusion is caused by the difference in path length for the same analyte species while passing the porous packaging material in the chromatographic column. The magnitude of Eddy diffusion is directly related to the particle size. The axial diffusion contributes to the band broadening due to the natural propensity of species to diffuse to areas of less concentration. The mass transfer resistance influences the chromatographic separation quality *via* the process of diffusion and convection from the species in the mobile phase to the stationary phase and the other way around (Figure 5) [10].

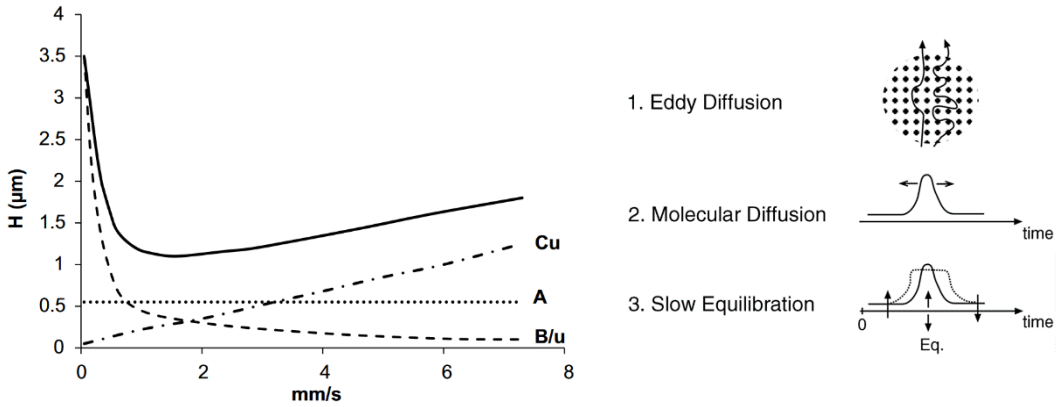

Figure 5: Left: Visual representation of the Van Deemter equation showing the influence of Eddy diffusion A, axial diffusion B and mass transfer resistance C on the plate height H of a chromatographic column (x-axis), depending on the flow rate in mm/s (y-axis). [10] *Right: Illustration of the three influencing factors 1) Eddy diffusion (A) 2) Molecular diffusion (B) and 3) Slow equilibration (C)* [11].

2.3. HPLC and UHPLC

High-performance liquid chromatography (HPLC) represents a special high-pressure technique in LC. It acquired its high reputation due to its high-resolution power, reliability in reproducibility between runs with the same column, the compatibility of the separation for very complex matrices and much more. The basics behind the HPLC technique are equal to the classic LC method, but with the advantages of less analysis time needed, better efficiency, and higher sensitivity of the HPLC technique [12]. Modern ultra-high-performance liquid chromatography (UHPLC) devices operate at pressures up to 1500 bar compared to 400 bar for modern classic HPLC devices. This increase in pressure results in a higher flow rate of the mobile phase through the column, when the particle size is the same. The plate number N is directly proportional to the square power of the time needed for the analysis, which influences the resolving power of the device [13].

2.4. Coupling of Chromatography and MS

The first use of chromatography with an MS device was described in the late fifties with the combination of gas chromatography and MS. Around 20 years later, the first direct interfacing of an LC column with an MS device was published [3]. The combination of MS with LC-separation ensures the identification of analytes with higher confidence, due to the increase in identification parameters for the individual analytes. This combination not only provides the m/z ratios and their intensities from the mass spectra, but also the retention times of the analytes from the ion chromatogram (Figure

6). Ionization techniques, like Electrospray ionization (ESI), atmospheric pressure ionization (APPI) or atmospheric pressure chemical ionization (APCI), are compatible for LC-MS setups. ESI represents the ionization method with highest reputation in LC-MS routine analysis [5].

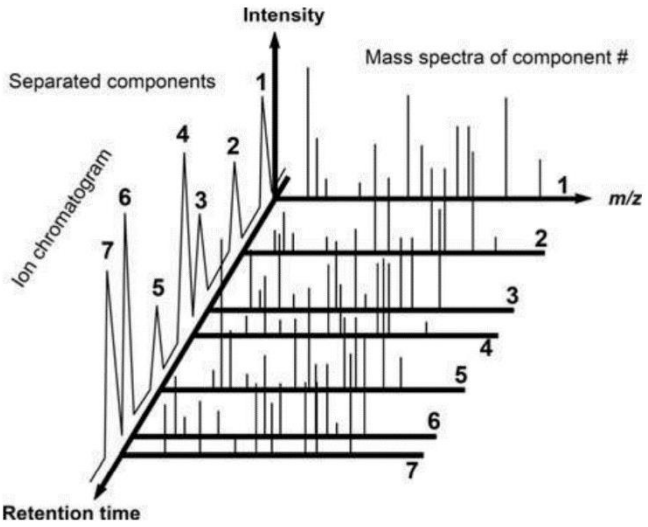

Figure 6: Illustration of the three parameters of identification provided by the combination of mass spectrometry with liquid chromatography. Each component of interest (1-7) is defined by its retention time (ion chromatogram) and its mass spectrum (m/z ratio versus intensity) [5].

2.5. Electrospray Ion Source

The principle behind the ionisation in an electrospray ionisation (ESI) source is based on the ionisation of species in a liquid phase and the evaporation of the solvent droplets to a point where the repulsion of the charged species between each other is bigger compared to the surface tension of the droplet. This leads to the release of individually charged species into the gas phase. The process from the injection of the diluted analytes from the sample vials into the ion source, to the transfer of the charged analytes to the mass spectrometer, is undertaken with high voltage (2,5-6 kV) applied to the tip of the ESI needle. This applied voltage results in a fine spray with charged droplets. Dry nitrogen flows (sheath gas and auxiliary gas) around the needle provide better nebulization and a more accurate spray direction to the mass spectrometer. The three following steps, occurring serially in the ion source, are 1) dispersion of the liquid to an electrostatically charged spray 2) evaporation of the solvent to the Rayleigh limits and Coulomb explosion/fission 3) ejection of the fully desolvated ions to the gas phase (Figure 7) [5],[6],[14],[15].

The ionization mechanism in the ESI source can be classified into the group of soft ionization methods. For example, electron ionization (EI) is a well-

known hard ionization method. The hardness of ionization determines the tendency of an ionization technique to produce fragments of analyte molecular ions [5].

The heated analogon to the ESI source is called a heated electrospray ionisation (HESI) source. The auxiliary gas flow in the HESI source is heated to temperatures up to 600°C, which results in an enhanced speed of evaporation. This increases the efficiency of ionisation, which is one of the main reasons of the massive gain of popularity of HESI sources in MS analysis [15].

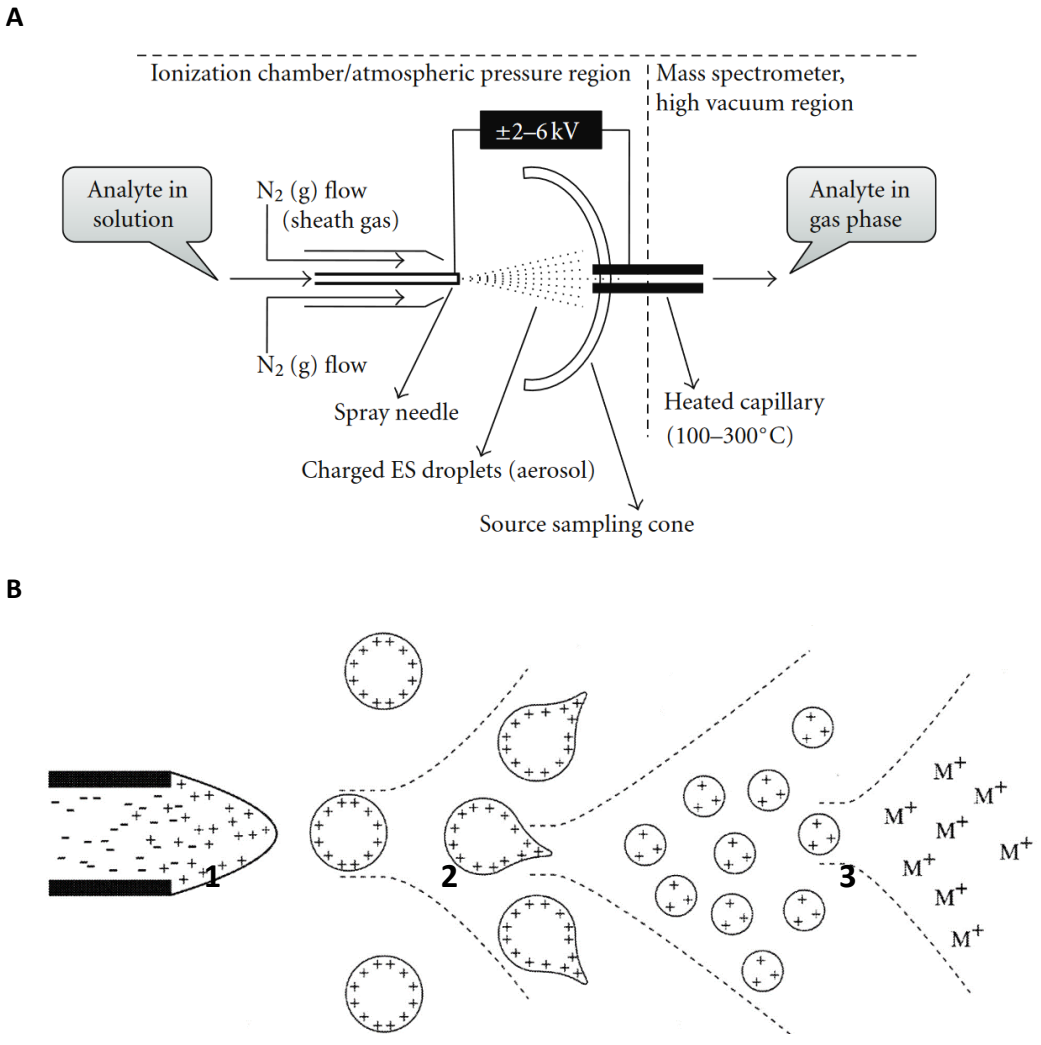

Figure 7: A) Schematic representation of the setup of an ESI -ion source, composed of the sample inlet with 2 individual N_2 gas flows, the spray needle with applied voltage, source amplifying cone and heated capillary [6]. *B) Basic principle behind the ionisation of analyte compounds in an ESI source* [14]. *1) Taylor cone formation 2) Evaporation of the electrochemically charged droplets to the Rayleigh limit and Coulomb explosion/fission 3) Ejection of the ions into the gas phase followed by their transport into the MS device.*

2.6. Trapped ion mobility-time of flight (TIMS-TOF) MS

Enhanced insight into the characteristics of the compounds of interest can be gained with trapped ion mobility mass spectrometry (TIMS), as a special technique in the ion mobility mass spectrometry (IMMS). The TIMS-technique uses the different behaviours of analytes in a gas flow and an electrical field in order to differentiate them, which opens the possibility of a deeper chemical interpretation of the analytes of interest. A constant gas flow along the drift tube results in a constant drag of the analytes depending on their cross-sections. The cross section represents a parameter with a high chemical informative value. A gradient in the electric field is applied along the drift tube, with increasing field strength towards the end of the tunnel. This leads to the stabilization of individual analytes at a position of a counterbalanced force of the electrical field and the counteracting force of the gas flow [16],[17],[18].

The general setup of the TIMS-TOF Pro device (Bruker Daltonics) can be seen in Figure 8.

Figure 8: Schematic 3D-drawing of the setup of the LC-MS device used for the analysis of the proteome of the sheep organ-samples. Left: Ultimate 3000 nano-LC. Right: TIMS-TOF Pro (Bruker Daltonics).

2.6.1. General setup

The main compartments of the TIMS-TOF Pro MS device are the ion interface, the Dual TIMS analyser, the ion transfer multipole, the quadrupole mass filter, the collision cell and the TOF analyser [19]. The individual compartments of the TIMS-TOF Pro MS device, with the characteristic processes occurring in the individual sections in the device, are illustrated in Figure 9. The processes in the individual TIMS-TOF sections are discussed in more detail in the following sections of this thesis.

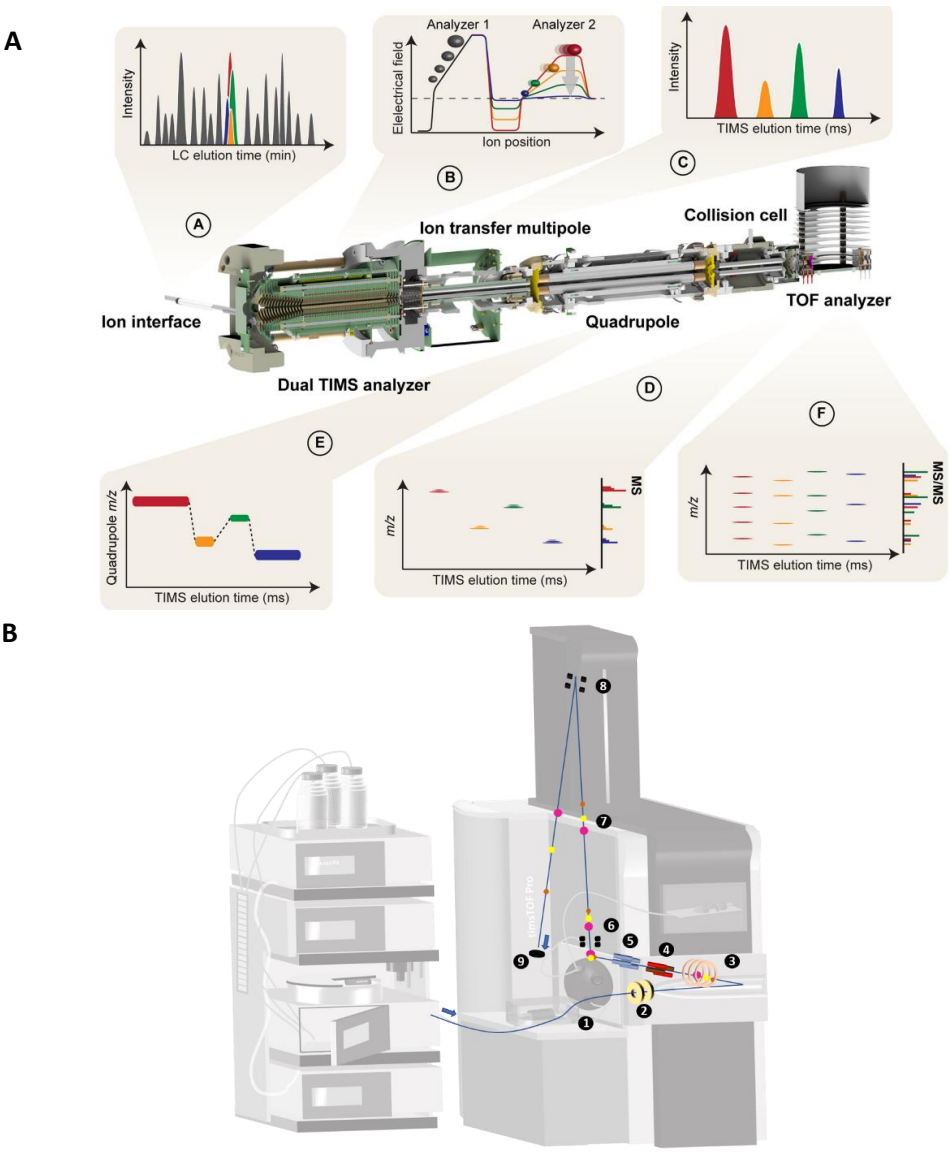

Figure 9: A) Schematic setup of the TIMS-TOF Pro. Processes occurring in the individual sections: A: Analytes eluting from the column. B: Dual TIMS analyser with one section trapping the ions and the second section separating them according to their mobility. C: and D: Mobility-dependent mass spectra gained via the variance of the field strength in the TIMS section. E: Synchronization of the TIMS elution window and the quadrupole analyser (PASEF-technology). F: MS/MS spectrum with resolved mobilities of the analytes [19]. *B) More detailed schematic internal setup 1. Electrospray Ionization 2. Focusing Lenses 3) TIMS-Cell 4) Quadrupole 5) Collision Cell 6) Accelerator 7) Flight Tube 8) Reflectron 9) Microchannel plate detector. Figure idea used from ref. [20].*

2.6.2. Time of flight (TOF) mass analyser

With its high speed of analysis, the TOF analyser represents a well-established analyser type, especially in peptide mass fingerprinting. A TOF analyser measures the difference in flight time between ions of different m/z in a drift tube, when the initial kinetic energies are the same for the individual species (Figure 10). This difference in flight time in the field-free drift tube results in different arrival times of the species at the detector [21].

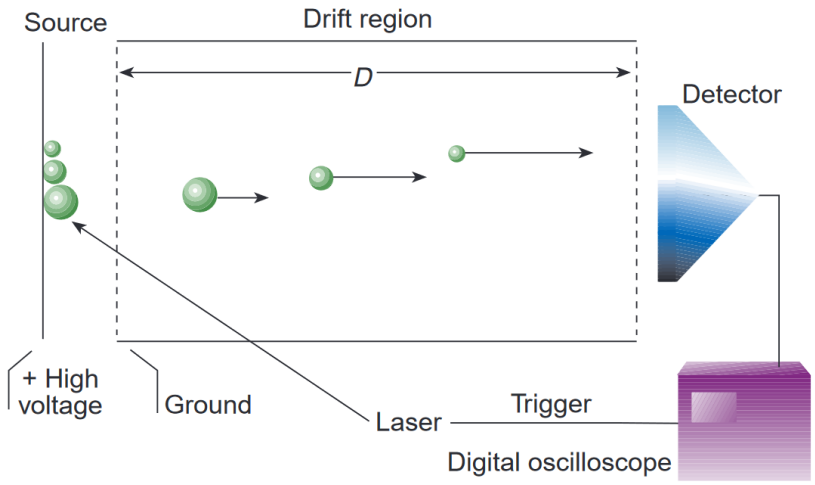

Figure 10: General principle behind a linear TOF-analyser, separating ions with lower masses from ions with larger masses. The lower masses have higher velocities, resulting in a smaller flight time through the field-free drift region with length D [22].

2.6.3. PASEF-technology

The parallel accumulation serial fragmentation (PASEF)- technology (Online-PASEF) enables more than 100 MS/MS scans per second. The main achievement is the maintenance of good sensitivity despite the enhancement in the sequencing speed [19]. Typically, classic MS/MS measurements only use a small percentage of the total ion beam for analysis. This inefficiency is improved by a difference in the passaging scheme of the precursor ions through the quadrupole in the instrument, being serially compared to the classic parallel passaging scheme. Timing the quadrupole selection window with the TIMS elution time, as the key point of the PASEF-method, the number of ions analysed per total ion beam is enhanced. The selection window of the quadrupole is altered in less than 1 ms, enabling outstanding efficiencies of MS/MS measurements [16].

Figure 11 shows the counterplay between the individually described techniques (TIMS and PASEF) and schematically depicts the steps during an analysis in the TIMS-TOF Pro.

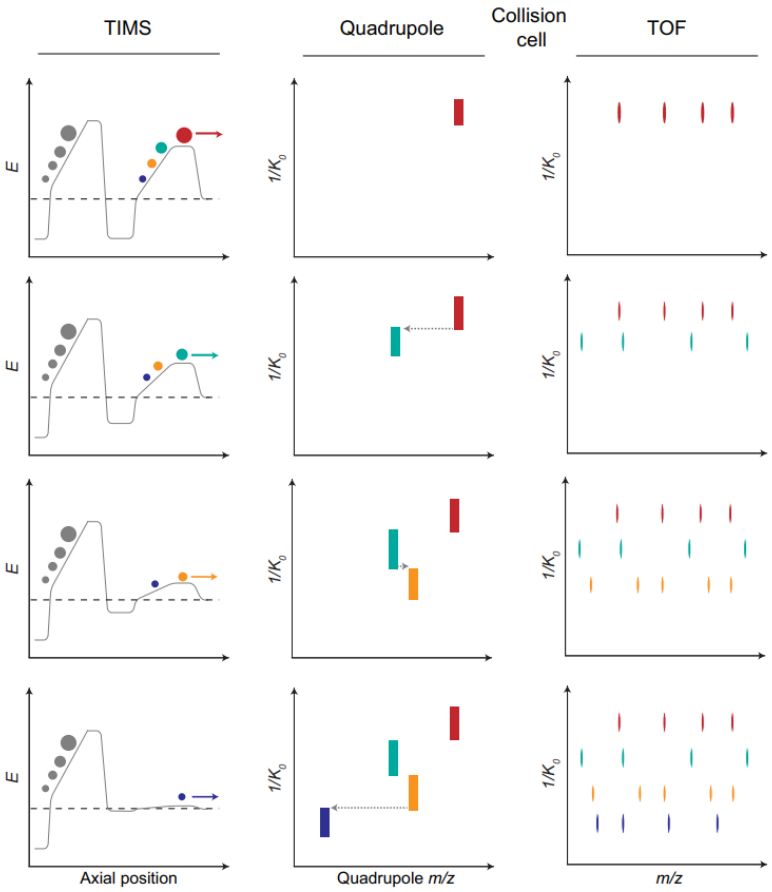

Figure 11: Schematic representation of the individual steps during an analysis run in the TIMS-TOF-Pro. 1) TIMS: separation of the precursor ions via the different behaviours in a gas flow and electric field. 2) Quadrupole: Serial selection of the precursor ions synchronized with the TIMS elution time (PASEF technique) 3) Collision Cell: Fragmentation of the precursor ions coming from the quadrupole 4) TOF: analysis of the m/z of the fragments [16].

2.6.4. TIMS-technology

The most important parameter of the TIMS-technology is the ion's mobility K. It describes the interaction of the individual analytes of interest with the inert gas. The electrical field applied results in a specific migration of the individual analytes through the inert gas stream, which can be described by the velocity v. This velocity is directly proportional to the parameter K, as described in Equation 2 [17],[18].

$$K = \frac{v_d}{E}$$

Equation 2: The correlation of the ion's mobility K, the electric field E and the migration velocity v_d of the analytes through the inert gas flow/steady state drift velocity [17],[18].

The core parameter K is dependent on the experimental parameters temperature and pressure. K can be expressed directly as the reduced mobility (K_0) during experiment performance under standard conditions or calculated afterwards as K_0 by using Equation 3 [17],[18].

$$K_0 = K\frac{T_0}{T}\frac{p}{p_0}$$

Equation 3: Conversion of K to K0 via the temperature and pressure for standard conditions T0 and p0 and the actual parameters temperature T and pressure p in the experimental setup [17],[18].

K_0 can further be used to calculate the collision cross section (CCS or Ω) of an analyte of interest, representing a parameter characteristic for the interaction of a charged analyte specie with the inert gas. The conversion of K_0 to CCS or Ω values can be seen below in Equation 4 [18].

$$\Omega = \frac{\frac{3}{16}\left(\frac{2\pi}{\mu k_b T}\right)^{\frac{1}{2}} ze}{N_0 K_0}$$

Equation 4: Relation between the reduced ion's mobility K0 and the collision cross section Ω [18].

With the CCS or Ω value, complex chemical information can be gained, for example the conformation of the analyte migrating through the gas flow. This opens another stage of certainty in identification, compared to classical MS techniques, especially for structurally close related compounds [18].

2.7. Vanquish Horizon UHPLC and Q Exactive high field (HF) hybrid Quadrupole-Orbitrap-MS

The Q Exactive HF mass spectrometer provides good quality-, high-resolution- and robust measurements. The device uses an ultra-high-field Orbitrap analyser, which enables superior resolutions at similar transient times, compared to the classic original Q Exactive MS device [23].

The general setup of the Vanquish Horizon UHPLC Q Exactive HF Hybrid Quadrupole-Orbitrap MS device can be seen in Figure 12.

Figure 12: Vanquish Horizon UHPLC – Q Exactive HF Hybrid Quadrupole-Orbitrap – combination. Schematic drawing of the MS device used for the eicosanoid analysis of the sheep organ samples.

2.7.1. Vanquish Horizon UHPLC

Modern UHPLC devices enable working pressures up to 1500 bar due to their special pumping techniques (dual piston pump-arrangement). The Vanquish UHPLC device features characteristic properties like high pressure limits in combination with less system volume. This combination ensures maximal performance of the UHPLC device [13]. A schematic illustration of the Vanquish Horizon UHPLC device can be seen in Figure 13.

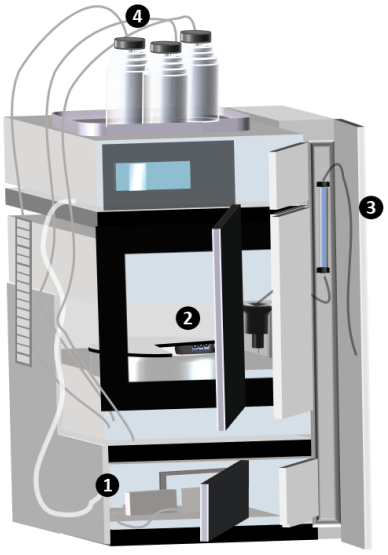

Figure 13: Individual building blocks of the Vanquish Horizon UHPLC with 1) pump system (SmartFlow-pumping algorithm; dual piston pump), 2) sample stack with autosampler, 3) column and 4) solvent reservoir.

2.7.2. Q Exactive HF Mass Spectrometer

In order to get an insight into the functions and interactions of complex compounds of biological samples, analysis with high sensitivity, robustness and speed is of paramount importance. All these requirements are fulfilled by the Q Exactive HF. The device consists of a high capacity transfer tube (HCTT), Advanced Active Beam Guide (AABG), the hyperquad Mass Filter with advanced quadrupole technology (AQT), and the HF Orbitrap analyser (Figure 14) [24]. With this setup, the Q Exactive HF shows outstanding performances compared to other MS devices.

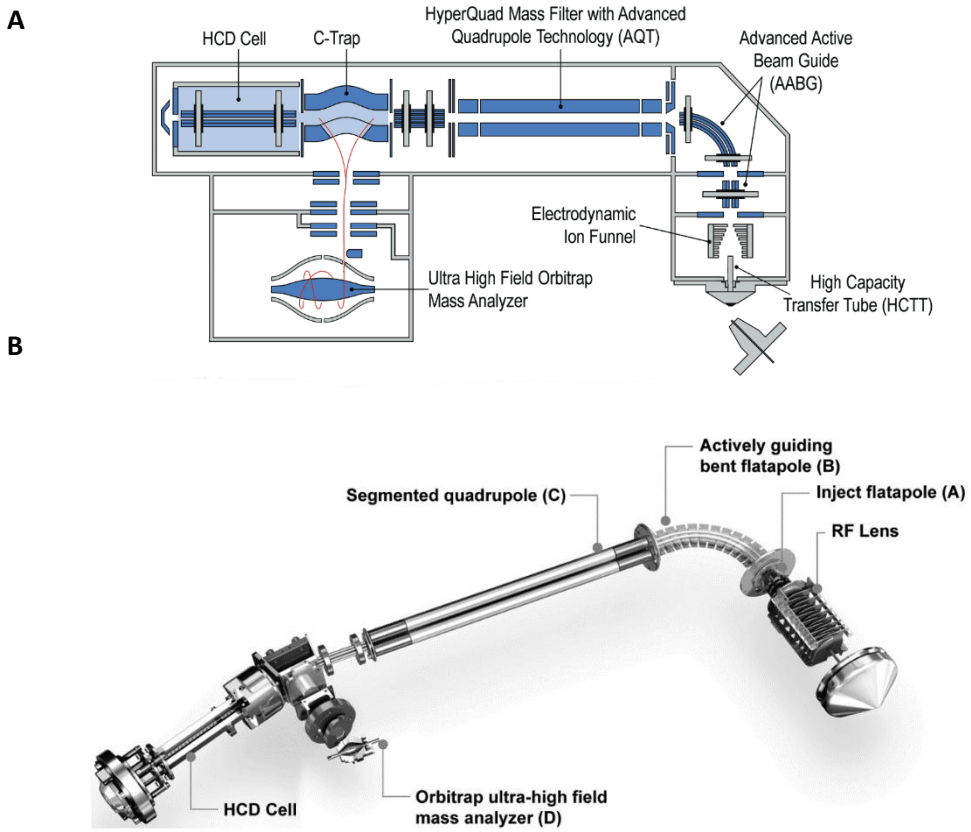

Figure 14: Q Exactive HF Hybrid Quadrupole-Orbitrap Mass Spectrometer. A) Schematic view of the internal arrangement. [24] *B) Realistic view of the internal organisation of a Q Exactive HF* [23].

2.7.2.1. Orbitrap Analyser and C-shaped Quadrupole Ion Trap

The internal organisation of an orbitrap mass analyser consists of an inner spindle-like electrode and an outer electrode, formed like a barrel. Ions, entering the analyser during the applied voltage ramp, undergo orbiting motions around the inner electrode combined with motions in the z-direction (Figure 15). The ion oscillation-frequency along the z-direction (f_z) represents the parameter of interest for detecting the m/z ratio of the individual ions by the amplifier (Equation 5) [25],[26],[27]**.** *Via* image current detection and Fourier Transformation, the ion species in the sample can be analysed very accurately according to their m/z ratios, due to the high precision of frequency measurements [27].

$$f_z \propto \frac{1}{\sqrt{\frac{m}{z}}}$$

Equation 5: Correlation of the ion oscillation-frequency in the z-axis in the orbitrap (fz) and the m/z ratio [27].

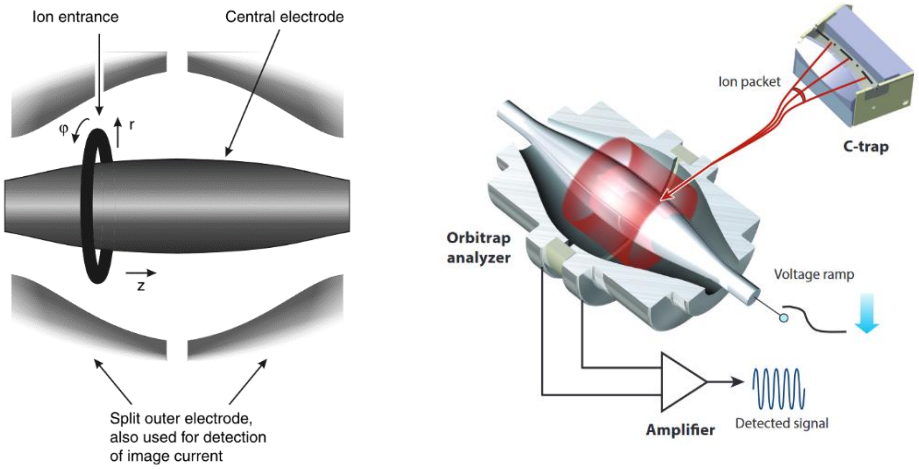

Figure 15: Left: Illustration of the inner and outer electrode of an Orbitrap mass analyser [27]**.** *Right: 3D representation of the trajectory of an ion packet going from the C-trap to the orbitrap mass analyser* [26]**.**

C-shaped quadrupole traps are generally used in Tandem-MS devices for the storage and cooling of ion packets prior to their transportation to the Orbitrap analyser. The C-shape of the electrodes results in a particular shaped potential field in the trap, with the exit of the storage device coinciding the entrance of the orbitrap. This ensures an accurate transfer of the analytes to the orbitrap analyser [27].

2.7.2.2. HF Orbitrap for enhanced scanning speed and resolution

The HF Orbitraps outer and inner electrode are smaller compared to the classic Orbitrap, thus enhancing the electric field [23]. The voltage of the Ultra-high field Orbitrap analyser is enhanced (around 5 kV), compared to classic Orbitrap analysers [24],[23]. This directly influences the scanning speed, resulting in roughly 1.8-times faster scanning times compared to other Q Exactive MS types with classic orbitrap analysers. Further, the resolution of a HF analyser compared to classic orbitrap analysers is tremendously improved, showing resolutions of 240,000 at 200 m/z compared to 140,000 at 200 m/z for the classical Q Exactive type [24].

2.7.2.3. Quadrupole Mass Filter and Octopole Ion guides

Ions of a specific m/z ratio are selected from the ion beam in the Q Exactive HF device *via* a quadrupole mass filter. This process can only be undertaken with unit resolution. Linear Quadrupole mass filters consist of four hyperbolic or cylindric rods, with an applied potential, with a DC voltage-(U) and a radiofrequency voltage compound (V). The total potential (Equation 6) applied is held at the same level for each set of rods on opposite sides (Figure 16) [5]**.**

$$\phi_0 = \mathrm{U} + \mathrm{V}\cos\omega\mathrm{t}$$

Equation 6: Description of the total potential applied to the rods of the quadrupole mass filter. The potential is composed of a DC voltage component (U) and a radiofrequency voltage (V) with the angular frequency ω and the parameter time t [5].

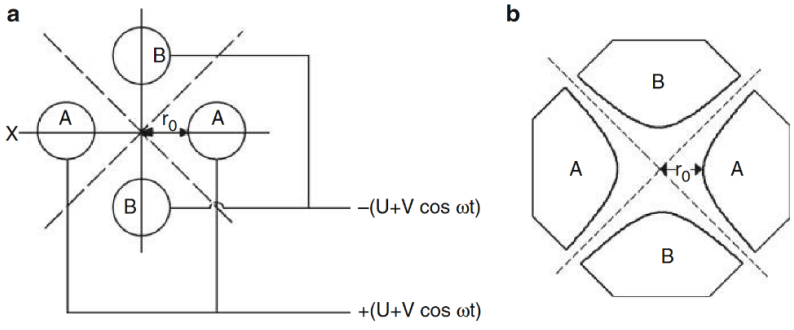

Figure 16: Schematic representation of the arrangement of the four a) cylindric or b) hyperbolic rods in a quadrupole mass filter and the potentials applied. r0 represent the distance of the centre of the device to the beginning of the rods [5].

Via an alteration of the total value of U and V, but with a constant ratio of U/V, the quadrupole mass filter can be scanned serially over the entire m/z range. This scanning scheme allow ions with increasing m/z ratios to pass

through the mass filter. This alteration in the voltage applied to the rods results in stable trajectories for the ions with m/z ratios of interest, compared to the other ions. This stability or instability of the trajectories of individual ions through the mass filter, depending on the applied potential, is visualized in Figure 17 [5].

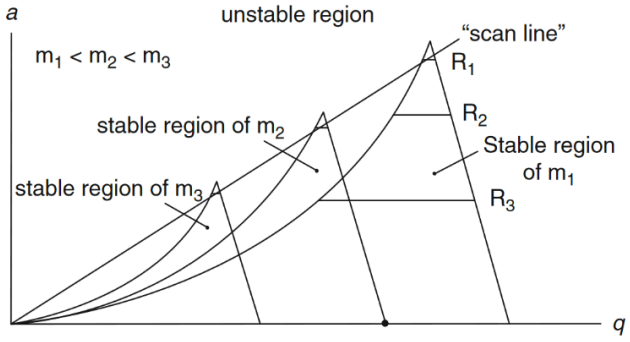

Figure 17: Visual representation of the scanning scheme of a quadrupole mass filter. The stable and unstable regions for the individual masses m1, m2 and m3 are defined via the difference in magnitude of U and V but with constant U/V ratio. R1, R2 and R3 represent the individual resolving powers. The x-axis a and y-axis q are parameters defined by the applied DC voltage U or radiofrequency V, the ion charge q, the ion mass m, the radius r and the frequency ω [5].

Alterations in the number of rods making up the device result in different possible applications. For example, octopoles, which contain eight rods, are mainly used as ion guides to ensure a transfer of the highest possible number of ions in an ion packet from one section in the device to another. The higher number of rods, compared to a quadrupole, directly results in higher potential walls at the edges of the octopole device, leading to higher ion transmission efficiencies (Figure 18) [5].

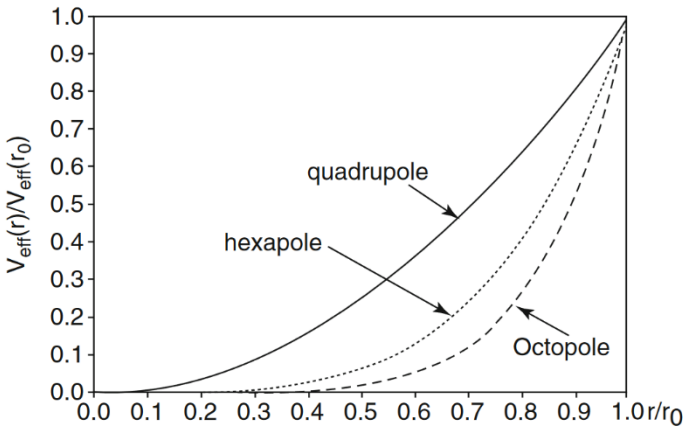

Figure 18: Differences in the effective potentials (V_{eff}) of quadrupoles, hexapoles and octopoles. r0 represent the distance of the centre of the device to the beginning of the rods (Figure 16). r represents the radius [5].

2.8. The omics-research fields and their applications

Genomics, transcriptomics, metabolomics, lipidomics, and proteomics are representing the main research fields in the general term of “omics”-research.

Metabolomics, as the discipline of determining metabolites (small molecules with masses < 1.5 kDa), provides a real-time view of the state of the system analysed. The metabolome is extremely sensitive to alterations in diet, drugs, and other environmental influences. On the one hand these different influences are very rapidly visible in the metabolome, which shows an advantage in research approaches aiming to detect food-, or drug-derived metabolites. However, on the other hand, these variations of the metabolome, can be substantial and can lead to confounded data interpretation [28]. Genomics, the oldest discipline in the omics research fields, focuses on analysing the entire genome of an organism of interest [29]. Genomics workflows (for example, whole genomic sequencing (WGS)) are well-established methods worth mentioning for their application in particular fields in routine analysis [30].

Combinations of different omics disciplines, called multi-omics approaches, can provide a massive gain in information about the biological processes in the system analysed, due to their complementary explanatory power. The combination of the analysis of diverse biomolecules provides a broader view of the processes occurring in the system of interest, which is especially relevant in the research field of specific complex diseases [28],[31].

The analytes of the individual omics disciplines and the biochemical pathways, starting from genes, to mRNA and proteins to metabolites, can be seen in Figure 19.

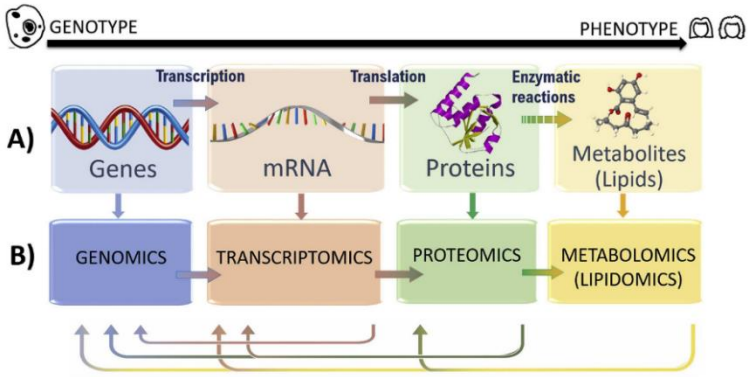

Figure 19: (A) The downstream information flow starting from genes, over mRNA and proteins to metabolites and (B) the upstream influence of the individual biomolecules among each other [32].

2.9. Lipidomics

Lipidomics represents a research area in the omics field aimed at analysing the entity of all lipids (lipidome) present in an organism of interest. The study of the overall lipidome from a system can provide highly informative value, like lipid biomarkers, in order to get a better understanding of complex diseases or in general medical applications [33]. The research field of lipidomics was first perceived in the year 2003, mainly driven by the formation of the website Lipid Maps. This website provides a database for a wide range of different lipidomics data [32].

Generally, lipids can be classified into eight classes, defined by the LIPID MAPS consortium, being fatty acids, glycerolipids, glycerophospholipids, sphingolipids, sterol lipids, prenol lipids, saccharolipids and polyketides (Figure 20) [34],[35]. To further differentiate the lipids in one class, a nomenclature scheme can be used which offers different stages of precision to describe the lipid structure in terms of the location of the double bonds. This annotation scheme is used to annotate the subclasses of lipids hierarchically. PC 18:0/18:2 represents a phosphatidylcholine with a fatty acyl chain with 18 C-atoms without double bonds at the sn-1 position and a fatty acyl chain with 18 C-atoms with two double bonds at the sn-2 position. The same lipid but with an unknown sn-position of the individual fatty acyl chains is written as PC18:0_18:2 [34].

Some of the main biological functions of lipids include their importance as membrane building blocks, their purpose in the haemostasis cascade, impulse transfer and in immune response, their function as vitamins, hormones and energy providers [36],[37]. Lipids show a substantial variety in their structure due to their proneness to oxidation and other modifications, which represents one of the main challenges in lipid analysis [37].

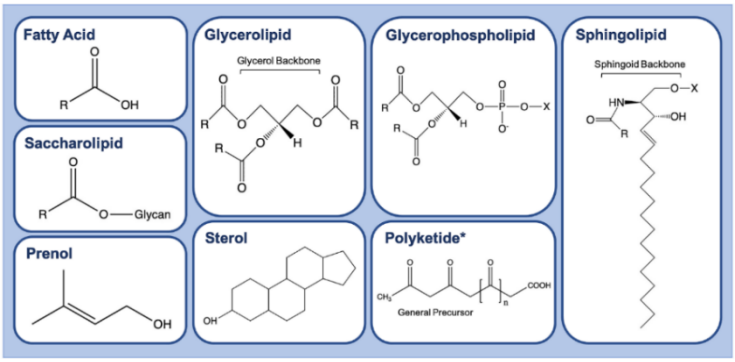

Figure 20: The eight classes of lipids [35].

2.10. Eicosanoids

The oxylipin-family covers a wide variety of highly reactive oxylipins, deriving from the precursor molecules arachidonic acid (AA), eicosapentaenoic acid (EPA), docosahexaenoic acid (DHA) and dihomo-gamma-linolenic acid (DGLA) [38],[39]. The hydroperoxylated, hydroxylated, oxygenated and epoxylated forms of polyunsaturated fatty acids (PUFAs), called oxylipins, derive from three main catalytical pathways with the enzymes cyclooxygenase (COX), lipoxygenase (LOX), cytochrome P450 (CYP) as enzymes. Further, the process can also be undertaken *via* non-enzymatic mechanisms. These oxidized products are known as essential mediators in many biological processes [39],[40].

AA, DHA and EPA can be classified into the family of PUFAs. This group of fatty acids is defined by more than one double bond in the structure. DHA and EPA are ω-3 fatty acids and AA is an ω-6 fatty acid, where the number in the nomenclature represents the position of the double bond nearest to the end of the fatty acly chain. Dietary linoleic acid (LA) and α-linolenic acid (ALA) are the precursors to be processed enzymatically in the body in order to form AA, EPA and DHA [38],[41]. The eicosanoid precursor molecules AA, DHA and EPA are incorporated into the cell membrane *via* the Lands' cycle and released *via* the enzyme Phospholipase A2 (pLA2), followed by the production of eicosanoids *via* different enzymatic reactions (Figure 21) [38],[42].

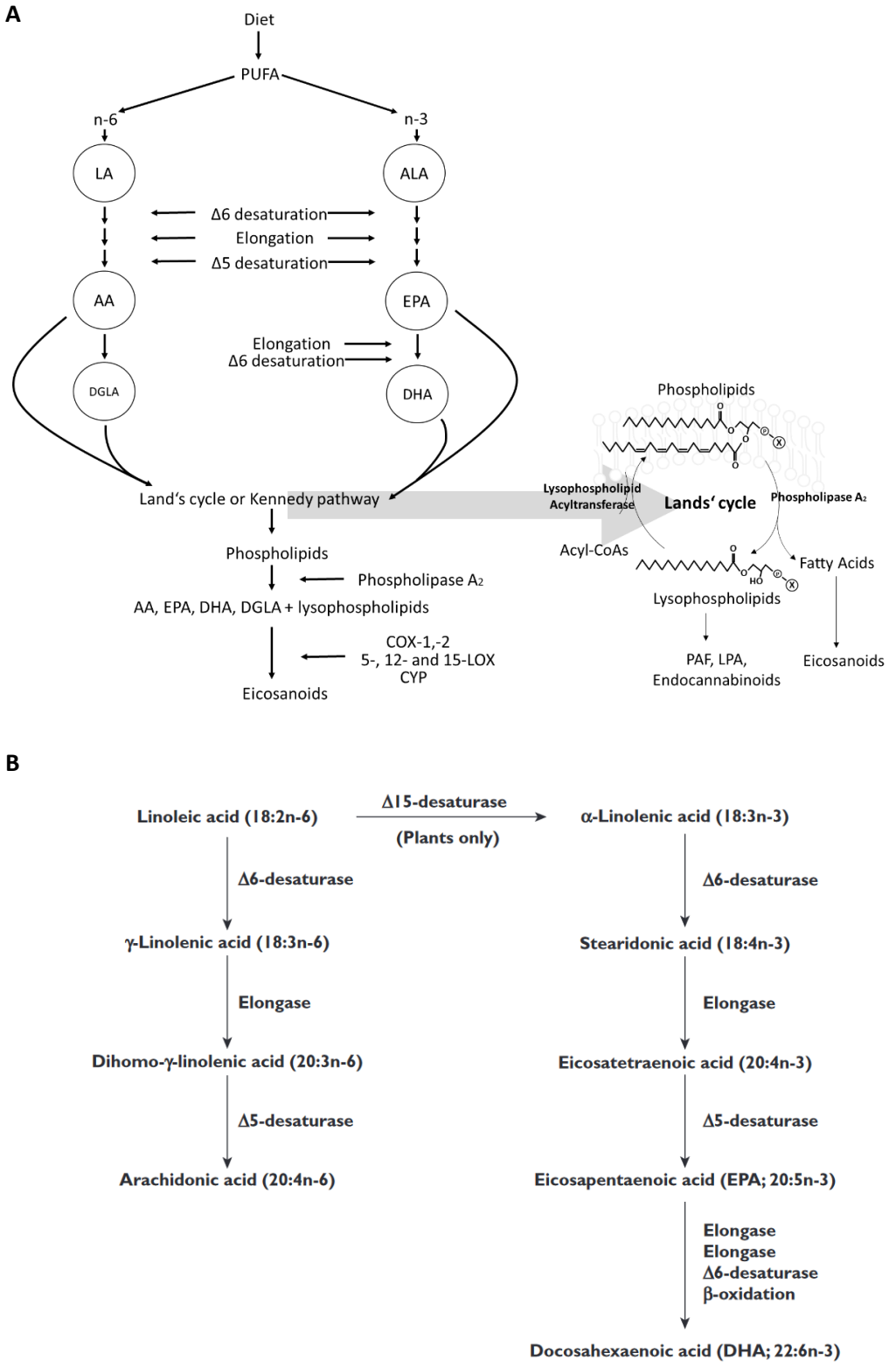

Figure 21: A) Left: Biochemical pathways starting from the PUFAs from the diet to the production of eicosanoids, as reproduced from ref. [38]. *Right: Lands' cycle representing how precursors are released from the cell membrane via Phospholipase A2 and integrated into the membrane via lysophospholipid acyltransferase as reproduced from ref.* [42] *B) More detailed view of the conversion of the ω-6 fatty acid Linoleic Acid to the ω-3 fatty acid alpha-Linolenic Acid and the precursor molecules of eicosanoids, being DHA and EPA as ω-3 fatty acids and AA as an ω-6 fatty acid* [41].

For example, AA linked to phospholipids in the cell membrane *via* an ester bond, is released *via* the activation of the enzyme pLA_2. From this step, different enzymatic pathways can lead to various highly active oxylipins, which mediate different bioactive pathways (Figure 22) [43].

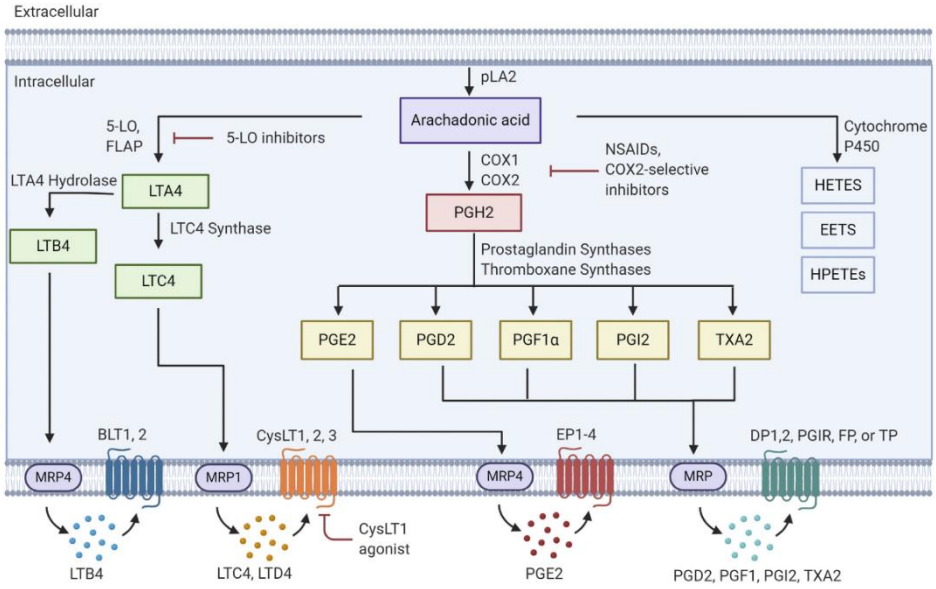

Figure 22: Overview of selected eicosanoid production pathways. Via the activation of pLA2, arachidonic acid is released from membrane phospholipids, which can be further converted enzymatically via the COX cycle, CYP cycle or LOX cycle leading to bioactive oxylipins, which can further interact with specific receptors in the cell membrane, mediating different biological processes [43].

The eicosanoids from the enzymatic pathways with AA as the precursor molecule generally show pro-inflammatory characteristics [44]. This precursor molecule can lead to hydroxyeicosatetraenoic acids (HETEs), dihydroxyeicosatetraenoic acids (DiHETEs), epoxyeicosatetraenoic acids (EETs), prostaglandins (PGs) and thromboxanes (TXs) [39]. The prostaglandin-family (Series 2) is produced *via* the catalytical pathway of the enzyme cyclooxygenase (COX), leukotrienes (Series 4) *via* 5-lipoxygenase (5-LOX) or 5-lipoxygenase activating protein (FLAP) and EETs and HETEs *via* the CYP enzymatic pathway (Figure 22) [43],[44]. In contrast to AA, generally forming pro-inflammatory eicosanoids, EPA and DHA represent the precursor molecules for producing anti-inflammatory eicosanoids [44].

Besides AA, EPA and DHA are also esterified to phospholipids in the cell membrane and released *via* specific stimuli. From free EPA, the series 3 prostaglandins are formed *via* the enzymatic pathway of COX-2 and the series 5 leukotrienes *via* the 5-LOX pathway. Free DHA is metabolized to,

for example, D-series resolvins, protectins and maresins (Figure 23) [41],[44].

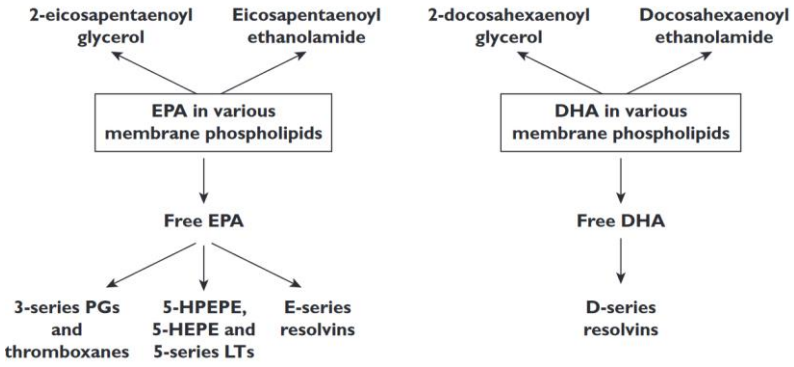

Figure 23: Overview of the metabolic pathways of EPA and DHA with the production of eicosanoids from free EPA and free DHA, being released by pLA2 from phospholipids in the cell membrane. Not the entire set of produced eicosanoids is noted in the picture [41].

2.10.1. Eicosanoids and their importance in various biochemical reactions and pathways

Eicosanoids are well-known actors in regulating inflammatory and other biochemical processes. The COX-cycle is the central catalytical path for producing the prostaglandin family, including for example PGI_2 and PGE_2. These two prostaglandins are reported to have distinct biochemical effects like vasodilation and an influence on the properties of platelets (Figure 25) [40],[45]. For example, PGI_2 is believed to reduce the adhesive ability of platelets on subendothelial regions, followed by a reduced aggregation which leads to changes in the thrombus-clot formation [46]. Further, eicosanoids are well known to play a significant role in the formation of cancer cells and cancer progression. Many studies focused on prostaglandin E_2, known to be produced by cancer cells. These pro-tumorigenic effects, like reported for PGE_2, were also found for other eicosanoids, for example leukotrienes [43]. Overall, prostanoids, summarizing prostaglandins (PGD, PGE and PGF), prostacyclin (PGI) and thromboxane (TXA), are known to have a distinct influence on angiogenesis, different processes occurring in cancer cells and chronic inflammation [47].

Besides the known effects of distinct members of the prostaglandin family on cancer development, these molecules also play a known role in other

biochemical mechanisms. For example, PGD_2 is reported to have a special role in sleep regulation (Figure 24). The process behind this is based on the circadian up- and downregulation of the concentration of the prostaglandin. Moreover, it is known to have a role in regulating special neuronal functions like memory formation [48].

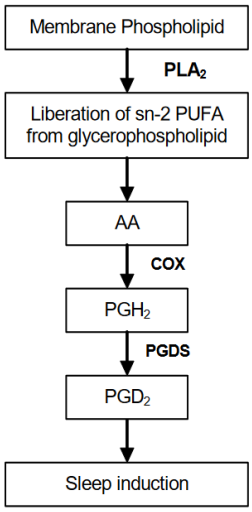

Figure 24: Schematic representation of the production of PGD2 from AA via the enzyme COX. PGD2 is known to have a direct effect on the induction of sleep [48].

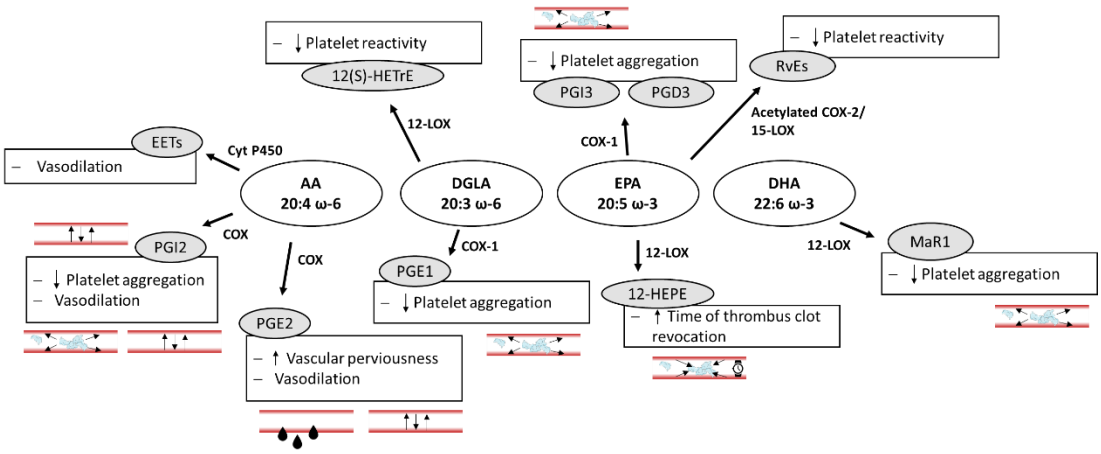

Figure 25: The four precursor molecules AA, EPA, DHA and DGLA and selected enzymatic eicosanoid products, classified into their influence on blood vessels, on the homeostasis cascade/ thrombus formation and platelet reactivity. Figure reproduced and modified from ref. [45].

2.10.2. The interplay of proteins and eicosanoids

Proteins, synthesized *via* the translation of gene codes from mRNA, represent highly bioactive molecules. They mediate an outstanding variety of biochemical pathways, ranging from electron transfer cascades and signal transductions up to immune responses and much more. [49] Not only the biochemical relevance of proteins by themselves represents their importance in our daily lives, but also their interaction with other bioactive molecules, like lipids, DNA and oxylipins. For example, albumin can act as a vector of highly bioactive oxylipins. The mechanism behind this process is based on passive adsorption or the formation of covalent bonds between the protein and the eicosanoid [50].

The signal transduction of a wide range of biological processes is mediated by receptors, for example G-protein coupled receptors (GPCRs). These receptors can interact with target molecules when triggered by external stimuli. Diverse metabolite GPCRs can affect the production of eicosanoids. For example the succinate receptor 1 (SUCNR1), which is highly expressed in platelets, is believed to promote platelet-PMN (polymorphonuclear leukocyte) interaction and the synthesis of LTC_4, a leukotriene acting as a proinflammatory agent. This signalling pathway is believed to occur when extracellular succinate levels are high, which indicates high levels of oxidative stress of the system of interest [51]. Further, eicosanoids can also directly bind to specific receptors. For example, human 12-(S)-hydroxy5,8,10,14-eicosatetraenoic acid-receptor (hGPR31), as a member of the GPCR 1 family, shows enhanced affinity towards the eicosanoid 12(S)-HETE compared to other HETEs. The binding of the signalling oxylipin to its receptor mediates a cascade of other biochemical pathways, like the mitogen-activated protein kinase (MAPK) pathway. Human oxoeicosanoid receptor 1 (OXER1), as another representant of the GPCR1-family, contains the binding side for its main eicosanoid ligand 5-oxo-6E,8Z,11Z,14Z-eicosatetraenoic acid (5-oxo-ETE) [52].

Analysis of different levels of bioactive molecules, like the protein level and lipid level provide complementary information about the system of interest. Proteome profiling, combined with oxylipin analysis, shows outstanding informative values in various research problems, for example in the research of the factors influencing long Covid [53].

2.11. Solid Phase Extraction

The basic idea behind solid phase extraction (SPE) is the trapping of an analyte of interest onto a solid phase while washing away other matrix components. By switching the composition of the eluent, the analyte of interest, trapped on the column, is eluted from the column. The trapping process is based on the exchange of the species between the two column phases, the sorbent material and eluent, when equilibrium is reached [54]. The general separation process *via* a SPE column can be seen in Figure 26.

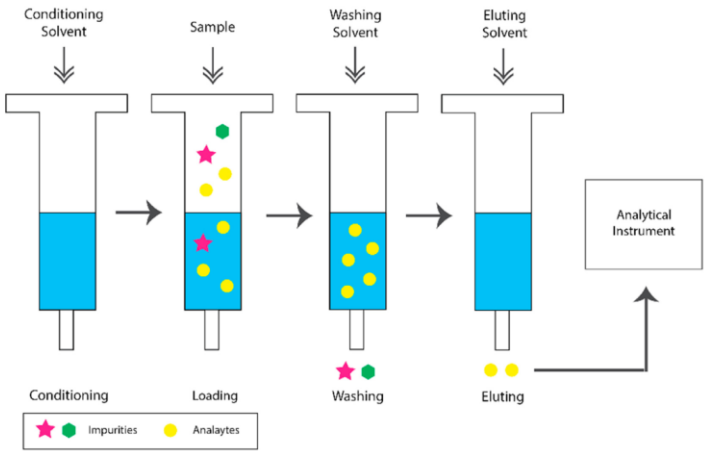

Figure 26: Visual representation of an SPE workflow consisting of the 1) Conditioning step 2) Sample application, 3) washing, and 4) elution of the analyte of interest [55].

Prior to the actual trapping and eluting steps, a conditioning step of the SPE column is necessary. This step ensures an effective interaction of the sorbent material with the analyte of interest in order to trap it on the column in the following sample application step [54]. SPE represents a crucial step to enrich the analyte of interest during the sample preparation. Therefore, this method is crucial for very low abundant molecules in a complex matrix.

2.12. Proteomics

The term proteome describes the entity of all proteins in an organism under specific, well-defined conditions. The first definition in the research field of proteomics was made by Marc Wilkins in 1996, who defined the term “proteome” as the “entire PROTein complement expressed by a genOME” [56],[57]. In 1838, Berzelius first mentioned the term “protein”, deduced from the word “proteios” with the origin in the Greek language, pointed out as the

“molecule of first rank” [58],[57]. The analysis of the proteome of a system gives insight into the mechanisms occurring in the observed organism. Besides the aim of identifying the overall protein content in the system of interest, abundances, modifications, and locations can provide a more complete overview of the biochemical processes occurring in the system [59].

The outstanding developments in mass spectrometry techniques in the past few years have driven tremendous progress in the field of proteomic research. Analyser types, like ion-traps, quadrupoles and TOFs are commonly used in the proteomics research field. Combinations of different analysers, called tandem MS devices, can be advantageous to gain more information about the analytes of interest [60].

Proteomics approaches can be classified into two research techniques, top-down and bottom-up. The bottom-up approach is based on an enzymatic fragmentation of the entire protein to gain peptides prior to the analysis step in the MS. The analysis can be undertaken on MS-1 or MS-2 level. Therefore, either the intact enzymatically digested peptides are analysed or the peptides are further fragmented in the MS device. The bottom-up approach, also called shotgun, is the more frequently used way to gain information in a proteomics workflow. In Top-down approaches, the intact proteins of the sample are fragmented only in the MS device (Figure 27) [61],[62].

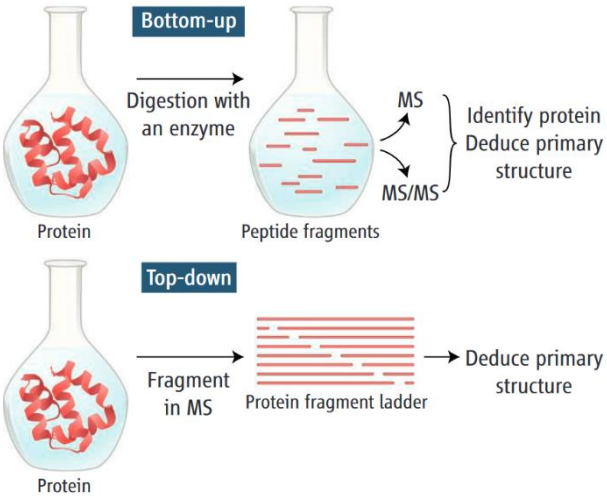

Figure 27: Comparison of the general workflow of a Bottom-Up and Top-Down Proteomics approach [61].

2.13. Genome-, Transcriptome- and Proteome-Atlases of Organisms

In order to gain a complete biochemical overview of individual organisms, atlases of different biomolecules from various systems have been of high interest in the past few years [63],[64]. For example, a research initiative, called the human protein atlas (HPA) was commenced in 2003 to collect information about the locations and expressions of proteins in human tissues. The first datasets were launched in 2005 in a publicly open database [65]. Spatially resolved antibody-based images of the proteins in different organs, combined with transcriptomics data and system biology, represents the basic idea behind the initiative. The data on the website is sectioned into ten subgroups: (1) the tissue atlas with protein distributions (2) Brain Section (3) Single Cell Type Section (4) Tissue Cell Type Section (5) Pathology Section (6) Immune cell Section (7) Blood Protein Section (8) Subcellular Section (9) Cell line Section (10) Metabolic Section [66],[67], [63]. The ten subsection in the HPA database are shown in Figure 28.

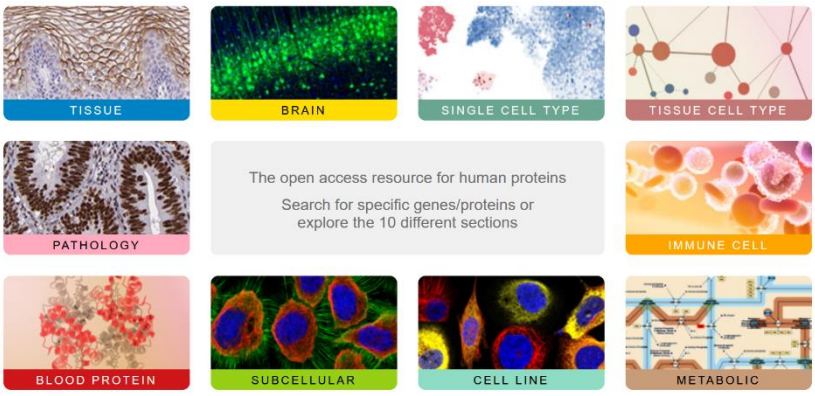

Figure 28: The ten subgroups of the human protein atlas project on the official HPA website: (1) tissue atlas (2) Brain atlas (3) Single-cell type (4) Tissue cell type (5) Immune cell (6) Metabolic atlas (7) Cell line atlas (8) Subcellular atlas (9) Blood protein (10) pathology atlas [67].

Progress in this field of research was also made for animal models, especially for the mouse. Several publications provide different information, like the spatially resolved protein composition of the mouse brain [68], local transcriptomics mouse brain analysis providing a spatially resolved view of the gene expression [69], organ-specificity of mouse-proteins [70] and much more. When looking at the genome level, initiatives like the Cancer Genome Atlas Organisation were launched from the National Institute of Health (NIH)

in 2005 to collect all significant cancer-causing abnormalities in the genome through extensive sequencing of genes [71].

2.14. Tissue-specific Eicosanoids

The eicosanoid composition of different organs can show significant alterations. For example, the expression of the human enzyme 12R-LOX shows local tissue-specific variations. It is described to be only expressed in the skin and tonsils. Therefore, the conversion of the precursor molecule AA to 12R-HETE, *via* the enzymatic path with 12R-LOX, is only feasible in these tissues [72]. Further, the expression among different cell types also shows differences when looking at 5-LOX, which is mainly expressed by leukocytes, macrophages and dendritic cells. Regiospecific alterations in the eicosanoid production are also known when looking at the thromboxan and prostaglandin family. Platelets are the main producers of the pro-thrombotic and vasoconstricting eicosanoid TxA_2 and PGE_2 is predominantly produced in kidneys and skin [50].

2.15. *In-vitro*- versus *in-vivo* models

The three main research approaches in natural sciences are *in-silico-, in-vitro*- and *in-vivo* models (Figure 29). *In-vitro* studies are undertaken outside of a living organism. The main advantage of these approaches is the ability to perform them under controlled conditions. Further, these types of models are generally low in time needed and ethically justifiable. The main disadvantage of *in-vitro* models is the lack of their ability to accurately predict the effects of a drug on the human or organism of interest in a real-life setting. *In-vivo* models are undertaken in a living organism, thus making their results more reliable [73].

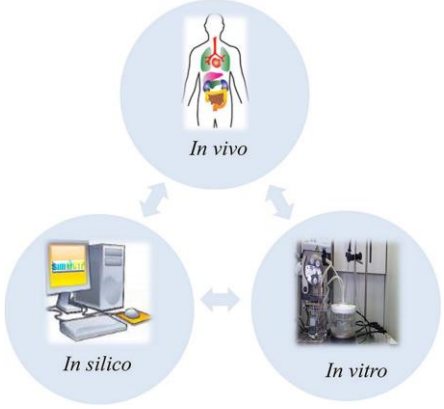

Figure 29: The three main research approaches, being in-silico, in-vitro and in-vivo [74].

2.16. Limitation of small animal models

Small rodent animals, like rats and mice, are one of the most frequently used animal models in natural science approaches. *In-vivo* models are well-established methods in research, due to their confidence in showing accurate predictions of the influences of drugs on a living organism. However, the pathophysiologic mechanisms of small rodent animal models in drug development approaches can alter tremendously from the mechanisms in the human body. These differences question their use as a model for the human system. Therefore, in the last few years, different organisations, like the European Medicines Agency (EMA) and the International Society for Stem Cell Research (ISSCR) recommended the use of large mammalian animal models, like pigs, sheep or horses. The motivation behind this is to better predict the human pathophysiological reaction on the drug [75]. For example, when looking at specific research settings, like gene therapy research approaches, large mammalian animals are well-established models. Their superiority is owed to their better performance in resembling the human biochemical responses, compared to smaller animals like mice [76].

2.17. Aim of this work

The aim of this work is to build up a protein abundance atlas of 13 sheep tissues: bone, brain, cartilage, heart, kidney, kidney mark, liver, lung, muscle, nerve, skin, spleen and tendon (Figure 30, Figure 31). Further, the eicosanoid composition of the individual tissue samples should be analysed. The assessment of the plausibility of the eicosanoid and protein expression distribution in the individual tissue samples, when looking at the eicosadomics and proteomics data set alone and in the combination of those two, should be undertaken in terms of biochemical pathways described in the individual tissue samples, cell type composition, similarities in tissue structure and further determining factors for possible similarities in the expression patterns.

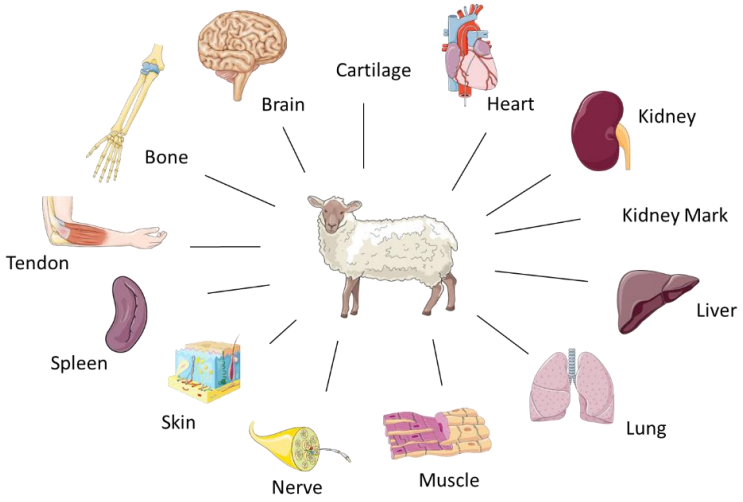

Figure 30: Tissue samples analysed in this work in order to build up an organ-atlas of the sheep for proteins and eicosanoid. Illustrations of organs and sheep used from ref. [1].

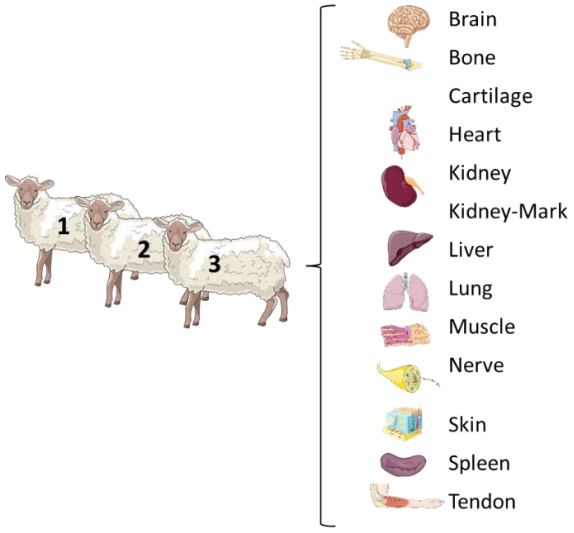

Figure 31: More detailed overview of the 13 sheep tissue samples analysed for the proteomics part, with three biological replicates (Sheep 1-3), making 39 samples in total for building up the protein abundance atlas of the sheep. The eicosadomics part only consists of 12 tissue samples analysed (the same samples as in proteomics part but without bone). Illustrations of organs and sheep used from ref. [1].

3.0. Materials and Methods

In this chapter, the materials and methods, used for the sample preparation and measurement steps for the two omics approaches in this thesis, eicosadomics and proteomics, can be seen. The ovine tissue samples, used for the proteomics- and eicosadomics part, were provided from Iris Gerner and Prof. Florien Jenner from the Veterinary University of Vienna. The ovine tissue samples used for this thesis were collected as by-products of the

animal experiment for the evaluation of the regeneration capability of tendon- and cartilage-injuries of adult- and fetal sheep of the Veterinary medicine university of Vienna. The ethical approval for euthanizing the sheep in this research setting was undertaken by the ethic commission of the Bundesministerium für Bildung, Wissenschaft und Forschung (engl.: Federal Ministry of Education, Science and Research) (BMBWF) (reference number of the approval = GZ 68.205/0100-V/3b/2018) and by the Veterinary medicine university of Vienna Ethic- and animal protection-commission. The collection of the tissue samples post-mortem, for setting up the protein-atlas and the analysis of the eicosanoid content in the different ovine tissue samples was confirmed by the Veterinary medicine university of Vienna, as the owner of the sheep.

3.1. Eicosadomics

The sample preparation steps for the eicosadomics part were undertaken on 12 ovine tissue samples: brain, cartilage, heart, kidney, kidney mark, liver, lung, muscle, nerve, skin, spleen and tendon. The sample preparation steps, standards used, MS device and the settings of the MS device are described below.

3.1.1. Internal deuterated standards

The standards used to analyse the eicosanoids were stored in aliquots at -80°C. Prior to their use, the individual aliquots were thawed at room temperature and kept on ice for further sample-preparation steps. In order to enable an overview of the sample-preparation and analysis quality, two standard mixtures were used, one prior to the extraction (“Eicos-pre-mix”) and one prior to the analysis via LC-MS (“Eicos-post-mix”). All standards were purchased from Cayman Chemicals. For the preparation of the Eicos-pre-mix and Eicos-post-mix, volumes from the individual thawed aliquots of deuterated standards, as listed in Table 1 and Table 2 ,were combined and filled up to 500 µL with ACN. The standard mixtures were stored at -80°C in aliquots of 70 µL each.

Table 1: Deuterated standards and volumes used for the preparation of the eicos-pre-mix.

Eicos-pre-mix	
Standard	V [µL]
15S-HETE-d8	4
12S-HETE-d8	4
5-oxo-ETE-d7	12
11,12-DiHETrE-d11	4
PGE2-d4	8
20-HETE-d6	4
In total	36

Table 2: Deuterated standards and volumes used for the preparation of the eicos-post-mix.

Eicos-post-mix	
Standard	V [µL]
5S-HETE-d8	4
14,15-DiHETrE-d11	4
8-iso-PGF2alpha-d4	8
In total	16

3.1.2. Sample-preparation procedure of the tissue samples

The sample preparation steps of the eicosadomics part were undertaken according to ref. [77]. The tissue samples were stored in ethanol at -20°C in 15 ml falcon tubes and kept on ice during the sample-preparation steps. For the cell lysis step an ultrasonic stick was used. Depending on the tissue structure a few short ultrasonic pulses were exerted on the tissue samples. In the eicosadomics part, only 12 tissue samples were analysed, due to problems in the collection of reproducible bone samples. Afterwards, the proteins were precipitated at -20°C for around 15 hours. The individual tissue samples were centrifuged 30 minutes at 4°C at 4536 g. The pellet consists out of tissue residues and proteins and the supernatant contains eicosanoids and other lipids. The supernatants of the individual tissue samples were transferred to falcon tubes with 500 µL ice cold LC-MS grade water. 5 µL of the Eicos-pre-mix were added to each falcon tube and vortexed shortly. The ethanol was reduced from the samples *via* centrifugation under vacuum at 37°C and the samples, reduced in volume, were kept on ice for the following extraction steps.

All the reagents and samples used in the extraction procedure were constantly kept on ice, if not mentioned at other conditions. The SPE columns (StrataX SPE columns (30 mg/mL; Phenomenex, Torrance, CA, USA)) were cleaned 2 times with 1 mL LC-MS grade methanol each, followed by an equilibration step with 2 times 1 mL of LC-MS grade water. The samples were loaded onto the columns with Pasteur pipettes and 2 ml of water was added to the falcons, vortexed and also transferred onto the column, which was undertaken twice. In order to ensure a good and reproducible binding of the eicosanoids to the solid phase, a constant flow rate of the liquid going through each column was tried to maintain. The SPE was flushed with another 1 mL of water. After this step the columns were shortly run dry. In order to elute the eicosanoids bound on the stationary phase, 500 µL of elution buffer (Methanol + 2% Formic acid (FA)) were added to each column. The eicosanoid samples were collected into 2 mL glass vials. The collected samples were dried under gentle N_2 stream at lukewarm conditions for around 1 hour. The dried samples were reconstituted in 150 µL reconstitution buffer (145 µl 35 % B (10 Vol-% Methanol, 90 Vol-% ACN and 0,2 Vol-% FA) (Table 3) + 5 µl Eicos-post-mix (Table 2)), containing the Eicos-post-mix, vortexed and transferred into glass inlets for MS vials. All samples were kept at +4°C in an autosampler and subsequently measured *via* LC-MS.

3.1.3. LC-MS method

The mobile phases for the LC-MS method used for the analysis of the eicosanoids can be seen in Table 3. The LC starting conditions for the eicosanoid analysis workflow was 65:35 vol-% (A:B). All tissue samples were not further processed prior to the LC-MS analysis despite the liver samples, which showed an oily film on top of the liquid. The liver samples were centrifuged and the supernatant was transferred into a new glass inlet for MS vials.

Table 3: Chemicals and percentages for the preparation of the elution buffer mixture and reconstitution buffer mixture.

Mobile phase A
Water + 0.2% FA

Mobile phase B	
Chemical	Vol-%
Methanol	10
Acetonitril (ACN)	90
FA	0,2

The glass inlets with the processed samples were placed into the autosampler from the LC-system (Vanquish Horizon UHPLC) at 4°C. 20 µl of each sample was injected into the LC-MS system. The detailed conditions of the eicosanoid LC-MS analysis workflow are listed in Table 4.

Table 4: Parameters of the LC-MS workflow used for the analysis of the eicosanoids in the sheep organ-atlas project.

Parameters of the LC-MS workflow for the eicosanoid analysis	
Instrument	Vanquish Horizon UHPLC - Q Exactive HF Hybrid Quadrupole-Orbitrap MS
Source	HESI
Measuring Mode	Negative (technical replicate)
Injection volume	20 µL
Column	Kinetex 150 x 2.1 mm, 2.6 µm, 100 Å
Flow rate	200 µL/min
Data processing	Trace Finder, Xcalibur

3.2. Proteomics

The sample preparation steps for the proteomics part were undertaken on 13 ovine tissue samples: bone, brain, cartilage, heart, kidney, kidney mark, liver, lung, muscle, nerve, skin, spleen and tendon. All steps undertaken during the sample preparation and the MS device with the settings used are described below. The sample preparation procedure for the ovine tissue samples was undertaken according to ref. [78] and the tissue proteomics procedure according to ref. [79].

3.2.1. Tissue sample preparation procedure

The tissue samples were kept in an Eppendorf tube at -80°C for long term storage and kept at -78 °C shortly before the lysis procedure. The dry organ samples were transferred into falcon tubes and 150 µL lysis buffer (LB) was added to each falcon. The individual samples were lysed *via* an ultrasonic stick, cleaned with water and ethanol after each organ sample. The samples were centrifuged at 5000 g, 23 °C for 5 minutes, lysed again with the ultrasonic stick, followed by another centrifugation step at 5000g, 23°C for 5 minutes (step 1, Figure 32). The tendon samples were spiked with another 100 µL LB. The bone, Cartilage, skin and tendon samples, which showed a less visible result of the cell lysis compared to the other samples, were centrifuged again at 5000 g, 23 °C for 3 min and again treated with the ultrasonic stick, followed by another centrifugation step with the same conditions for 5 min. The supernatant was transferred to Eppendorf tubes and shaken for 5 min at 95°C and afterwards centrifugation at 5000g for 5 min. The supernatants of all samples were transferred into Eppendorf tubes and the protein concentration was analysed *via* BCA. The individual tendon samples were again spiked with different amounts of LB and treated with a small pestle for further cell lysis and in order to be able to take a supernatant (step 2). The supernatant of the further lysed tendon samples was combined with the supernatant of the first lysis steps. Afterwards, a BCA assay was done to identify the protein concentration. The individual samples were diluted to 20 µg protein in 50 µL LB buffer for the following digestion procedure. A detailed version of the procedure to analyse the proteome abundance atlas of the proteomics tissue samples can be seen in Figure 32.

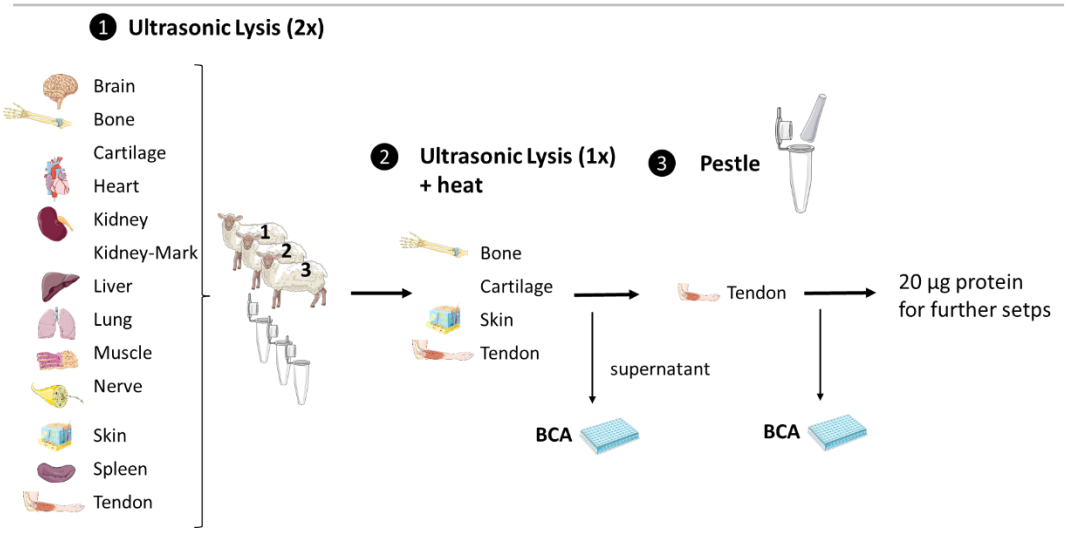

Figure 32: Overview of the sample-preparation steps for the analysis of the proteins for building up the protein-abundance atlas of the sheep consisting of 39 tissue samples (three biological replicates (sheep 1-3) for each tissue.) Illustrations of organs, sheep and lab equipment used from ref. [1].

3.2.1.1. Protifi S-Trap Mini protocol

The supernatants of the tissue samples, diluted to 20 µg protein in 50 µL Lysis Buffer (LB) each, were digested using the Protifi S-Trap Mini protocol. The composition of the LB is listed in Table 5. 50 µL Dithiothreitol (DTT) was added to each sample in order to reduce disulfide bonds followed by an incubation time of 10 minutes at 95°C and 300 rpm. Afterwards, the samples were cooled to room temperature and shortly spun in the centrifuge to collect all the liquid at the bottom of the Eppendorf tube. With 12.5 µL of Iodacetamide (IAA) in each Eppendorf tube and an incubation time of 30 min at 30 °C and 300 rpm, the thiol groups of the opened disulfide bonds were modified in order to prevent them from rebuilding disulfide bonds. 11.25 µL of 12 % phosphoric acid was added for acidification, followed by the addition of 866 µL S-Trap buffer in each Eppendorf tube. The mixtures were added to the columns, which were placed into 2 mL Eppendorf tubes in order to collect the liquid going through the column in the first washing steps. The columns were centrifuged at 1000 g for 1 min, followed by an equivalent centrifuging step but with 180° rotated Eppendorf tube. 400 µL of S-Trap buffer were added to each column and centrifuged to wash away any salts. This step was repeated 3 times with 180° rotations of the Eppendorf tubes between each centrifugation run. The columns were then transferred to new Eppendorf tubes to collect the eluted proteins. 20 µg of Trypsin/LysC mixture were dissolved in 1000 µL digestion buffer and kept on ice for the following steps. 4000 µL digestion buffer were pipetted into a 5 ml Eppendorf tube and the dissolved Trypsin/LysC mix was added. 125 µL of this mixture was added to each column (0,5 µg enzyme). The trapped proteins on the S-Trap Columns in the Eppendorf tubes were undertaken a digestion procedure for 2 h at 37 °C in an incubator. In order to elute the digested proteins 80 µL digestion buffer was pipetted directly onto the solution with the peptides followed by a centrifugation step at 1000 g. Afterwards, 80 µL 0,2 % FA was added, centrifuged and 80 µL 50 % ACN were added, again centrifuged and lastly the eluted peptides were dried in the speedvac at 40°C. The dried peptides were stored at -20°C prior to the analysis step.

Table 5: Volumes of the chemicals used for the preparation of the lysis buffer needed in the Protifi S-Trap Mini protocol for digesting proteins.

Lysis Buffer (pH 7.55)		
Chemical	Volume [mL]	Mass [g/10 mL]
Urea	-	4,80
1 M Tetraethylammoniumbromide (TEAB)	0.5	-
20 % Sodiumdodecylsulfate (SDS)	2.5	-

3.2.1.2. BCA-assay

For the calibration of the method, 10 different volumes of a Bovine serum albumin (BSA) standard (1 µg/µL), starting from 0 µl BSA standard to 9 µL BSA in 1 µL steps, were pipetted into a 96 well plate. Water and LB were added to each well as listed in Table 6. To analyse the protein amount in the individual samples, 1 µL sample was spiked into 9 µL of H_2O. Lastly, 200 µL working reagent solution was added to each sample and each well with the BSA standard for calibration. Working reagents, A and B, for the preparation of the working reagent solution, were combined only shortly before their use in a ratio of 98:2 (Table 7). The 96 well plate was kept at reduced light exposure as far as possible in the further shaking and incubation steps. The plate was shortly shaken at 1100 rpm and incubated for 30 min at 60 °C in the dark followed by the measurement of the absorbance at 562 nm.

Table 6: Volumes of the BSA standard, H2O, Lysis buffer and working reagent used for the calibration of the BCA assay.

Calibration BCA-assay				
Std.	BSA standard (1 µg/µL) [µL]	H_2O [µL]	LB [µL]	Working reagent [µL]
1	0	9	1	200
2	1	8	1	200
3	2	7	1	200
4	3	6	1	200
5	4	5	1	200
6	5	4	1	200
7	6	3	1	200
8	7	2	1	200
9	8	1	1	200
10	9	0	1	200

Table 7: Preparation scheme of 100 ml of the working reagent A and working reagent B and the working reagent solution as a combination of working reagent A and B for the protein quantification via the BCA-assay.

Working reagent A (100 mL)	
Chemical	Amount [g]
Bicinchoninic acid	1
Sodium carbonate	2
Sodium tartrate	0,16
Sodium bicarbonate	0,95
→ dissolve in 100 mL H_2O and pH adjustment to 11,25 (3M NaOH)	

Working reagent B (10 mL)	
Chemical	Amount [g]
Copper sulfate · 5 H_2O	0,5
→ dissolve in 10 mL H_2O	

→ Working reagent solution: 98:2 vol-% (A:B) with 200 µL for each sample/standard well

4.0. Data-Evaluation

The data evaluation was undertaken with various software packages. All programs and packages used for the evaluation of the data from the eicosadomics and proteomics part are described in this section.

4.1. Proteomics

The first search for the identification of proteins and label-free quantification (LFQ) was performed using the MaxQuant software package. The obtained data was further processed with the Perseus software (version 1.6.14.0). The LFQ-values of each organ, with the three biological- and two technical replicates were processed separately. In Perseus, five main filtering steps were undertaken. The data matrix was reduced by the values only identified by site, followed by a filtering step of the values that could not be found when searching the data in reverse and potential contaminants were filtered. The data was log2-transformed in order to achieve a variance of the data which is not concentration-dependent. Afterwards, the technical replicates of the individual organs were categorically annotated as one group and the mean of the groups were calculated, followed by another filtration step of the matrix, removing the rows containing less than 2 valid

entities in the total data set of the individual organs. For the specification of the proteins, the following requirements had to be fulfilled: a limit of at least 2 peptides found per protein, FDR < 0.01 for proteins and peptides, the protein had to be found in at least 2/3 of the samples in one group and the protein was annotated as specific if it was not found in all other samples. Afterwards, the matrices, with the filtered data of the individual organs, were further processed in excel in order to visually present the organ-specificity of the analysed proteins with bar plots.

Furthermore, the list of accession numbers, specific for the individual tissue samples, were loaded into R (version 4.2.2) to put specific proteins into biologic context. GO Term annotation was downloaded from UniProt. The GO database was used with the classification “Biologic Process”, “Cellular Compartment” and “Molecular Function”. An enrichment analysis was undertaken with the clusterProfiler package (version 4.6.0) [80],[81]. The p-value was adjusted according to Benjamini-Hochberg [82]. An adjusted p-value of less than 0.05 was considered to be significant. The enrichment results were visualized using the enrichplot package (version 1.18.3). GO semantic similarity analysis (version 2.25.0) was used to show the similarity of the enriched GO terms of the specific proteins per organ. GO Term similarity was determined using the Jaccard index as the distance metric. GO Terms were clustered using hierarchical clustering and complete linkage.

Lastly, a list of all proteins found per organ, with their corresponding LFQ values, was loaded into R to form a heatmap. To do so, the LFQ values were z-transformed. The z-transformation represents a standardization of the data to a Gauss distribution with the mean value zero and standard deviation +1/-1. By undertaking this transformation, the data of the individual tissue samples is better comparable. Prior to the z-transformation of the protein data set, the missing values were filled up using Perseus.

4.2. Eicosadomics

For the data processing, Xcalibur Qual Browser Version 4.1.31.9 Thermo Fischer Scientific and TraceFinder Version 4.1 Thermo Fischer Scientific were used. The deuterated standards used are references for the retention times of the analytes of interest. An equal distribution of the individual standards over the entire retention time window/gradient of the analysis is aimed to cover a sufficient comparison of the entire set of analytes of interest to the standards used in the method. A list of 300 eicosanoid compounds that could be found in the sample analysed was loaded into TraceFinder as the Compound Database. Parameters like the compound

name, retention time, m/z value, polarity (negative), adduct (hydrogen-loss), height threshold (10 000), area threshold (10 000), collision energy (24 eV) and retention time window (15 sec) were set. The internal standards were set as references for the retention time of the individual eicosanoids in the master method. During the search run, the software searches for MS-1 features in the sample data set at the retention times of the eicosanoids in the uploaded compound database, considering the set parameters. Manually, the sample with the feature at the right retention time is opened in Xcalibur and the MS-2 spectrum of the feature is compared to either a theoretical MS-2 spectrum of the expected eicosanoid in the compound list or the MS-2 spectrum of the particular standard. Afterwards, the eicosanoid is defined as identified if the retention time (MS-1 level) and the fragment spectrum (MS-2 level) of the feature identified in the sample matches the theoretical data or measured standards. The identified features were manually integrated. The areas under the curve (AUC) of the integrated peaks were read using the R software package (version 4.2.0). The data was log2-transformed to achieve a constant variance over the whole concentration-window. Afterwards, the mean values of the standards were subtracted from the mean values of the analytes for normalization. In order to achieve a data set with values close to proteomics LFQ-values, 20 was added to the areas. Missing values were filled up with the minProb function of the imputeLCMD package (version 2.1). This data was further processed with excel and the R software package (RStudio version 2022.12.0).

Further, the eicosanoids analysed were assigned to their precursor molecules and enzymatic pathways. The concentration values of the eicosanoids with distinct precursors and enzymes, were z-transformed and plotted in a heatmap to visually present the concentration differences of the eicosanoids in the different tissue samples and to visualize the overall concentration differences of the eicosanoids with different precursors and enzymes. The evaluation steps undertaken for the proteomics and eicosadomics part, with the individual software packages used in each step, are summarized in Figure 33.

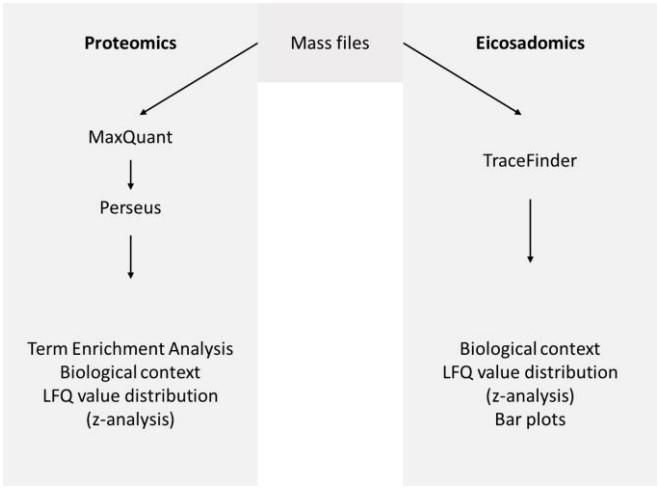

Figure 33: Overview of the data-evaluation scheme of the eicosadomics- and proteomics-part using MaxQuant, Perseus, TranceFinder and various R-packages.

5.0. Results

This section shows the results from the different data evaluation approaches of the eicosadomics- and proteomics-part.

5.1. Eicosadomics

A total number of 176 different eicosanoids were found in the tissue samples analysed. 129 of them were able to be annotated as distinct eicosanoids according to their retention time and mass. All eicosanoids identified *via* standards can be seen in Table 18 in the supplementary section. 47 features found in the mass spectra were listed as no-name features. These no-name features could be ascribed to the general group of eicosanoids due to specific fragments found in the mass spectrum, specific for individual eicosanoid class candidates, and the retention time.

5.1.1. Z-transformed LFQ-value distribution

71 of the 129 annotated eicosanoids could be assigned to a distinct precursor molecule and enzymatic pathway. The z-transformed concentration values of these 71 eicosanoids, with their precursor molecules (AA, ALA, EPA, DHA, DGLA and Linoleic Acid) and enzymatic pathway (COX, COX-ASA, LOX or CYP) can be seen in Figure 34, visualized in a heatmap.

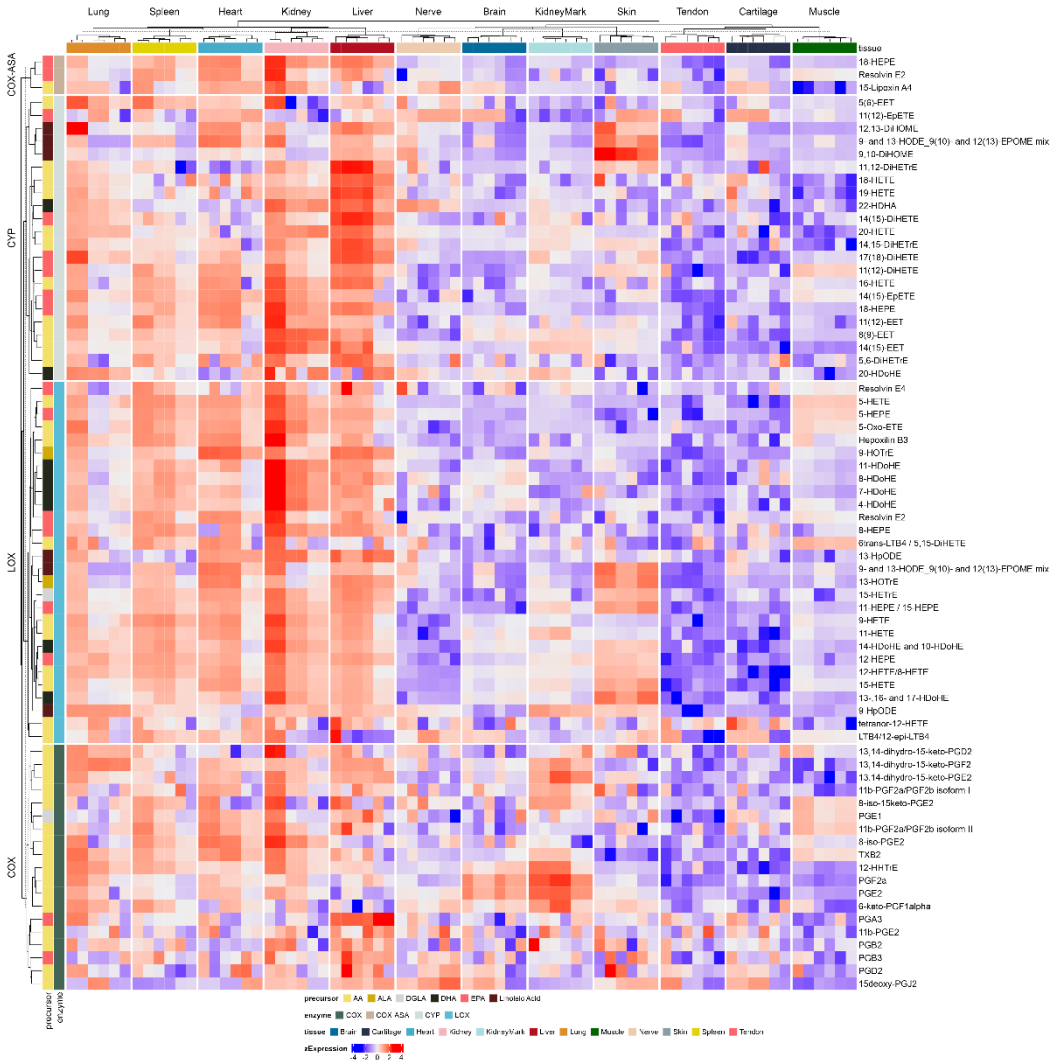

Figure 34: Heatmap of the z-transformed concentration values of the eicosanoids analysed.

The z-transformed LFQ value patterns can be interpreted *via* different approaches: the extent of similarity of the eicosanoid patterns in the heat map between organs with similar cell type composition, tissue texture, biological function or in literature described eicosanoid pathways.

When looking at the heatmap of the eicosanoid evaluation, several similarities between the expression patterns of the organ samples can be seen. Firstly, the 13 organ samples can be roughly categorized into three groups, showing similarities in their eicosanoid expression patterns. Group 1 consists of nerve, brain, kidney mark, skin, tendon, cartilage and muscle. This group is defined by an overall lower expression of eicosanoids, compared to the other two groups. Group 2, consisting of lung, spleen and heart, is defined by overall higher abundance values, visualized by a higher amount of red across the columns in the heat map. Group 3, formed by kidney and liver, shows expression patterns with the highest concentration

values over the entire columns in the heat map, compared to the other two groups.

5.1.1.1. Interpretation according described eicosanoid pathways

In this section, the individual tissue groups, defined by similarities in their expression patterns in the heatmap (Figure 34), are evaluated *via* described eicosanoid pathways. This interpretation approach should give an insight into whether the tissue group formation could be explained with a similarity in the day-to-day biological processes, mediated by signalling molecules, between tissue samples in one group. This section also covers the comparison of the results found here with eicosanoids found in different tissue samples in the literature.

Group 1: Nerve, brain, kidney mark, skin, tendon, cartilage and muscle

The skin, with the main functions as a protective barrier of our body to the environment, regulation of heat and much more, shows a high metabolic conversion of PUFAs. For example, the dietary PUFA linoleic acid (LA) is known to have an important role in maintaining the normal function and appearance of the skin. When looking at specific enzymatic pathways, the 15-LOX pathway is especially active in the skin epidermis. This enzymatic pathway predominantly catalyses the conversion of the precursor molecule AA to the oxylipin 15S-HETE. On top, the same metabolic pathway with 15-LOX as enzyme but with LA as precursor leads to the formation of 13S-HODE and to 15S-HETrE with DGLA as precursor molecule [83]. These three oxylipins, 15-HETE, 15-HETrE and 13-HODE were all found with an elevated abundance in the skin tissue samples, compared to the other eicosanoids found in the skin.

Group 2: Lung, spleen and heart

The heart can metabolize free AA *via* COX, LOX or CYP. Myocardial-, endothelial- and vascular smooth muscle cells are the three main contributors in the metabolic turnover of cardiac AA. Several oxylipin LOX-products, with the main myocardial enzymatic pathways being 12-LOX (eg.12-HETE) with traces of 15-LOX (eg.15-HETE), are described in a previous study in different heart regions of rat hearts and cultured myocytes. Further, some special COX-products, like PGF2a, are also generally known to have distinct signalling- or physiological roles in the cardiac myocytes [84].

Group 3: Liver and kidney

Several renal eicosanoid pathways are described in literature, covering the three major enzymes COX, LOX and CYP. For example, AA is metabolized *via* the renal COX-pathway to primarily form the prostaglandins PGE2 and PGI2. These oxylipins are described to have functions as renal vasodilators. Both, PGE2 and PGI2, are shown to have significant influences on maintaining normal kidney functions during special circumstances like hypovolemia [85].

The major pathway of the conversion of AA to bioactive oxylipins in the kidney is *via* the enzyme CYP. Firstly, AA is metabolized by CYP to form different EETs (5,6-, 8,9-, 11,12- and 14,15-EET) with the main renal EET being 14,15-EET. For example, renal EETs are found to have anti-inflammatory effects by inhibiting the NF-kB cascade. Further, HETEs are formed *via* the enzymatic pathway of CYP. It has been described that 11-HETE and 15-HETE (*via* CYP2J5 in mouse kidney) and 20-HETE and 19-HETE (*via* CYP ω-hydroxylase) are formed in tubular cells in the kidney, with 20-HETE being the main HETE produced by CYP ω-hydroxylase in the kidney with AA as precursor. 20-HETE, formed in renal tubules, thick ascending rings, different regions of the renal cortex and outer medulla, has several effects on renal functions. For example, the oxylipin can completely bind to vasoconstrictors like angiotensin II. When looking at the LOX pathway, renal LTs and LXs, as the major oxylipins in this enzymatic process, are described to have special functions in kidney inflammation [86].

The liver is also described to produce high levels of EETs, with 14,15-EET and 11,12-EET being the main hepatic EET CYP products. For example, EETs, prostaglandins (e.g. PGE_2) and thromboxanes (e.g. LTB_4) have been found to play a crucial role in promoting liver regeneration after surgical partial hepatectomy [87].

The heatmap with the z-transformed LFQ values (Figure 34) shows slightly elevated abundance values of the two HETEs, 19- and 20-HETE, in the tissue representatives of Group 3, compared to the members of the other two groups. When looking at the two candidates in Group 3, the liver shows higher abundance levels of the two oxylipins, compared to kidney.

Further, when looking at the EET family, the high amount of 14,15-EET found in the kidney and liver are in accordance with the literature, as described above.

Numerous hepatic AA-derived oxylipins are described in literature. The liver is mainly composed of hepatocytes, Kupffer cells and endothelial cells with all three of them showing metabolic turnover of AA to form oxylipins. Firstly, Kupffer cells are known to form PGs and LTs, with the major AA-derived oxylipins being PGD2, PGE2, TXA2, LTB4 and LTC4. Hepatocytes are

known to produce PGI2, PGE2, PGF2a and TxA2, but in lower concentrations. These cell types are believed to have a higher importance in the PG metabolization compared to PG production. And lastly, hepatic endothelial cells are known to produce PGI2 as the main AA derived oxylipin [88].

5.1.1.2. Interpretation according biological function

Another interpretation approach can be undertaken when looking at the functions of the individual organs analysed. For examples, skin, lung, liver and kidney can be summarized as barrier organs. Especially the skin and the lung have to deal with the exposure to environmental toxins in the first place. Therefore, these barrier organs play a crucial role in immunology defence. The kidney and liver (Group 3) are major players in clearance processes, the elimination of toxins or the degradation of drugs. To do so, these two barrier organs, especially the liver cells, have a high amount of the enzyme Cytochrome-P450 enzymes. Cytochrome P450 is a well-known enzyme in the regulation and elimination of toxins from the environment and drugs. This high amount of CYP in renal and hepatic cells, needed for the day-to-day clearance and segregation processes, could be the reason for the high amount of CYP-derived oxylipin products found in the kidney and liver samples.

After exposure to toxins from the environment, the body can react *via* two different mechanisms to fight the unwanted substance, *via* an inflammation - or immune-system process. The liver has to deal with many challenges day-to-day, also owed by the location of the organ in the human body, placed directly after the intestinal tract. Even the body itself, especially the small and large intestines, accommodating the so-called microbiome, representing all bacteria in the intestinal tract subsequent to living, can trigger toxin elimination processes in the liver. Generally, prostaglandins are known oxylipin mediators in inflammatory processes. Therefore, for example, the upregulation of certain prostaglandins could be owed to the general day-to-day hepatic function of toxin elimination.

5.1.1.3. Interpretation according tissue texture

Another way to interpret the formation of the three groups of the eicosanoid data in the heat map could be to look at the texture of the organ samples analysed. Lung, spleen, heart, kidney, liver, kidney mark and brain can be seen as softer organs and muscle, tendon, cartilage, skin and nerve as more stiff organs. This difference in the texture of the samples analysed could have an influence on their lysability during the sample preparation

steps. Five of the seven mentioned stiffer organs are in Group 1, characterized by the overall lowest expression values of the eicosanoids measured. None of the stiffer organ samples are in the other two groups, showing higher overall eicosanoid expression values.

5.1.2. Bar-plots

The plots shown below, divided into three subsections, visually present the eicosanoid distribution with one specific precursor molecule classified into the different enzymatic pathways (COX, LOX and CYP). Further, this section visualizes the enzyme ratio of the eicosanoid production with one specific precursor and the Omega-3/Omega-6 ratio in the 12 tissue samples analysed. Therefore, this section outlines the distribution of eicosanoids within one enzymatic pathway, the contribution of a single enzyme to the eicosanoid production with one specific precursor and the Omega-3/Omega-6 ratio for the individual tissue samples.

5.1.2.1. COX-, LOX- and CYP- derived eicosanoids with AA as precursor

The distribution of eicosanoids, derived from different enzymatic pathways (COX, LOX and CYP) and different precursor molecules (AA, EPA, DHA and DGLA), is shown as a collectivity in a heatmap in section 4.1.1. The same data is presented in bar-plots in this section. These plots are focused only on a selected set of eicosanoids, derived from one enzymatic pathway and one precursor molecule. This visualization aims to present the data in a more clearly arranged way. Figure 35-37 show nine selected eicosanoids derived from COX, LOX and CYP with AA as precursor molecule. For example, when looking at the COX-derived eicosanoids with AA as precursor, PGF2a shows the highest abundance in the kidney mark and the lowest abundance in tendon.

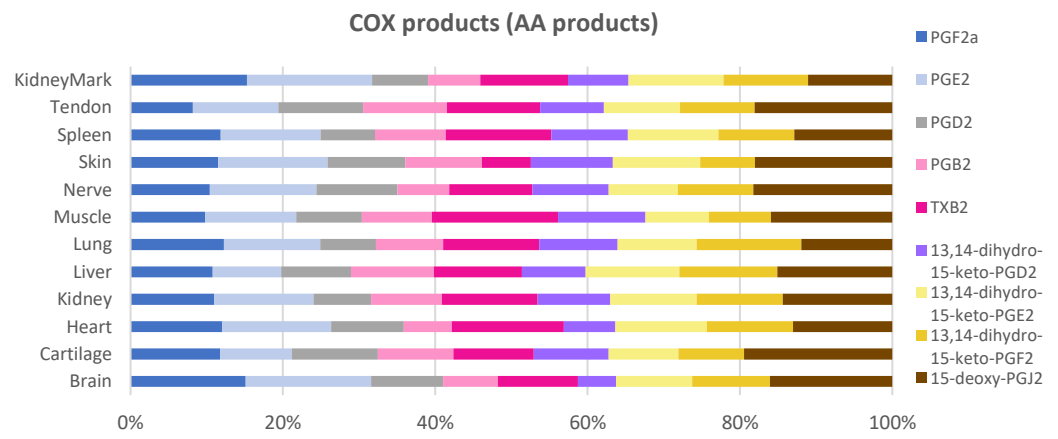

Figure 35: Distribution of 9 selected eicosanoids (PGF2a, PGE2, PGD2, PGB2, TXB2, 13,14-dihydro-15-keto-PGD2, 13,14- dihydro-15-keto-PGE2, 13,14- dihydro-15-keto-PGF2 and 15-deoxy-PGJ2) in the 12 tissue samples analysed with AA as precursor molecule and COX as enzymatic pathway.

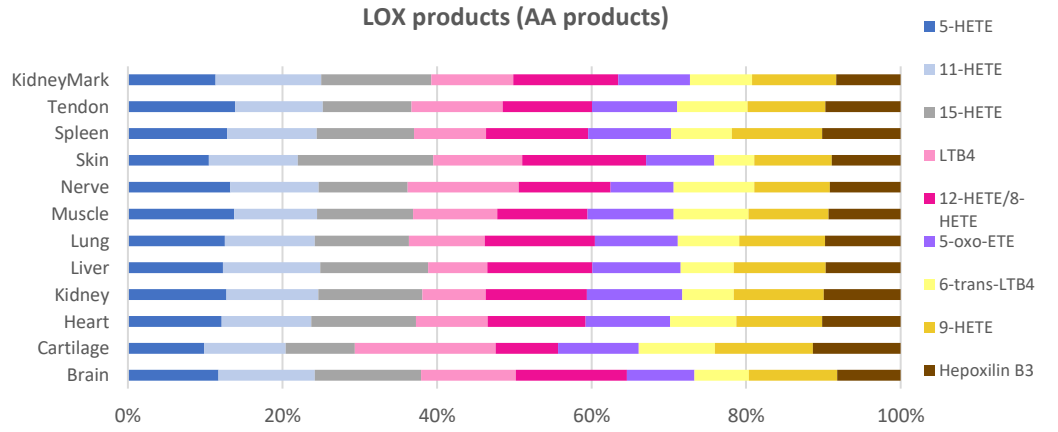

Figure 36: Distribution of 9 selected eicosanoids (5-, 9-, 11-, 15-HETE, 12-HETE/8-HETE, LTB4, 6-trans LTB4, 5-oxo-ETE and Hepoxilin B3) in the 12 tissue samples analysed with AA as precursor molecule and LOX as enzymatic pathway.

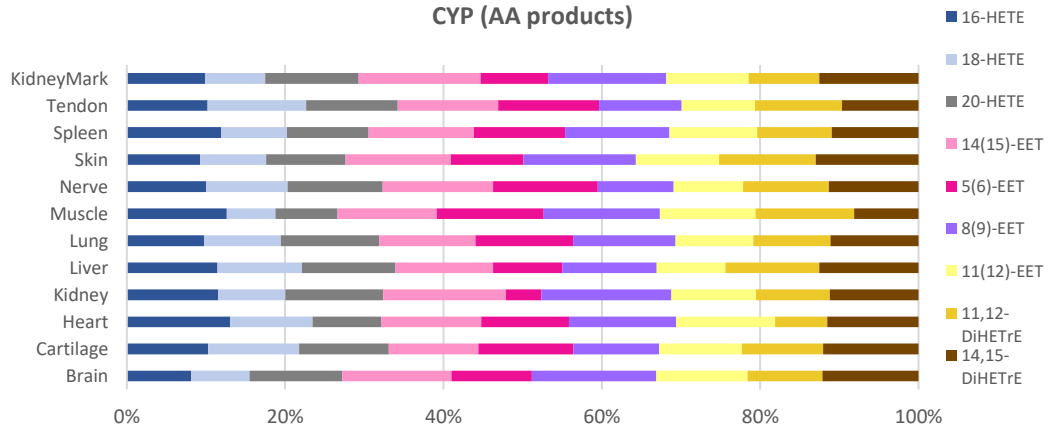

Figure 37: Distribution of 9 selected eicosanoids (16-, 18-, 20-HETE, 5(6)-, 8(9)-, 11(12)-, 14(15)-EET, 11,12-DiHETrE and 14,15-DiHETrE) in the 12 tissue samples analysed with AA as precursor molecule and CYP as enzymatic pathway.

5.1.2.2. Enzyme ratio of AA-derived eicosanoids

Figure 38 represents the distribution of the summed-up abundance values of a selected set of 9 AA-derived eicosanoid products, divided into their enzymatic origin (CYP, COX or LOX). This representation of the eicosadomics data set should provide information about the enzymes which show the highest significance in the metabolic rate in the AA-derived eicosanoid production, in the individual tissue samples. When comparing the three enzymes COX, LOX and CYP (Figure 38), it is clear to see that LOX shows the highest metabolic turnover of AA in the muscle and CYP the lowest. In the kidney mark, AA is predominantly converted by COX in order to form eicosanoids. However, it is essential to mention that this presentation only involves the summed-up abundance values of nine selected eicosanoid products for each enzyme.

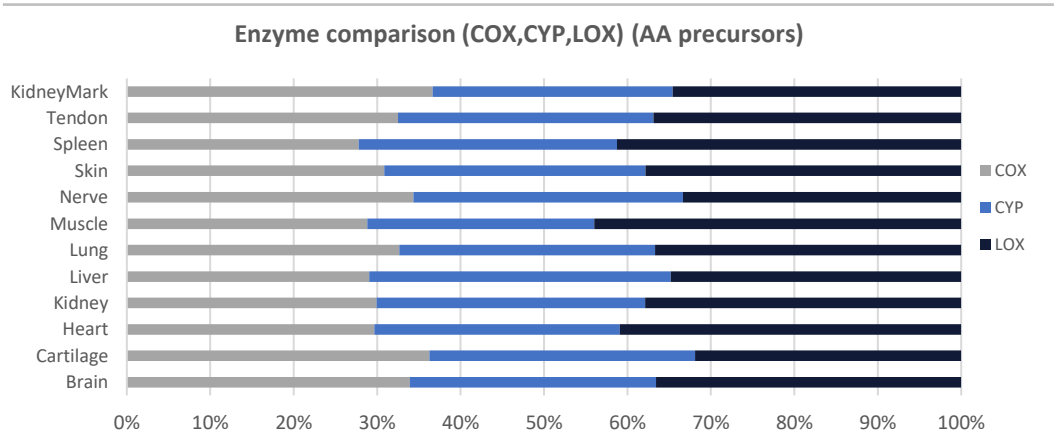

Figure 38: Distribution of the eicosanoids derived from the three enzymatic pathways CYP, COX and LOX in the 12 tissue samples analysed. 9 selected eicosanoids (CYP: 16-, 18-, 20-HETE, 5(6)-, 8(9)-, 11(12)-, 14(15)-EET, 11,12-,DiHETrE and 14,15-DiHETrE; COX: PGF2a, PGE2, PGD2, PGB2, TXB2, 13,14-dihydro-15-keto-PGD2, 13,14- dihydro-15-keto-PGE2, 13,14- dihydro-15-keto-PGF2 and 15-deoxy-PGJ2 and LOX: 5-, 9-, 11-, 15-HETE, 12-HETE/8-HETE, LTB4, 6-trans LTB4, 5-oxo-ETE and Hepoxilin B3) were chosen for each enzymatic pathway and the sum is plotted for each tissue.

5.1.2.3. Omega-3 versus Omega-6 ratio

Figure 39 shows the ratio of omega-3 and omega-6 fatty acids across the set of tissue samples analysed. The oxylipin precursor molecules AA and DGLA are belonging to the group of omega-3 PUFAs and EPA and DHA to the omega-6 fatty acids. This representation of the data set gives insight into the differences in the abundances of the omega-3 or omega-6 fatty acid precursor molecules in the individual tissue samples. This visualization could show the difference in the extent of the omega-3 or omega-6 fatty acid conversion in the individual tissues. As expected, the omega-3 levels in the brain are higher compared to the other organ samples. It can be clearly seen

that the omega-3 levels are low in muscle and cartilage, compared to all other tissue samples.

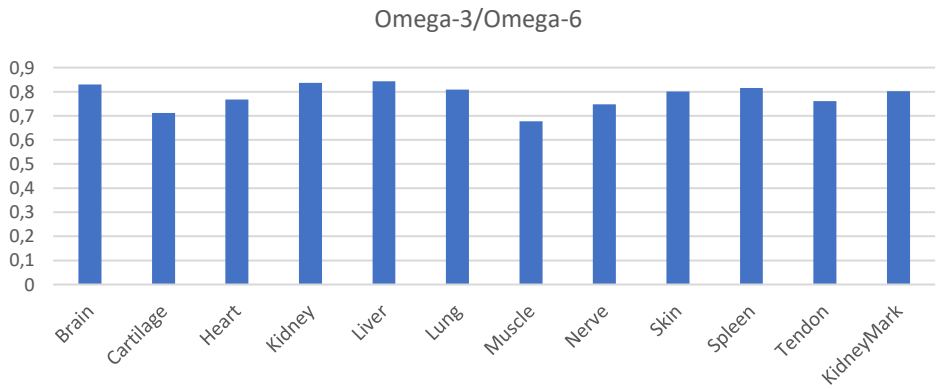

Figure 39: Omega-3 (AA + DGLA) versus omega-6 (EPA + DHA) ratio in the 12 tissue samples analysed.

5.2. Proteomics

In this section, the results of the proteomics evaluation steps (protein-specificity, GO-term enrichment analysis, z-transformed LFQ-value distribution) are presented and discussed.

5.2.1. Specific proteins

A total number of 4 702 different proteins were detected in all tissue samples analysed. The individual numbers of detected proteins are listed in Table 8. Table 8 also shows the number of proteins only found in one organ type.

Table 8: Total number of proteins found per organ and the number of specific proteins.

Organ	Number of detected proteins	Number of organ-specific proteins
Bone	491	1
Brain	2761	445
Cartilage	171	15
Heart	1428	24
Kidney	2486	106
Kidney mark	2091	60
Liver	1860	87
Lung	2577	68
Muscle	1046	63
Nerve	1992	29
Skin	1757	87
Spleen	2696	194
Tendon	295	2

Figure 40 visually depicts the differences in the number of specific proteins found per organ analysed. The number of specific proteins, compared to the total number of proteins found per organ can be seen in Figure 41.

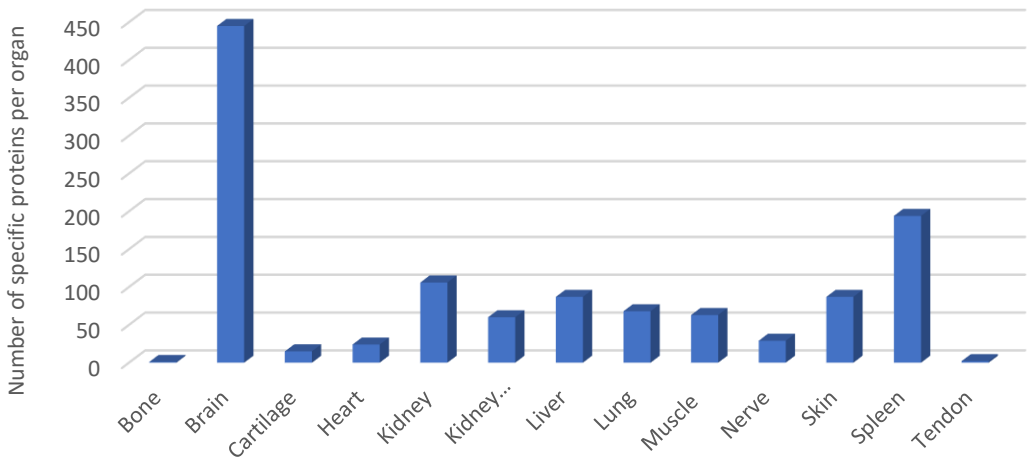

Figure 40: Visual presentation of the number of specific proteins found per organ. The corresponding data is listed in Table 8.

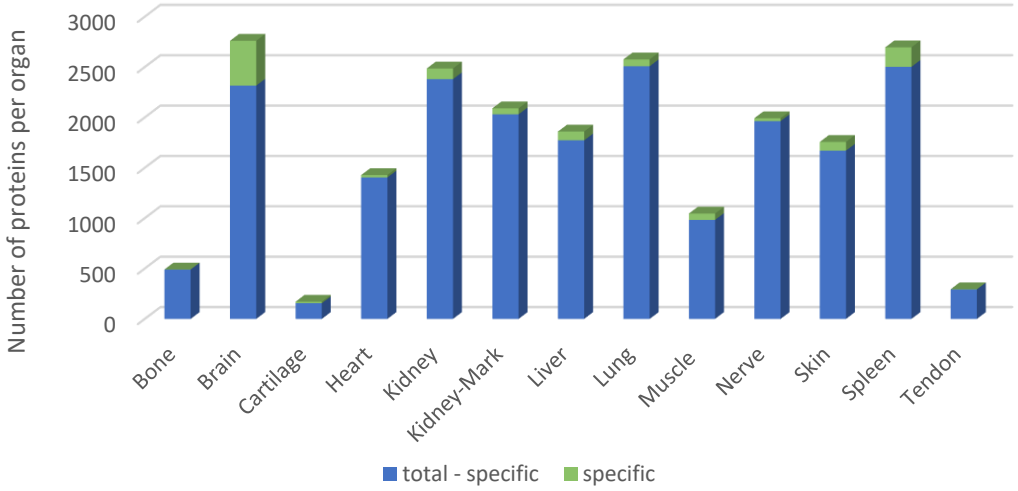

Figure 41: Visual presentation of the total number of proteins found per organ (blue + green), composed of the number of specific proteins (green) and the total number of proteins found per organ minus the number of specific proteins (blue).

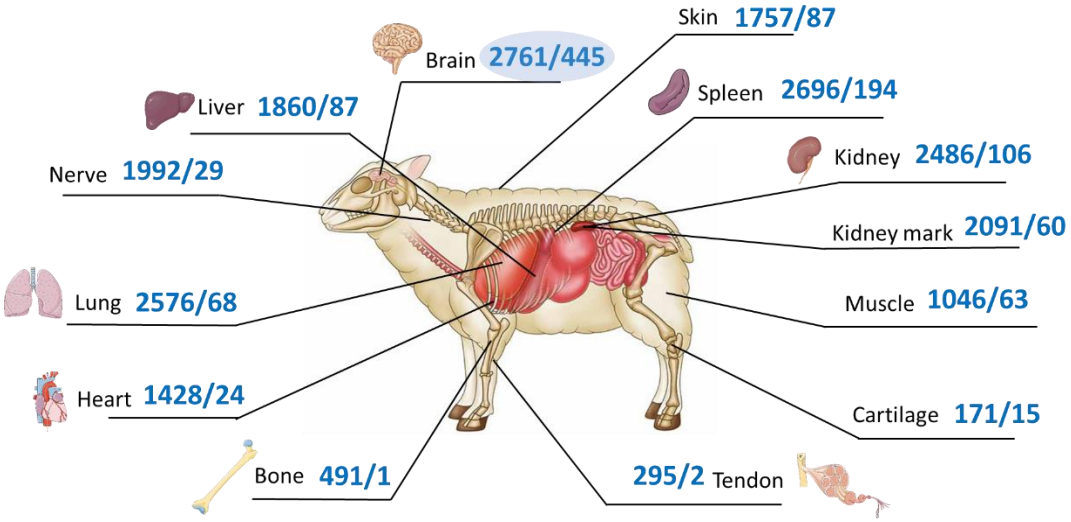

Figure 42: Organ-atlas of the 13 tissue samples analysed. The visual presentation of the data follows the scheme: total number of identified proteins/number of specific proteins. The data was used from Table 8.

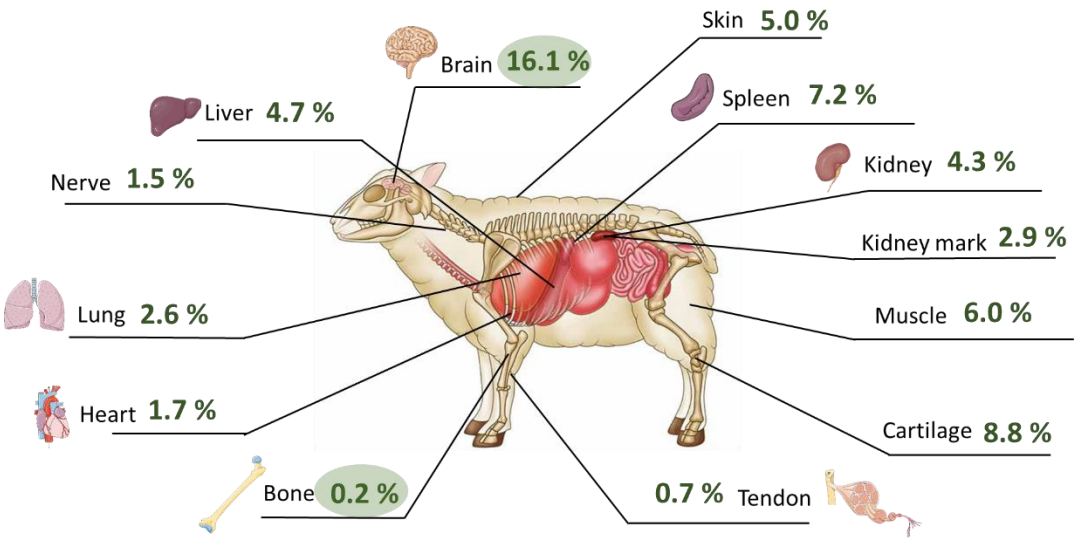

Figure 43: Organ-atlas of the 13 tissue samples analysed. The data presented shows the percentage of specific proteins found in the total number of proteins found per organ analysed.

5.2.2. Comparison of the tissue-specificity with the Human Protein Atlas project

In this section, the tissue-specificity of the proteins for the individual organs found in this study is compared to the results found in the human protein atlas project [67],[63]. The HPA initiative was established to provide a comprehensive overview of expression patterns of RNA and proteins over

many human tissue samples. For example, when looking at the 87 proteins found to be specific for the liver samples, 38 of them were found to have some information about the RNA- and protein expression in different organs listed in the HPA. Nine of the 38 proteins (23.7%) found with information in the HPA database showed selective, distinct or high expression of the protein in the liver, compared to other tissues and the RNA of the protein was found to be either tissue enriched or enhanced in the liver. Those nine proteins, found with information about the expression in the liver on both levels, RNA and protein, are listed in Table 9. Four of the 38 proteins (10.5%) were found only with the term “tissue enriched in liver” or “tissue enhanced in liver”, when looking at the tissue RNA expression, but showed no distinct expression in the liver on the protein level. However, these four proteins were annotated in the HPA database to be expressed in a set of organs including liver. The other proteins were annotated with “low tissue specificity”, showed only expression in the liver on the RNA level or were described to be expressed enriched or enhanced in another tissue.

The comparison of the proteins, found in this study to be specific for the liver, with the HPA database, showed that some proteins were described in the HPA to be expressed selectively in the liver and some proteins were found to be expressed in a set of different tissues, including, or not including liver. But, many proteins of the liver-specific proteins found in this master’s thesis were also described to be expressed in the liver alone or a set of organs, including liver.

Table 9: The nine proteins of the overall 38 liver-specific proteins found in the HPA database showing a selective, distinct or high expression of the protein in the liver and tissue enrichment or enhancement of the RNA in the liver.

Protein name	Gene name	HPA: Tissue RNA expression	HPA: Protein expression and localisation
Aldo-keto reductase family 1 member D1	AKR1D1	Tissue enriched (liver)	Selective cytoplasmic expression in liver.
Asialoglycoprotein receptor 1	ASGR1	Tissue enriched (liver)	Distinct cytoplasmic expression in hepatocytes.
Asialoglycoprotein receptor 2	LOC101115381	Tissue enriched (liver)	Cytoplasmic expression in hepatocytes.
Bile salt export pump	ABCB11	Tissue enriched (liver)	Distinct expression in liver bile canaliculi.
Cytochrome P450 2E1 (EC 1.14.13.n7) (EC 1.14.14.1)	CYP2E1	Tissue enriched (liver)	Selective cytoplasmic expression in hepatocytes.

Cytochrome P450 4V2	LOC101116121	Tissue enhanced (liver)	Cytoplasmic expression in several different tissues, highest in the liver.
Formimidoyltransferase cyclodeaminase	FTCD	Tissue enriched (liver)	Selective cytoplasmic expression in hepatocytes and renal tubules.
Solute carrier family 27 member 5	SLC27A5	Tissue enriched (liver)	Selective cytoplasmic expression in hepatocytes.
Glycogen [starch] synthase (EC 2.4.1.11)	GYS2	Tissue enriched (liver)	Cytoplasmic expression in hepatocytes

5.2.3. GO-Term Enrichment Analysis

This section shows the plots of the GO-term enrichment analysis results of three selected tissue samples, brain, kidney and liver, with interpretations. The plots of the enrichment analysis of the other tissue samples can be seen in the supplementary section.

5.2.3.1. Brain

The results of the GO-term Enrichment Analysis of the significant proteins found in the brain tissue samples showed that the ten most significant (q-value 7.85 e^{-12} – 2.89 e^{-06}) enriched GO-terms were “neuron projection”, “presynaptic membrane”, “gamma-aminobutyric acid signaling pathway”, “synaptic vesicle”, “synapse”, “regulation of ARF protein signal transduction”, “positive regulation of excitatory postsynaptic potential”, “GABA-A receptor activity” and “synaptic vesicle membrane” (Figure 44 B). All listed terms are directly related to brain processes or brain-related biological functions. The proof of accordance of the GO-terms found to be enriched for the brain samples in the enrichment analysis with general functions and biological processes occurring in the brain on a day-to-day basis can be seen in the discussion below, which outlines the reliability of the results of this evaluation.

The hierarchical cluster analysis of the enriched GO-terms (Figure 44 A) visually presents the extent of the similarity between the 20 most significantly enriched GO-terms in the brain (q-value 6.28 e^{-12} – 2.51 e^{-3}) and classifies them into different groups. The results of the hierarchical clustering of the enriched terms in the brain were “dendrite GTPase

activator glutamatergic", "phospholipid ARF binding protein", "neuron positive vesicle excitatory", "presynaptic, postsynaptic membrane" and "extracellular GABA-A acid channel".

The C-net plot (Figure 44 C) puts together a network of the five most significantly enriched GO-terms. The protein symbols, showing more than one of the five most significantly enriched GO-terms annotated in the database used for the evaluation, represent the connecting points of the GO-term-network. All protein symbols having only one of these terms listed in the database are connected only to the corresponding GO-term. For example, the proteins with the protein symbols SNAP25 (Synaptosomal-associated protein) and LIMK1 (LIM domain kinase 1) are both annotated with the enriched GO-terms "synapse" and "neuron projection". LIM kinases can be classified into the group of serine-threonine-kinases [89]. SNAP25 is a member of the SNARE (Soluble N-ethylmaleimide-sensitive factor attachment protein receptor) complex having an essential role in the exocytotic neurotransmitter release in the process of synapse information flow [90]

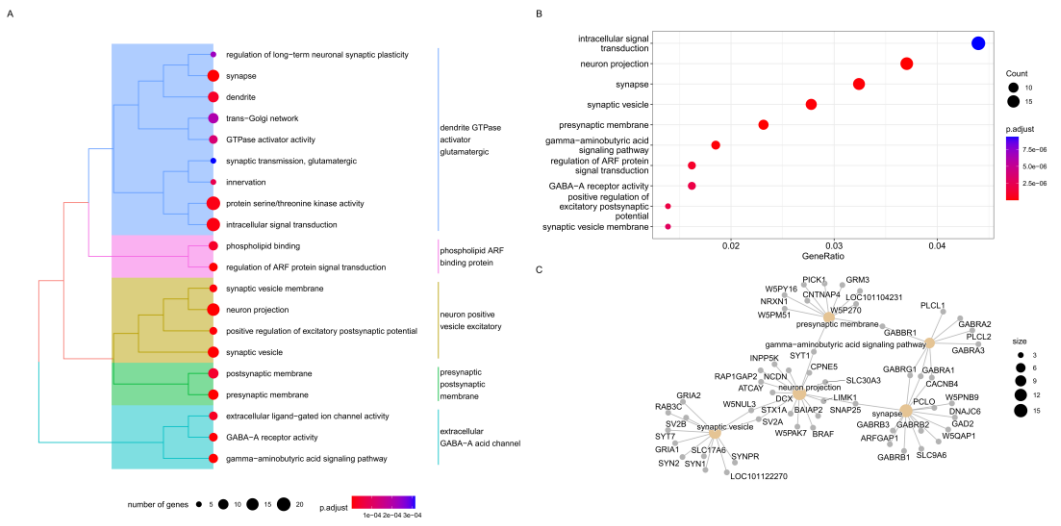

Figure 44: Results of the Term Enrichment Analysis of the Brain tissue samples presented as a A) tree plot B) dot plot and C) C-net plot.

When looking at the general process of signal transduction in the brain, four main signalling pathways can be distinguished, with one of them being the pathway of the activation of G-protein-coupled receptors (GPCR) *via* neurotransmitter. The activated GPCR can influence ion channels or trigger other neuronal processes (Figure 45 A). One G-protein, known to have a role in the complex process of neurotransmitter release at synapses, is the ADP-ribosylation factor (ARF). The general process of signal transduction

in neurons is undertaken *via* a cascade of second messenger processes, induced *via* first messengers. Neuronal biological information flow and subsequent biological processes can also be induced through the activation of protein tyrosine kinases *via* first messengers (Figure 45 B). This further triggers diverse biological processes, where, for example, protein serine-threonine kinases are involved [91].

The Gamma-Aminobutyric acid type A receptors (GABA-A-Rs) represents the most prominent inhibitory receptor class in the central nervous system, activated by neurotransmitters as first messengers. 20-50% of all synapses in the human brain use Gamma-Aminobutyric acid (GABA) as a ligand [92].

Therefore, the receptors and messengers involved in the processes in the day-to-day information flow and transduction of the brain are in good accordance with the GO-terms found to be enriched in the brain samples.

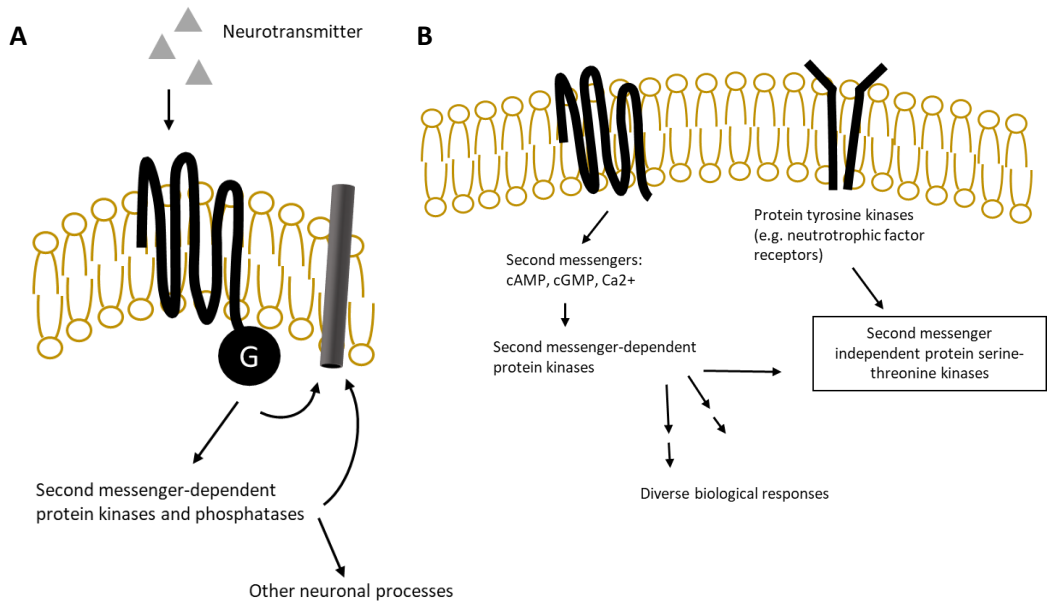

Figure 45: A) One of the four main signal transduction processes in the brain. Neurotransmitter trigger the activation of the GPCR. The activated proteins can have an influence on ion channels or trigger further neuronal processes. B) Two selected signal transduction pathways in neurons. Figures reproduced from ref. [91].

5.2.3.2. Kidney

The results of the GO-term Enrichment Analysis of the significant proteins found in the kidney tissue samples showed that the 10 most significant (q-value 9.01 e^{-06} – 7.97 e^{-02}) enriched GO-terms were “brush border membrane”, “apical plasma membrane”, “excretion”, “transmembrane transport”, “metallopeptidase activity”, “transporter activity”, “ruffle membrane”, “dendritic shaft”, “positive regulation of transforming growth

factor beta receptor signalling pathway" and "endoplasmic reticulum membrane" (Figure 46).

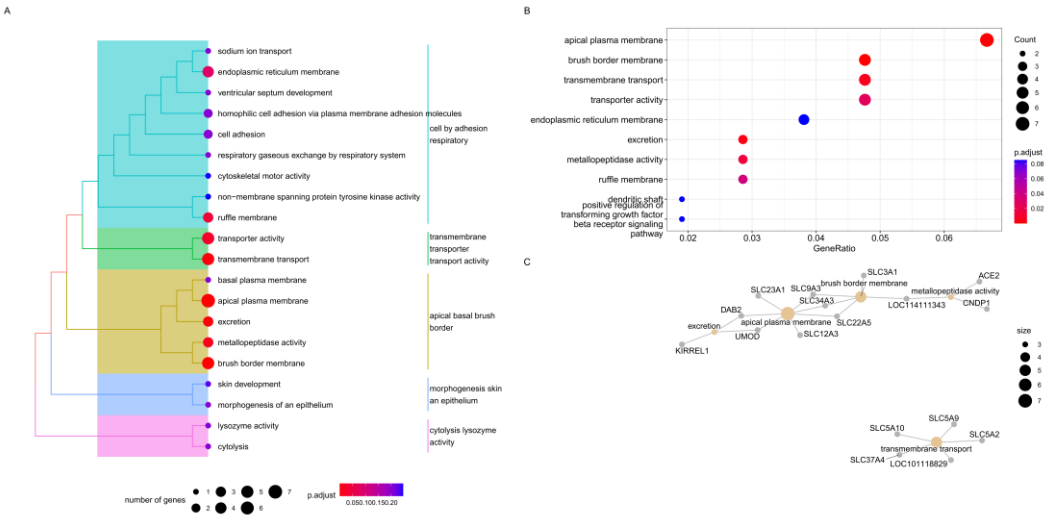

Figure 46: Results of the Term Enrichment Analysis of the kidney tissue samples presented as a A) tree plot B) dot plot and C) C-net plot.

When looking at the GO-term enrichment results for the kidney, all terms can be classified into 5 groups *via* a hierarchical cluster analysis of the 20 most significantly enriched terms (q-value 4.08 e-^{08} – 3.27 e^{-2}) (Figure 46 A). The kidney is known for its unique role in the body to eliminate toxins from the environment and for drug and xenobiotic metabolism. When looking at the renal clearance mechanism in more detail, three main sub-mechanisms cooperate in order to achieve the segregation of drugs and other substances: glomerular filtration, renal tubular secretion and reabsorption. To do so, the kidneys use carriers and transporters, which can be classified into two prominent transporter families, being ATP-binding cassette transporters (ABCs) and solute carriers (SLCs). The SLC group consists of more than 400 membrane proteins which can be further classified into over 60 different families [93].

18 of the overall 68 membrane proteins of different SLC families found in the proteomics data set were found to be specific for the kidney (Table 10). Further evaluation of the different solute carrier proteins according to their function in more detail can be seen in section 4.3.1.

The active renal secretion of drugs and xenobiotics is undertaken *via* membrane transport mechanisms. Carriers and transporters located at the brush border and basolateral membranes of epithelial cells play crucial roles during the secretion step, especially when looking at cationic drugs. For

example, in the human body, the secretion of cationic drugs into the urine is undertaken by well-studied renal organic cation transporters (OCTs) and multidrug and toxin extrusion proteins (MATEs). One renal protein transporter family is the SLC 22 family of the OCTs, located at the basolateral membrane [94].

5 of the 18 solute carrier proteins found to be specific for the kidney were members of the SLC 22 family.

The need for transporters and carriers of various different families, located at different regions of the membrane in the kidney, in order to maintain the essential process of renal secretion and clearance, is in good accordance with the enrichment of the GO terms “brush border membrane”, “apical plasma membrane”, “transmembrane transporter” and “transporter activity” in the kidney samples. Nevertheless, it has to be mentioned that not only the kidney requires many cooperating transmembrane processes, mediated by carriers and transporters, but also other organs, which will be discussed below.

Table 10: All transporter proteins classified as members of the solute carrier family found specific for the kidney.

Protein name	Gene name
Solute carrier family 12 member 3	SLC12A3
Solute carrier family 13 member 3	SLC13A3
Solute carrier family 22 member 10-like	LOC101118829
Solute carrier family 22 member 2	LOC101111810
Solute carrier family 22 member 5	SLC22A5
Solute carrier family 22 member 6	-
Solute carrier family 22 member 8	SLC22A8
Solute carrier family 23 member 1	SLC23A1
Solute carrier family 25 member 21	SLC25A21
Solute carrier family 27 member 6	SLC27A6
Solute carrier family 3 member 1	SLC3A1
Solute carrier family 37 member 4	SLC37A4
Solute carrier family 5 member 10	SLC5A10
Solute carrier family 5 member 2	SLC5A2
Solute carrier family 5 member 9	SLC5A9
Solute carrier family 6 member 20	SLC6A20
Sulfate transporter (Solute carrier family 26 member 2)	SLC26A2
Multidrug and toxin extrusion protein	SLC47A2
Solute carrier family 34 member 3	SLC34A3

5.2.3.3. Liver

The results of the GO-term Enrichment Analysis of the significant proteins found in the liver tissue samples showed that the 10 most significant (q-value 4.46 e^{-14} – 1.88 e^{-02}) enriched GO-terms are “hexosyltransferase activity”, “iron ion binding”, “heme binding”, “monooxygenase activity”, “oxidoreductase activity, acting on paired donors, with incorporation or reduction of molecular oxygen”, “oxidoreductase activity, acting on paired donors, with incorporation or reduction of molecular oxygen, reduced flavin or flavoprotein as one donor, and incorporation of one atom of oxygen”, “oxidoreductase activity”, “flavin adenine dinucleotide binding”, “endoplasmic reticulum membrane” and “transporter activity” (Figure 47).

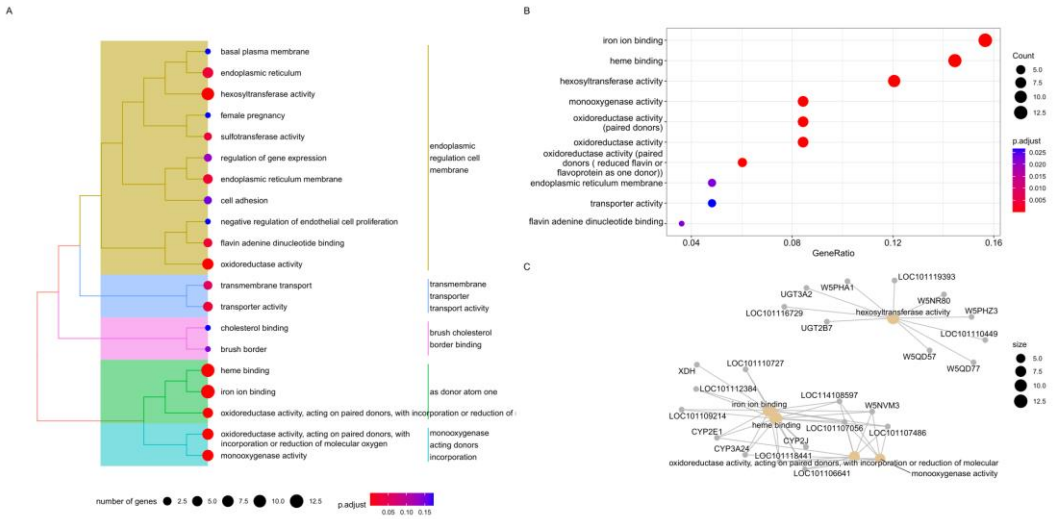

Figure 47: Results of the Term Enrichment Analysis of the Liver tissue samples presented as a A) tree plot B) dot plot and C) C-net plot.

One property worth mentioning is the extent of blood flowing through the individual organs. This property differs profoundly throughout the samples analysed. For example, the kidneys, heart and liver are one of the organs with the highest throughput of blood. The tissue samples were not perfused with water to remove the blood prior to the sample preparation processes. Therefore, the GO-terms “heme binding” and “iron ion binding” could be ascribed to the high blood content in the liver.

CYP, as one of the main enzymes in drug and xenobiotic metabolism in the liver, is located in the endoplasmic reticula of hepatocytes and other liver cells. Besides the well-known enzyme CYP, co-working proteins, like electron donor enzymes, play important roles in both, the biotransformation

of drugs and xenobiotics and the production of biochemically relevant endogenous substances, like bile acids. This cooperating enzymatic complex of hepatic microsomal CYP, needed for the electron transfer to the enzyme, is known as the flavoprotein NADPH-cytochrome P450 oxidoreductase (POR). [95] Therefore, the enrichment of many GO-terms listed above could be explained by the fact of cooperation taking place between the flavoprotein POR with the enzyme CYP for the day-to-day hepatic function of biotransformation of xenobiotics and drugs and the biosynthesis of important substances like bile acids.

Like described for the kidney, the liver is also in use of many different transporter molecules. Many transporters are described to be expressed in both, the kidney and liver, but some transporters are also known to have strong concentration differences between the two organs. Hepatic OCTs, organic anion-transporting peptides (OATPs), and organic anion transporters (OATs) are primarily needed for the uptake of xenobiotics and drugs into hepatocytes. For example, human OCT1, represented by the gene name SLC22A1, is described to be expressed primarily in the liver and only in small concentrations in the kidney [94],[96]. After the processing of the drugs and xenobiotics in the liver cells, the transfer to the bloodstream is mediated by multidrug resistance-associated proteins 3 (MRP3) and 4 (MRP4). For example, bile acids, being toxic for hepatocytes, have to be removed effectively from the liver cells. This process is undertaken by one major transporter called the bile salt export pump (BSEP) [96].

All solute carrier proteins explicitly found in the liver or kidney and liver and the BSEP, found expressed specifically in the liver, can be seen in Table 11.

Table 11: Selected transporter-proteins found specific for liver or for kidney and liver.

Protein name	Gene name	Organ
Solute carrier family 2, facilitated glucose transporter member 2 (Glucose transporter type 2, liver)	SLC2A2	Liver, kidney
Solute carrier family 22 member 1	SLC22A1	Liver, kidney
Solute carrier family 22 member 18	SLC22A18	Liver, kidney
Solute carrier family 25 member 15	SLC25A15	Liver, kidney
Bile salt export pump	ABCB11	Liver
Solute carrier family 22 member 9	LOC101119087	Liver
Solute carrier family 22 member 9-like	LOC101119346	Liver
Solute carrier family 27 member 5	SLC27A5	Liver
Solute carrier family 39 member 14	SLC39A14	Liver
Solute carrier organic anion transporter family member	LOC101120653	Liver

5.2.4. Z-transformation of LFQ values

Figure 48 shows the heatmap of the z-transformed LFQ values of all proteins found per organ. When looking at the hierarchical clustering of the data set, it can be seen that the protein patterns of the organs can be classified into six groups. Group 1 is formed by muscle and heart with an overall very low abundance pattern with one higher abundant region showing overlapping proteins for the two candidates in this group. Group 2 is represented by liver and kidney, Group 3 is composed of spleen and lung and Group 4 of kidney mark, skin and nerve. Group 5 is composed of bone, cartilage and tendon, showing a nearly identical protein expression pattern in the heatmap. The brain, as the only representative of Group 6, shows no significant similarity in the expression pattern compared to all other organ samples.

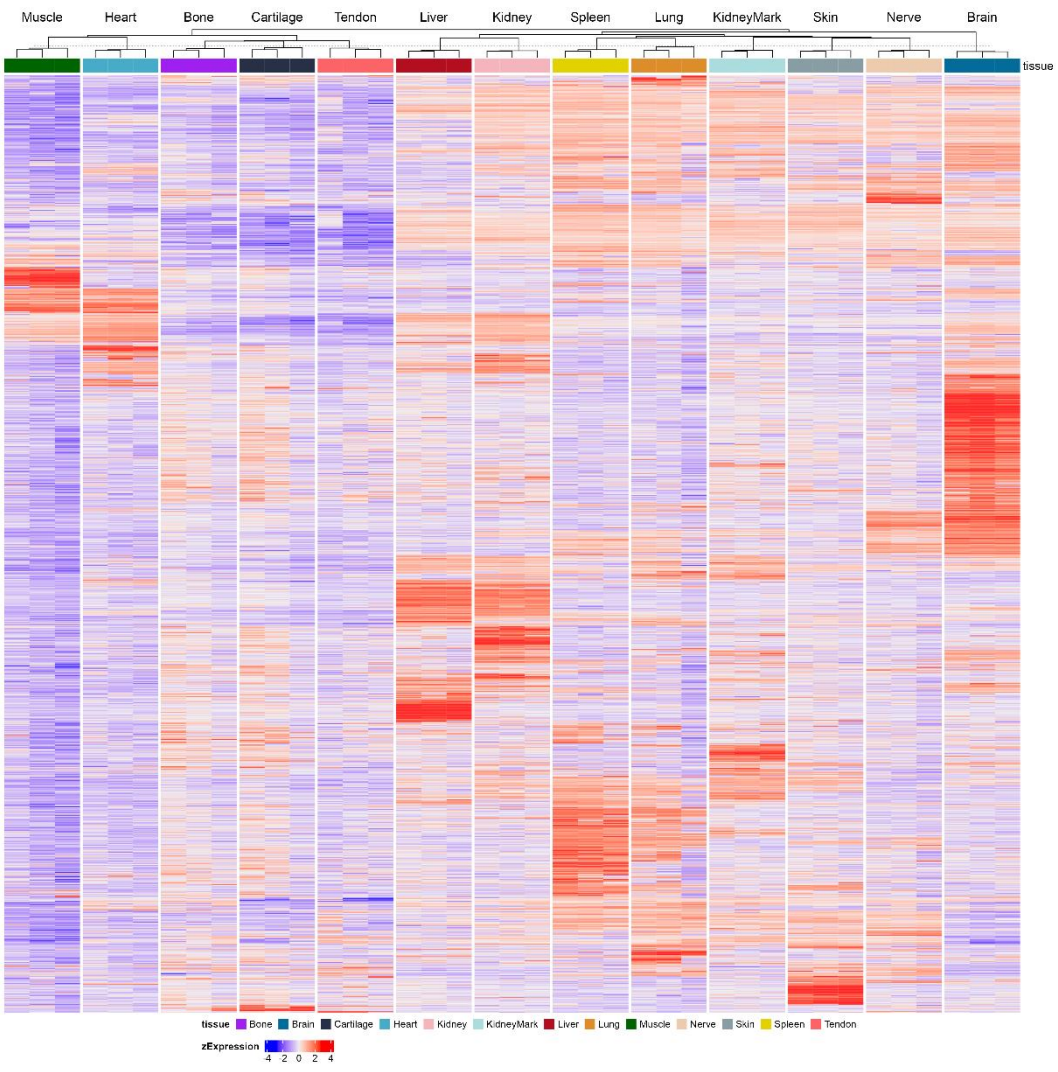

Figure 48: Heatmap of the z-transformed LFQ values of all proteins found per organ.

5.2.4.1. Group 1: Muscle and heart

The first group, represented by heart and muscle, is defined by tissue mainly composed of myocytes. There are several similarities between cardiomyocytes (cardiac muscle cells) and skeletal muscle cells. One main similarity between those muscle cell types is their high number of mitochondria. [97] It is generally known that skeletal muscle has high energy requirements. A previous study showed that under resting conditions, the heart and kidney are reported to have the highest metabolic rate, followed by the brain and liver. [97],[98] Another similarity, cardiac and skeletal muscle, both classified as striated muscles, are composed of subunits called sarcomeres [97].

A previous study showed similarities between cardiomyocytes and skeletal muscle cells in their expression of proteins related to contraction movements, like members of the myosin (e.g. MYL3) and troponin (e.g. TNNC1) family. Further, proteins like LIM-domain binding 3 (LDB3), Hedgehog Acyltransferase Like (HHATL) and Calsequestrin (CASQ) were also found to be expressed with elevated levels in both, cardiac and skeletal muscle cells. LDB3 plays a special role in the organization of sarcomeres and CASQ was found to be functionally involved in calcium ion transport [97].

All these mentioned proteins were also found here to be expressed specifically in both, heart and muscle. On top, three more proteins from the myosin family (MYL1, Myosin VC and Myosin-3) were found in both organs (Table 12).

Table 12: Seven of the 40 specific proteins found in heart and muscle.

Protein name	Abbreviation
Myosin light chain 3	MYL3
Myosin light chain 1	MYL1
Myosin VC	-
Myosin-3	-
Hedgehog acyltransferase like	HHATL
LIM domain binding 3	LDB3
Calsequestrin	CASQ

The energy requirements are high for both representatives in Group 1. This characteristic can be seen when looking at the mitochondrial proteins and key enzymes in energy production pathways. For example, known enzymes in energy production are NADH-ubiquinone oxidoreductase, ATP synthase, Cytochrome C and corresponding coenzymes. These enzymes were

previously found to be highly elevated in the heart, muscle, brain and stomach [99].

27 subunits of the three mentioned enzymes were found in the entire proteomics data set. 23 of the 27 subunits were found in the heart and 22 in the muscle samples. 20 of those subunits were found in heart and muscle, but also in other tissues like, for example, the brain, liver, lung, kidney, nerve, skin and spleen. Two of the overall 12 subunits found of the enzyme NADH-ubiquinone oxidoreductases (Table 13) were only found in muscle (NADH-ubiquinone oxidoreductase B17 subunit) or heart (NADH-ubiquinone oxidoreductase ESSS subunit). All other subunits were expressed in more than one tissue sample analysed.

Table 13: The 12 NAHDH-ubiquinone oxidoreductase subunits found in the proteomics data set. Grey: Subunits found only in muscle (NADH-ubiquinone oxidoreductase B17 subunit) or heart (NADH-ubiquinone oxidoreductase ESSS subunit).

Protein name	Gene name
NADH:ubiquinone oxidoreductase subunit A9	NDUFA9
NADH-ubiquinone oxidoreductase 75 kDa subunit, mitochondrial	NDUFS1
NADH-ubiquinone oxidoreductase subunit B14.5a	NDUFA7
NADH-ubiquinone oxidoreductase 23 kDa subunit	NDUFS8
NADH-ubiquinone oxidoreductase B22 subunit)	NDUFB9
NADH-ubiquinone oxidoreductase B17 subunit	NDUFB6
NADH-ubiquinone oxidoreductase 24 kDa subunit	NDUFV2
NADH-ubiquinone oxidoreductase ESSS subunit	NDUFB11
NADH-ubiquinone oxidoreductase PDSW subunit	NDUFB10
NADH-ubiquinone oxidoreductase B15 subunit	NDUFB4
NADH-ubiquinone oxidoreductase 9 kDa subunit	NDUFV3
NADH-ubiquinone oxidoreductase B14 subunit	NDUFA6

5.2.4.2. Group 2: Kidney and liver

Generally, when glucose levels are low, fatty acids are metabolized to provide the energy needed to maintain the biochemical pathways essential for life. This process is called mitochondrial fatty acid beta-oxidation (FAO). In the heart, skeletal muscle and kidney, FAO is a crucial energy-supplying mechanism even with sufficient amounts of available glucose. The energy-providing step occurs in mitochondria, when fatty acids are transferred over the cell membranes *via* specific proteins like CD36, facilitating the process of the uptake into the cytosol. Acyl-CoA synthetase is further needed to form activated acyl-CoA esters. The carnitine cycle with L-carnitine and different enzymes plays a crucial role for the importing process into the mitochondria due to the impermeability of the mitochondrial cell membrane to the

activated esters. Inside the mitochondria, the activated acyl CoA esters are metabolized *via* four main enzymatic steps to provide energy. Around 20 different proteins are known to have a specific role in the FAO in mitochondria [100]. In eukaryotic cells, peroxisomes cooperate with mitochondria in a close manner to provide a refined association for optimizing energy metabolism. The kidney and liver are described to have the highest amount of peroxisomes. Very long-chain fatty acids (over 22 carbon atoms) are shortened in peroxisomes. These fatty acids are further metabolized in the mitochondria, preferentially using medium- or short-chained fatty acids for the FAO. Besides cardiac muscle, skeletal muscle and kidney, the renal cortex also strongly depends on the energy provided *via* FAO. The first step in the peroxisomal FAO of very-long-chain fatty acids is undertaken by the enzyme Acyl-CoA oxidase (ACOX). After the initial step, a cascade of different enzymes is needed for the overall reaction [101].

Nine selected proteins from the proteomics data set, described to be involved in the peroxisomal FAO and mitochondrial FAO, can be seen in Table 14. Five of the nine described proteins were only found in kidney and liver. One protein (Solute carrier family 22 member 5) was found to be specific for the kidney. All other proteins listed in Table 11 were found to be expressed in more than two organ samples analysed.

Table 14: 9 selected proteins with their gene names, known for having different roles in mitochondrial and peroxisomal FAO, found in different organ samples in the proteomics data set.

Protein name	Gene name	Biochemical function	Organs
Acyl-coenzyme A oxidase	ACOX1, ACOX2	Peroxisomal FAO [102]	kidney, liver
Acyl-coenzyme A thioesterase 4	LOC101103726	Peroxisomal FAO [102]	kidney, liver
Carnitine O-acetyltransferase	CRAT	Peroxisomal FAO [102]	brain, heart, kidney mark, kidney, liver, lung, muscle, nerve, skin, spleen
Carnitine O-octanoyltransferase	CROT	Peroxisomal FAO [102]	kidney, liver
Acyl-CoA-binding domain-containing protein 5	ACBD5	Peroxisomal FAO [103]	liver, kidney
Solute carrier family 22 member 5	SLC22A5	Mitochondrial FAO [104]	kidney
Carnitine O-palmitoyltransferase (EC 2.3.1.21)	CPT1A	Mitochondrial FAO [100]	brain, kidney, kidney mark, Liver., Lung
Carnitine O-palmitoyltransferase (EC 2.3.1.21)	CPT1B	Mitochondrial FAO [100]	heart, kidney, liver, muscle

Acyl-CoA dehydrogenase family member 11	ACAD11	Mitochondrial FAO [103]	liver, kidney

5.2.4.3. Group 6: Brain

In the brain, neurons are embedded between Ependymal cells, microglial cells and macroglial cells (astrocytes and oligodendrocytes). There are several neuroglial proteins described. For example, well-known neuroglial proteins are the glial fibrillary acidic protein (GFAP), myelin basic protein (MBP), neurofilament light chain (NFL) and tau and ubiquitin carboxy-terminal hydrolase L1 (UCHL1) with all of them previously shown to be selectively expressed in various cell types throughout the central nervous system [105]. GFAP represents a well-known astrocyte marker and MBP and proteolipid protein 1 (PLP1) was found to be expressed highly enriched in the brain and have an influence on the process of myelination [106],[107]. Further, some microglial signature genes are described to be highly expressed in different distinct regions throughout the body, like for example arachidonate 5-lipoxygenase (ALOX5) in the spleen. Further, neuronal protein examples, like phosphodiesterase 1B (PDE1B) and many more are also described to be found in neuronal cell bodies in the brain [107].

All these mentioned proteins were found in the brain samples. One example (ALOX5) was found to be expressed specifically in the spleen. MBP was only expressed in the brain and nerve and UCHL1 in the brain, nerve and spleen samples. All other examples and their expressions can be seen in Table 15.

Table 15: The neuroglial proteins GFAP, MBP and NEFL and UCHL1 and microglial signature gene ALOX5 and the neuronal protein PDE1B found in different organ samples analysed.

Protein name	Gene name	Expression
Glial fibrillary acidic protein	GFAP	brain, nerve, heart
Myelin basic protein	MBP	brain, nerve
Ubiquitin carboxyl-terminal hydrolase (EC 3.4.19.12)	UCHL1	brain, nerve, spleen
Neurofilament light	NEFL	brain, nerve, lung, spleen
Proteolipid protein 1	PLP1	brain, nerve, cartilage
Arachidonate 5-lipoxygenase	ALOX5	spleen
Phosphodiesterase (EC 3.1.4.-)	PDE1B	brain, kidney mark

5.2.4.4. Group 5: Bone, cartilage, tendon

The group composed of bone, cartilage and tendon can be summarised as connective tissues. There are several types of connective tissues, characterized by their composition. For example, tendon can be classified into the group of dense/fibrous connective tissue, whose extracellular matrix is composed of collagen fibrils aligned along tensile stress. [108] Overall, 28 different collagen types were found in the proteomics data set, with eight of them showing specificity for only one organ and one found in two organs in the connective tissue family (Table 16). All other collagen types were found in at least more than three organs.

Table 16: Tissue-specific collagen types found in the proteomics data set and one collagen type specific for two organs in the connective tissue family.

Protein name	Gene name	Organs
Collagen type IX alpha 2 chain	COL9A2	Cartilage
Collagen type II alpha 1 chain	COL2A1	Cartilage
Collagen type IX alpha 1 chain	COL9A1	Cartilage
Collagen type XXII alpha 1 chain	COL22A1	Bone
Collagen type XI alpha 2 chain	COL11A2	Bone, Cartilage
Collagen type IV alpha 6 chain	COL4A6	Lung
Collagen type XXVIII alpha 1 chain	COL28A1	Nerve
Collagen type III alpha 1 chain	COL3A1	Skin
Collagen type XVII alpha 1 chain	COL17A1	Skin

5.3. Eicosadomics with Proteomics

This section combines the findings of the proteomics- and eicosadomics part. The combination of the findings in this thesis with known eicosanoid pathways with distinct receptors and transporters, could maybe lead to connections between tissue-specific proteins and enhanced eicosanoids in the individual tissue samples.

5.3.1. Described eicosanoid transporters

Eight ABC/MRP types are known for the efflux of eicosanoids through the cell membrane. These transporters are annotated with the abbreviations MRP/ABCC1-6, MRP7 and MRP8. MRP1/ABCC1 is the natural receptor of the endogenous oxylipins LTC4, LTD4 and LTE4 (reduced glutathione-conjugated forms), MRP2/ABCC2 of LTC4, PGA2, MRP3/ABCC3 of LTC4,

MRP4/ABCC4 targets the endogenous ligands PGE2, PGF2α, PGD2, TXB2, LTB4 and LTC4, MRP5/ABCC5 targets cyclic nucleotides, MRP6/ABCC6 is the receptor of LTC4, MRP7 of LTC4 and MRP8 of LTC4. Besides the listed eicosanoids, these transporters also target drugs, different metabolites and other endogenous bioactive substances [109]. MRP2 is known to be expressed in renal proximal tubule brush borders and is believed to play a role in the urinary excretion process and general transport of prostaglandins conjugated with glutathione. The expression of this transporter is known to be limited to kidney, liver and small intestine. When looking at the second major renal transporter class, being the SLC family, SLC22 is also known to transport prostaglandins and it is believed that SLC22 mediates the renal secretion of prostaglandins into the urine. Further, two members of the OAT family, OAT1 and OAT3, are described to be expressed in the basolateral proximal tubule membrane. It is believed that these two transporters play a role in the secretion of the prostaglandin PGE2 into the urine [110]. The spatial distribution of members of the OAT, ABC/MRP and MATE transporter classes in the kidney proximal-, distal-tubules and tubular cells and in liver hepatocytes can be seen in Figure 49. As shown in Table 17, OAT1, OAT3 and MRP1 were found in the proteomics data set to be specifically expressed in the kidney and MRP4 in the kidney mark. As stated above, these findings are in accordance with the expression of the members of these transporter families described in previous studies.

When looking at the MRP4 transporter, found expressed specifically in the kidney mark, connections between the organ-specificity of the transporter and the content of individual eicosanoids, described to act as endogenous natural ligands of the transporter can be seen. The MRP4 transporter is described to bind to the eicosanoid ligands PGE2, PGF2α, PGD2, TXB2, LTB4 and LTC4 [109]. In the heat map of the eicosadomics evaluation in this study (Figure 34), when comparing the kidney mark samples with the other tissues analysed in this study, the two prostaglandins, PGE2 and PGF2α, show the highest abundance in kidney mark over the entire set of organs analysed. As stated above, PGE2 and PGF2a represent endogenous ligands for many transporters of different transporter families over the entire organ samples analysed. Therefore, the specificity of the MRP4 transporter for the kidney mark found in this study and PGE2 and PGF2a, showing the highest abundances in the kidney mark compared to all other tissue samples, establishes no basis for a direct relation between the findings in the eicosanoid and proteomics data set.

In the kidney, cationic drug compounds are excreted into the urine *via* two main mechanisms, with MATE (SLC47) and SLC22 as major transporters of the SLC family. For example, MATE2-K (gene name: SLC47A2) is described to be expressed predominantly in the kidney. The transporter is

mainly located at the renal Brush-border membrane. In the human kidney, the interplay of MATE2-K and MATE-1 with OCT2, located at the basolateral membrane, is of paramount importance for the general renal secretion process of cationic compounds. However, there are differences between the expression and local distribution of these transporters, important in the secretion process, when comparing rodent animals and humans (Figure 49 A) [94]. These two transporters were found to be expressed specifically in the kidney samples analysed in this study.

Table 17: Selected transporters from the OAT, ABC/MRP and MATE family found in different organs of the proteomics data set with their eicosanoid ligands described in literature.

Protein name	Alternative name	Gene name	Organs	Eicosanoid ligands
ABC-type glutathione-S-conjugate transporter	-	ABCC2	kidney, liver, lung, muscle, nerve	LTC4, PGA2 [109]
ABC-type glutathione-S-conjugate transporter	-	ABCC6	brain, kidney, liver	LTC4 [109]
Solute carrier family 22 member 6	Human: OAT1 [103]	-	kidney	Assumed: PGE2 secretion [110]
Solute carrier family 22 member 8	Human: OAT3 [103]	SLC22A8	kidney	Assumed: PGE2 secretion [110]
Multidrug resistance-associated protein 4	MRP4	LOC101106534	kidney mark	PGE2, PGF2α, PGD2, TXB2, LTB4 and LTC4 [109]
Multidrug and toxin extrusion protein	Human: MATE-2 [103]	SLC47A2	kidney	-
Multidrug resistance protein 1-like	MRP1	LOC101112460	kidney	LTC4, LTD4, LTE4 [109]
Solute carrier family 22 member 2	Human: OCT2 [103]			

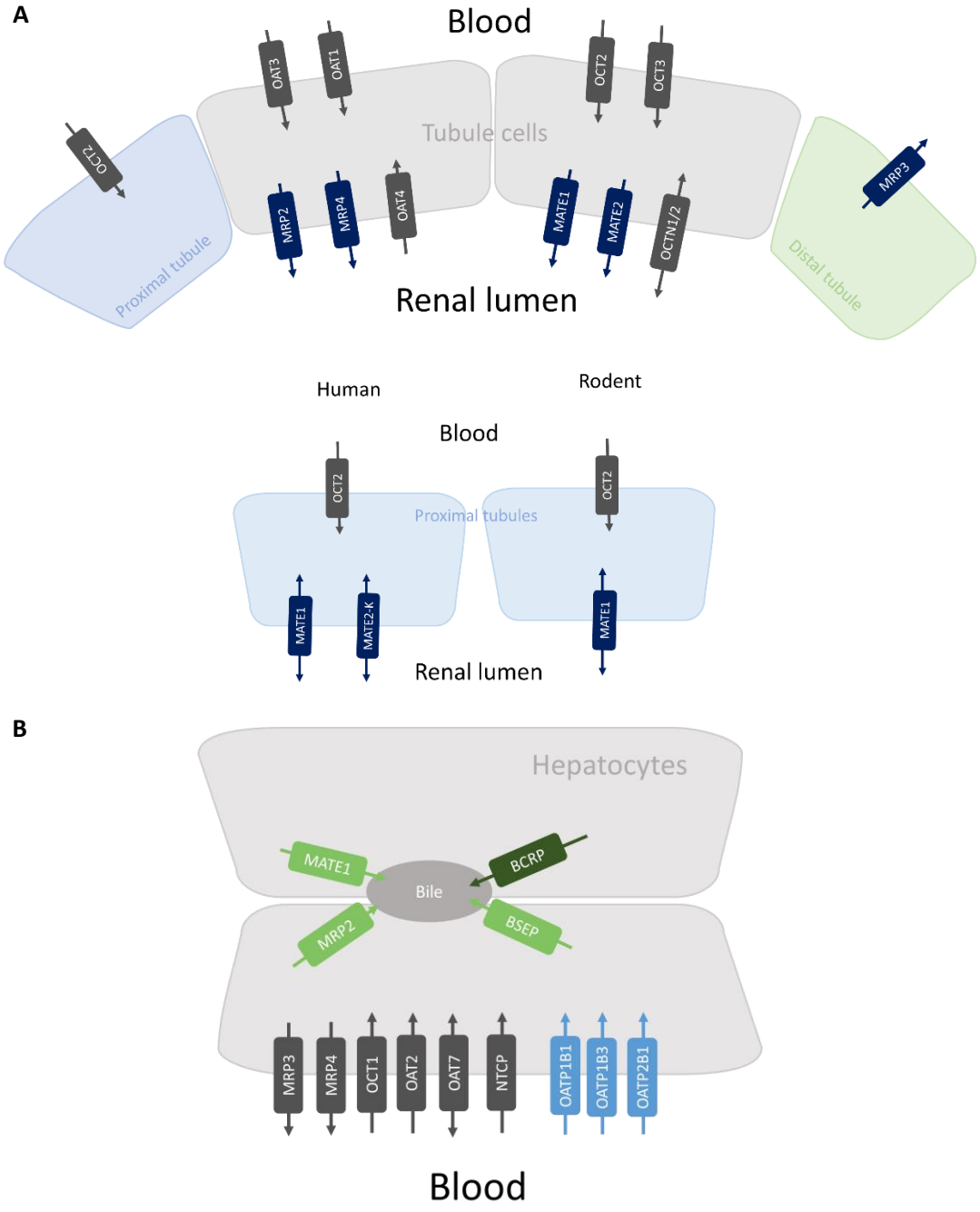

Figure 49: The major drug transporters for A) kidney, with the local distribution of the transporters between proximal tubules, distal tubules and tubular cells and the differentiation of the transports to transfer drugs into or out of the distinct cell types and the difference between the transporters essential for the renal secretion of cationic compounds in human and rodent (OCT-1 and 2 and MATE-1 and 2). Figures reproduced/modified from ref. [111] *and* [94]. *B) liver with the transporters located at the hepatocyte membranes and transporters for bile acids. Figure reproduced/modified from ref.* [112].

20-HETE represents one of the major oxylipins of the CYP (4A CYP450 family of hydroxylases) enzymatic pathway with AA as precursor molecule in mammalian proximal tubules in the kidney. 20-HETE is known to

influence renal tubular sodium uptake. It is assumed that 19-HETE and 20-HETE have a counterplaying role in regulating the sodium transport, with 19-HETE showing stimulating characteristics and 20-HETE inhibiting the uptake. As another essential AA-derived oxylipin class arising from the CYP enzymatic pathway, EETs mediate many important mechanisms in the kidney. EETs are known to be produced in the renal proximal tubules, influencing the tubule sodium uptake process. EETs are also described to play a crucial role as second messengers in the renal proximal tubules for angiotensin II [110].

In general, several eicosanoid receptor types are characterised until now. The main receptors are rhodopsin-like, transmembrane domain-containing G-protein coupled receptors (7 different types) and G-protein-coupled prostanoid-receptors (9 different types: TX-receptor TP, prostacyclin-receptor IP, PGF2a-receptor FP, PGD-receptors DP1 and DP2 and PGE2 receptors: EP 1-4). The receptors can be further classified into three groups, according to their functions and the second messenger pathways they mediate. IP, DP1, EP2 and EP4 can be summarized as smooth-muscle-relaxing receptors. These receptors undertake the signalling cascade *via* an increase in cyclic AMP (cAMP) in the cell, mediated by the G-protein-subfamily G_s. The other group, consisting of FP, TP and Ep1, summarized as “contractile” prostanoid-receptor subgroup, undertakes the signalling transduction *via* the increase of calcium in the cell with the help of the G-protein-subfamily G_q as a mediator. Further, eicosanoids can also interact with peroxisomal proliferator-activated receptors (PPAR) [113]. One of the best-described eicosanoids as natural ligands of one of the three members of the PPAR-family are 8-HETE and LTB4 activating PPARα, 15-HETE activating PPARβ/δ and 15d-PGJ2, 15-HETE, 9-HODE and 13-HODE activating PPARγ [114]. No subunit of the receptors mentioned in this section was found in the proteomics data set.

5.3.2. Similarity in group-formation

When comparing the similarity in the group formation of the heatmap patterns in the proteomics data set (Figure 48) and the eicosadomics data set (Figure 34), some similarities can be seen. The proteomics data set revealed the formation of six groups with similarities in the abundance patterns of the z-transformed LFQ-values: Muscle and heart (Group 1), liver and kidney (Group 2) spleen and lung (Group 3) kidney mark, skin and nerve (Group 4), bone, cartilage and tendon (Group 5) and brain (Group 6). The eicosadomics data set showed the formation of three groups with similarities in the eicosanoid expression pattern: nerve, brain, kidney mark,

skin, tendon, cartilage and muscle (Group 1), lung, spleen and heart (Group 2) and kidney and liver (Group 3). It is clear to see that in both data sets, kidney and liver form a group, owed by the similarities in the patterns in the heatmaps. As described in section 18.1.1., this similarity could be owed to the fact of the high content of CYP and CYP-derived oxylipins in both representatives in this group. Both organs have a high metabolic turnover of CYP due to their day-to-day clearance and segregation mechanisms. Therefore, the several CYP subunits and CYP-derived oxylipins could be the reason for the formation of a group composed of kidney and liver in both omics fields in this thesis. Lung and spleen are the representatives of one group in both data sets, where the group in the eicosadomics data set also shows heart in the same group.

6.0. Summary

The results of the MS-based proteome-analysis in this work provide information about the tissue-specificity of the proteins found in the 13 sheep organ samples analysed: bone, brain, cartilage, heart, kidney, kidney mark, liver, lung, muscle, nerve, skin, spleen and tendon. A total number of 4 702 proteins were found in all tissue samples analysed. The brain showed the highest percentage of specific proteins, being 16.1 % (445 specific proteins) and bone the lowest, being 0.2% (1 specific protein). A GO-term enrichment analysis provided further insight into the specific proteins found per organ. The results of the terms, found to be enriched in only one organ sample, were evaluated according their plausibility by looking at the biological processes in the organs and the mediators, receptors and transporters needed. The enriched GO-terms of the term enrichment analysis for brain, kidney and liver, chosen to be evaluated in detail in this work, showed good accordance with biochemical pathways and their mediators, described in literature. The protein patterns of the z-transformed LFQ-value distribution of the individual tissue samples showed the formation of six groups with similarities in their expression patterns: Muscle and heart (Group 1), liver and kidney (Group 2) spleen and lung (Group 3) kidney mark, skin and nerve (Group 4), bone, cartilage and tendon (Group 5) and brain (Group 6). The confirmability of the formation of these groups was evaluated and interpreted *via* different approaches, like the similarities in day-to-day biological processes described for candidates in the same groups, the tissue texture and further characteristics. Further, 12 organ samples (brain, cartilage, heart, kidney, kidney mark, liver, lung, muscle, nerve, skin, spleen and tendon) were analysed for their eicosanoid content. A total number of 176 eicosanoids (129 explicitly annotated eicosanoids and 47 no-name features) were found in the tissue samples analysed. The eicosadomics data set, visualized *via* expression patterns in a heatmap, showed the

formation of three groups with high similarity in the patterns: nerve, brain, kidney mark, skin, tendon, cartilage and muscle (Group 1), lung, spleen and heart (Group 2) and kidney and liver (Group 3). The data was interpreted *via* different approaches, like the confirmability of similarity of the expression pattern in the heat map between organs with similar cell-type composition, tissue texture, biological function or in literature described eicosanoid pathways. The combination of the eicosanoid and protein data set revealed some apparent correlations between the organ-specificity of proteins and the concentration of eicosanoids in this organ. The approach of the data set and the evaluation steps undertaken in this thesis do not form a sufficient basis for the establishment of a direct relation or the formation of a linkage between the findings of the eicosadomics- and proteomics-data set.

Abstract

Proteome, oxylipin and fatty acid analysis of 13 ovine tissues (bone, brain, cartilage, heart, kidney, kidney mark, liver, lung, muscle, nerve, skin, spleen and tendon) provided information about the tissue-specificity of proteins and differences in expression patterns of eicosanoids over the set of tissue samples analysed. The presentation of the proteomics- and eicosadomics-data sets as heatmaps of the z-transformed abundance values revealed the formation of different groups with similarities in their expression patterns. These formations of the groups were evaluated for both, proteomics and eicosadomics, *via* different approaches: the extent of similarity of the expression pattern between organs with similar cell type composition, tissue texture, biological function or in literature described day-to-day biological processes. Further, the evaluation of the proteomics data set *via* a GO-term enrichment analysis showed good accordance between the enriched GO-terms found per organ and day-to-day biochemical processes described for the individual organs. The identified molecules bear a distinct relation to the functionality of the individual organs and their enzyme-compositions. However, the data comprehensiveness was not yet sufficient for the calculation of significant correlations between the proteomics- and eicosadomics-data sets.

Zusammenfassung

Die Resultate der Massenspektrometrie-basierten Proteom-, Oxylipin und Fettsäuren-Analyse von 13 Gewebeproben vom Schaf (Knochen, Gehirn, Knorpel, Herz, Niere, Nierenmark, Leber, Lunge, Muskel, Nerven, Haut, Milz und Sehne), geben einen Einblick in die Organspezifität der gefundenen Proteine und der Verteilung der Eikosanoide. Die Darstellung der Protein- und Eikosanoid-Daten mittels einer Heatmap aus z-transfomrierten Abundanz-Werten in den verschiedenen Gewebeproben ergab die Formation von Gruppen mit Ähnlichkeiten in deren Expressionsmuster. Die Nachvollziehbarkeit der Formation der verschiedenen Gruppen wurden mittels diversen Interpretationsstrategien ermittelt: das Ausmaß der Ähnlichkeit des Expressionsmusters von Kandidaten mit ähnlicher Zelltyp-Zusammensetzung, Gewebsbeschaffenheit, biologische Funktionen oder in der Literatur beschriebenen biologische Prozesse. Die Evaluierung des proteomics Datensatzes mittels einer GO-term Enrichment Analyse zeigte gute Übereinstimmungen der angereicherten GO-Terme für die einzelnen Gewebeproben mit in der Literatur beschriebenen biologischen Prozessen. Die identifizierten Moleküle weisen einen deutlichen Bezug zur Funktionalität der entsprechenden Organe und deren Enzym-Ausstattung auf, zur Berechnung signifikanter Korrelationen waren die erhobenen Daten jedoch noch nicht ausreichend.

Supplementary Figures and Tables

In this section, bar-plots showing the concentration distributions of selected eicosanoids found for the pathway with LOX as enzyme and DHA and EPA as precursor molecules can be seen in Figure 50 and Figure 51.

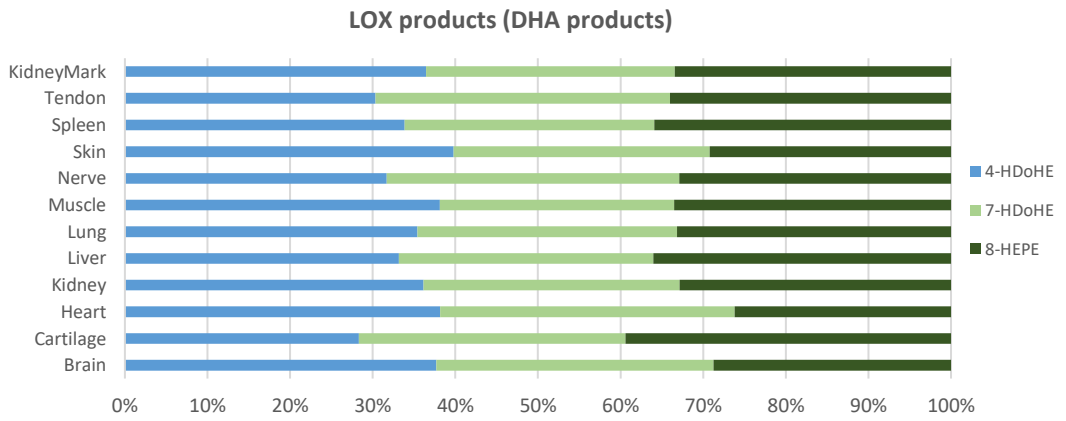

Figure 50: Distribution of 3 selected eicosanoids (4-, 7-HDoHE and 8-HEPE) in the 12 tissue samples analysed with DHA as precursor molecule and LOX as enzymatic pathway.

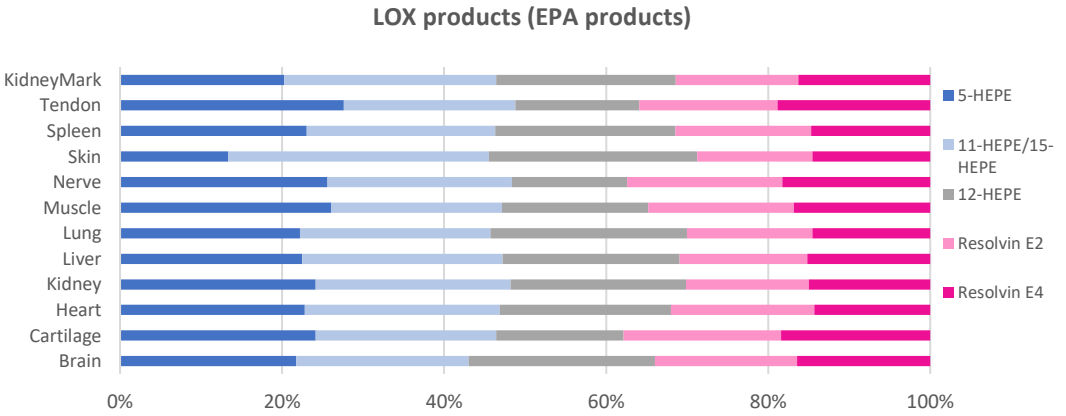

Figure 51: Distribution of 5 selected eicosanoids (5-, 11-/15-HEPE and Resolvin E2 and E4) in the 12 tissue samples analysed with EPA as precursor molecule and LOX as enzymatic pathway.

Further, Table 18 lists all eicosanoids identified *via* standards.

Table 18: Eicosanoids identified via standards.

Eicosanoids identified *via* standards	
11(12)-DiHETE	8(9)-EET
11(12)-EET	8-HDoHE
11(12)-EpETE	8-HEPE
11,12-DiHETrE	8-iso-15keto-PGE2
11b-PGF2a/PGF2b	8-iso-PGE2
11-HDoHE	9- and 13-HODE
11-HETE	9,10-DiHOME
12,13-DiHOME	9-HETE
12-HEPE	AA
12-HETE/8-HETE	a-Linolenic Acid
12-HHTrE	Cholic Acid
13,14-dihydro-15-keto-PGD2	Deoxycholic Acid
13,14-dihydro-15-keto-PGE2	DHA
13,14-dihydro-15-keto-PGF2	DPA
14(15)-DiHETE	EPA
14(15)-EET	g-Linolenic Acid
14,15-DiHETrE	Glycocholic Acid
14-HDoHE and 10-HDoHE	Glycodeoxycholic Acid
15-Lipoxin A4	Glycolithocholic Acid
11-HEPE / 15-HEPE	Linoleic Acid
15-HETE	LTB4/12-epi-LTB4
16-HETE	Oleic Acid
17(18)-DiHETE	Palmitic Acid
18-HEPE	PGA3
18-HETE	PGB2
20-HDoHE	PGB3
20-HETE	PGD2
22-HDHA	PGE2
14(15)-EpETE	Resolvin E2
4-HDoHE	Resolvin E4
5(6)-EET	Stearic Acid
5,6-DiHETrE	Stearidonic Acid
5-HEPE	Taurocholic Acid
5-Oxo-ETE	tetranor-12-HETE
5-HETE	TXB2
6-keto-PGF1alpha	AA-EA
6trans-LTB4 / 5,15-DiHETE	DHA-EA
7-HDoHE	

Further, Figure 52-60 show the results of the GO-term enrichment analysis of cartilage, heart, kidney mark, lung, muscle, nerve, skin, spleen and tendon, presented in 3 different ways (tree plot, dot plot and C-net plot).

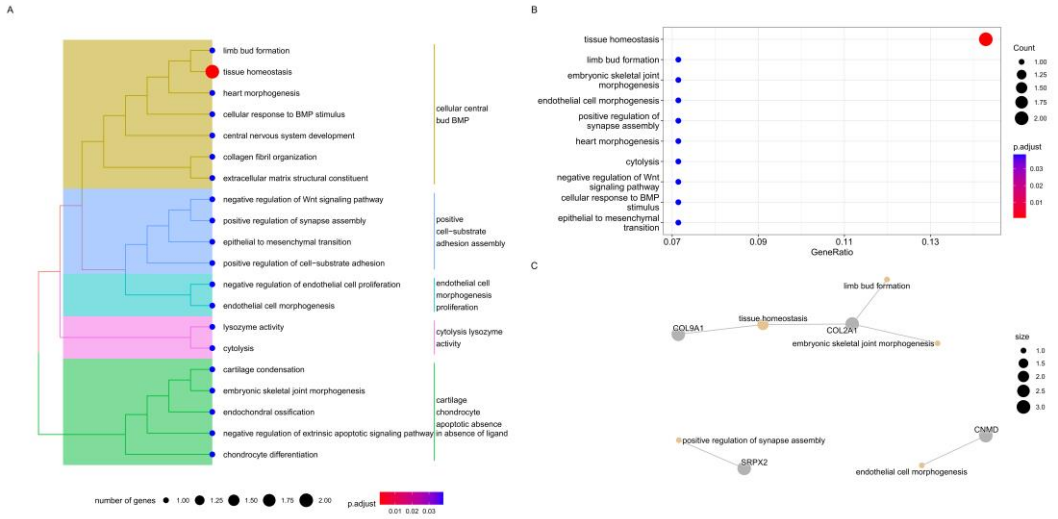

Figure 52: Results of the Term Enrichment Analysis of the Cartilage tissue samples presented as a A) tree plot B) dot plot and C) C-net plot.

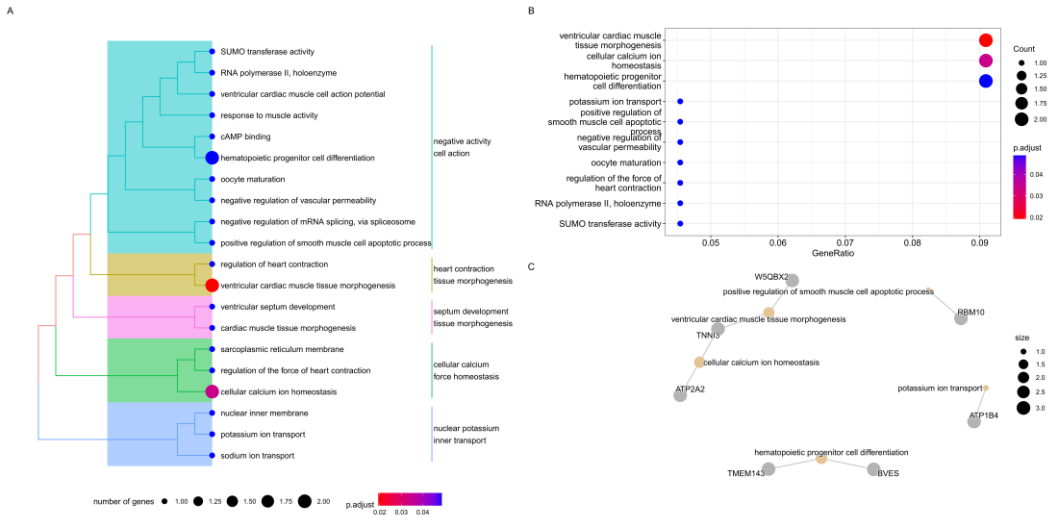

Figure 53: Results of the Term Enrichment Analysis of the Heart tissue samples presented as a A) tree plot B) dot plot and C) C-net plot.

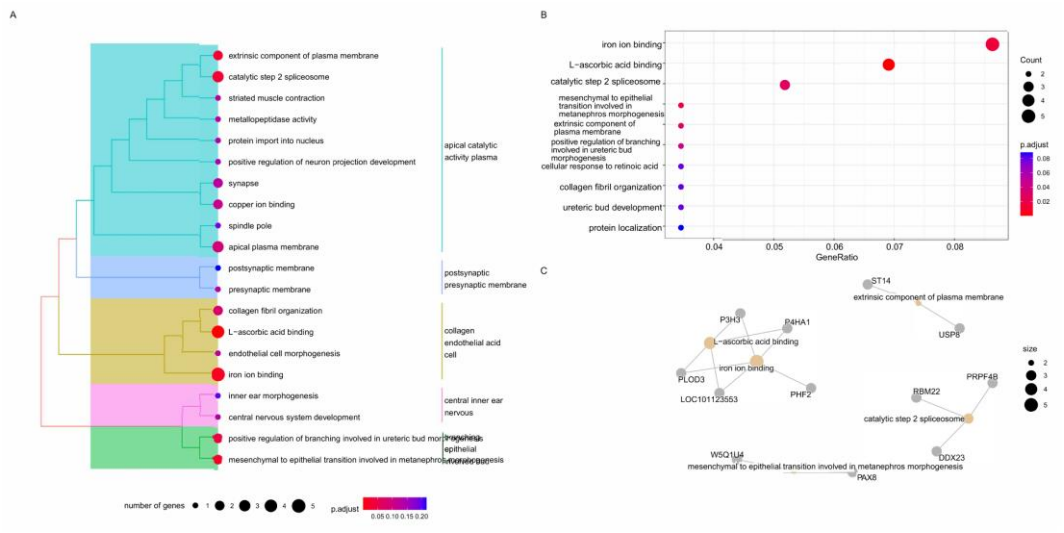

Figure 54: Results of the Term Enrichment Analysis of the kidney mark tissue samples presented as a A) tree plot B) dot plot and C) C-net plot.

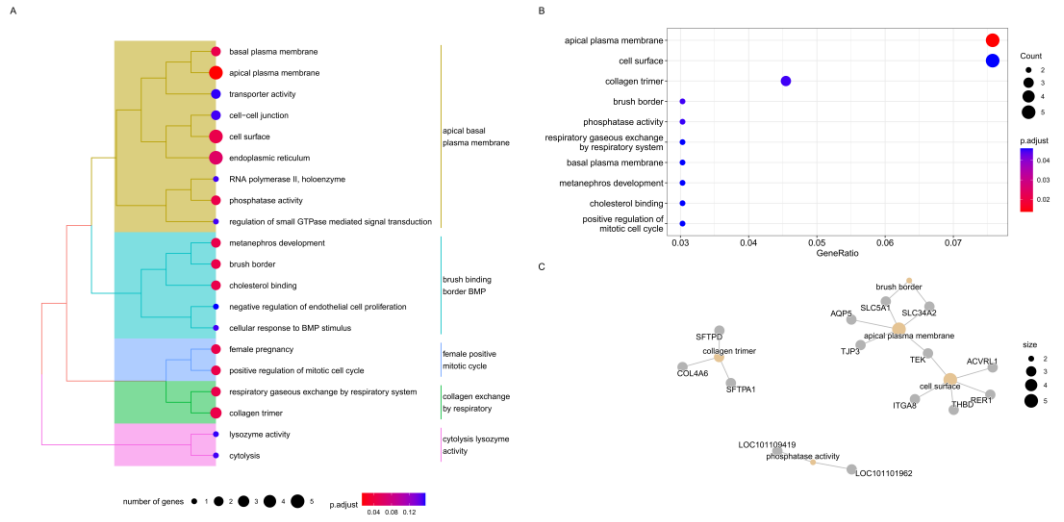

Figure 55: Results of the Term Enrichment Analysis of the Lung tissue samples presented as a A) tree plot B) dot plot and C) C-net plot.

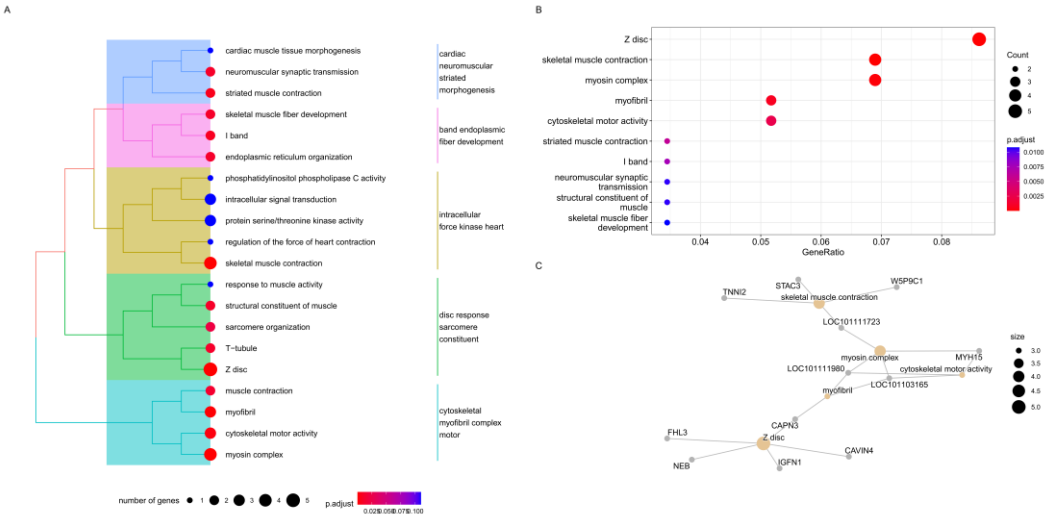

Figure 56: Results of the Term Enrichment Analysis of the Muscle tissue samples presented as a A) tree plot B) dot plot and C) C-net plot.

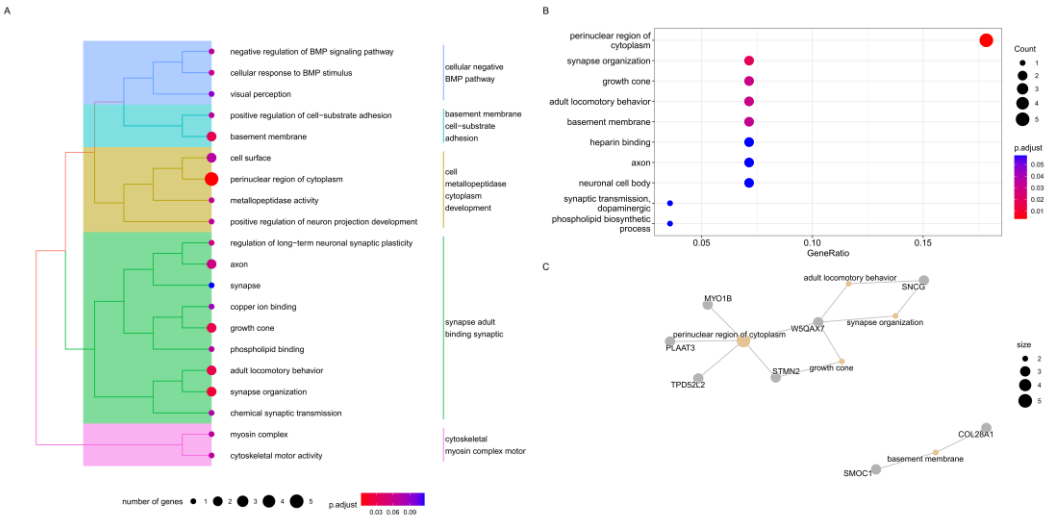

Figure 57: Results of the Term Enrichment Analysis of the Nerve tissue samples presented as a A) tree plot B) dot plot and C) C-net plot.

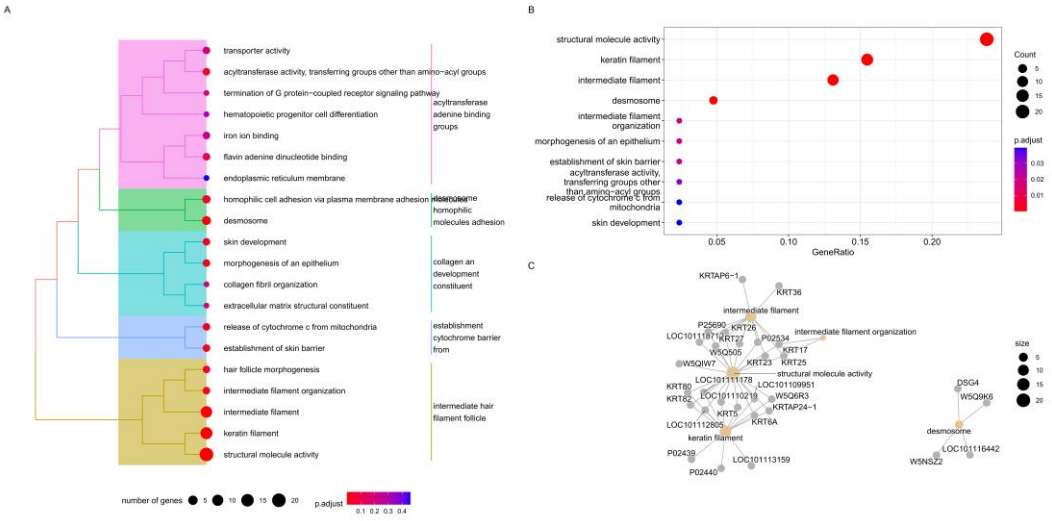

Figure 58: Results of the Term Enrichment Analysis of the Skin tissue samples presented as a A) tree plot B) dot plot and C) C-net plot.

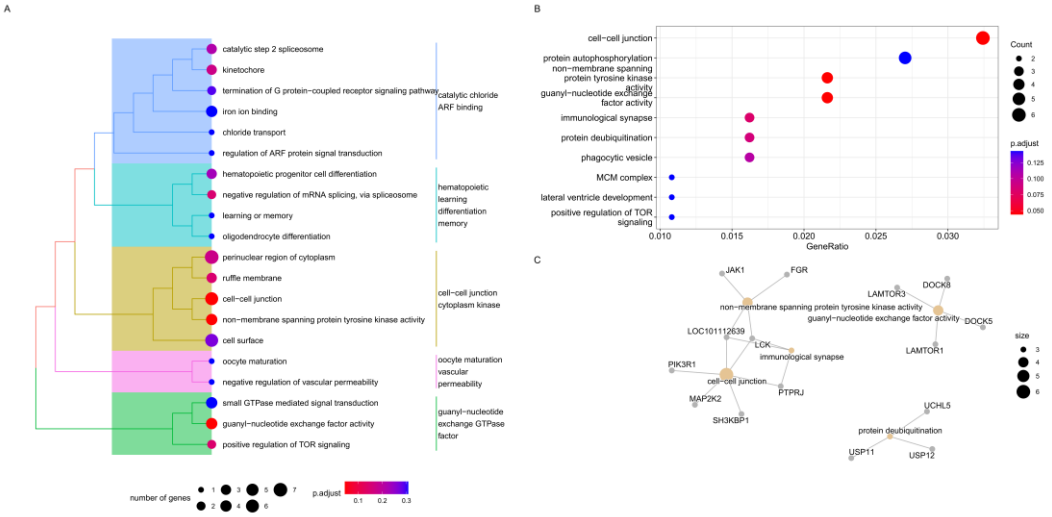

Figure 59: Results of the Term Enrichment Analysis of the Spleen tissue samples presented as a A) tree plot B) dot plot and C) C-net plot.

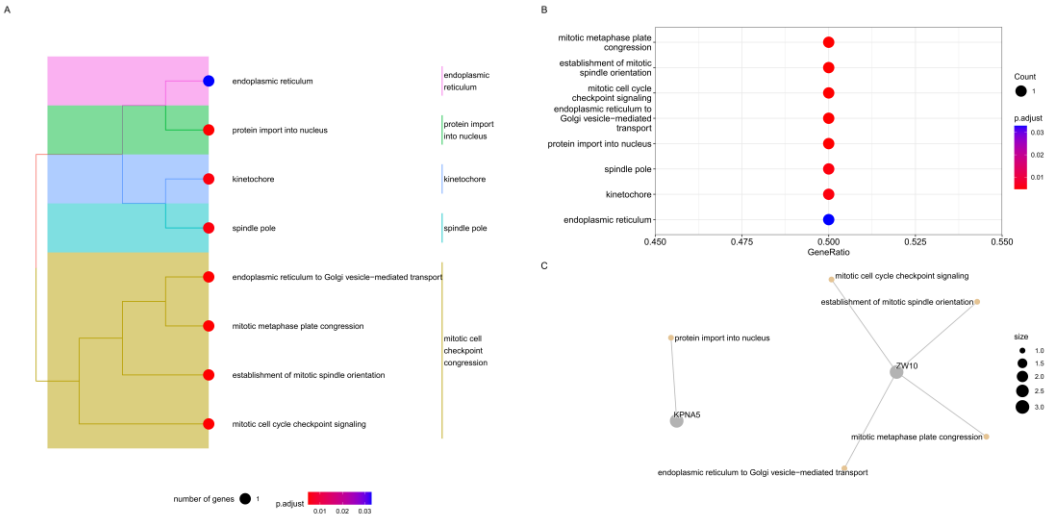

Figure 60: Results of the Term Enrichment Analysis of the Tendon tissue samples presented as a A) tree plot B) dot plot and C) C-net plot.

References

[1] Servier Medical Art (https://smart.servier.com/) accessed on 28.03.2023

[2] De Bruycker K, Welle A, Hirth S, Blanksby S J and Barner-Kowollik C 2020 Mass spectrometry as a tool to advance polymer science *Nat. Rev. Chem.* **4** 257–68

[3] Wanner K T and Höfner G 2007 *Mass Spectrometry in Medicinal Chemistry* (Wiley-VCH Verlag GmbH & Co. KGaA)

[4] Glish G L and Vachet R W 2003 The basics of mass spectrometry in the twenty-first century *Nat. Rev. Drug Discov.* **2** 140–50

[5] Gross J H 2017 *Mass Spectrometry* (Cham: Springer International Publishing)

[6] Banerjee S and Mazumdar S 2012 Electrospray Ionization Mass Spectrometry: A Technique to Access the Information beyond the Molecular Weight of the Analyte *Int. J. Anal. Chem.* **2012** 1–40

[7] Ferrante L and Cameriere R 2009 Statistical methods to assess the reliability of measurements in the procedures for forensic age estimation *Int. J. Legal Med.* **123** 277–83

[8] Unger K K, Lamotte S and Machtejevas E 2017 Column technology in liquid chromatography *Liquid Chromatography* (Elsevier) pp 39–89

[9] Lembke P, Henze G, Cabrera K, Brünner W and Müller E 2001 Liquid Chromatography *Handbook of Analytical Techniques* ed H Günzler and A Williams (Weinheim, Germany: Wiley-VCH Verlag GmbH) pp 261–326

[10] Lundanes E, Reubsaet L and Greibrokk T 2014 1. General Concepts *Chromatography: Basic Principles, Sample Preparations and Related Methods* (Wiley-VCH Verlag GmbH & Co. KGaA) pp 1–16

[11] Fornstedt T, Forssén P and Westerlund D 2015 Basic HPLC Theory and Definitions: Retention, Thermodynamics, Selectivity, Zone Spreading, Kinetics, and Resolution *Analytical Separation Science* ed Ja L Anderson, A Berthod, V Estevez and A M Stalcup (Weinheim, Germany: Wiley-VCH Verlag GmbH & Co. KGaA) pp 1–24

[12] Abdu Hussen A 2022 High-Performance Liquid Chromatography (HPLC): A review *Ann. Adv. Chem.* **6** 010–20

[13] De Vos J, Stoll D, Buckenmaier S, Eeltink S and Grinias J P 2021 Advances in ultra-high-pressure and multi-dimensional liquid chromatography instrumentation and workflows *Anal. Sci. Adv.* **2** 171–92

[14] Ho C S, Lam C W K, Chan M H M, Cheung R C K, Law L K, Lit L C W, Ng K F, Suen M W M and Tai H L 2003 Electrospray ionisation mass spectrometry: principles and clinical applications. *Clin. Biochem. Rev.* **24** 3–12

[15] Lu W, Bennett B D and Rabinowitz J D 2008 Analytical strategies for LC–MS-based targeted metabolomics *J. Chromatogr. B* **871** 236–42

[16] Meier F, Park M A and Mann M 2021 Trapped Ion Mobility Spectrometry and Parallel Accumulation–Serial Fragmentation in Proteomics *Mol. Cell. Proteomics* **20** 100138

[17] Ridgeway M E, Lubeck M, Jordens J, Mann M and Park M A 2018 Trapped ion mobility spectrometry: A short review *Int. J. Mass Spectrom.* **425** 22–35

[18] Dodds J N and Baker E S 2019 Ion Mobility Spectrometry: Fundamental Concepts, Instrumentation, Applications, and the Road Ahead *J. Am. Soc. Mass Spectrom.* **30** 2185–95

[19] Meier F, Brunner A, Koch S, Koch H, Lubeck M, Krause M, Goedecke N, Decker J, Kosinski T, Park M A, Bache N, Hoerning O, Cox J, Räther O and Mann M 2018 Online Parallel Accumulation–Serial Fragmentation (PASEF) with a Novel Trapped Ion Mobility Mass Spectrometer *Mol. Cell. Proteomics* **17** 2534–45

[20] Sinha A and Mann M 2020 A beginner's guide to mass spectrometry–based proteomics *Biochem. (Lond).* **42** 64–9

[21] Li C, Chu S, Tan S, Yin X, Jiang Y, Dai X, Gong X, Fang X and Tian D 2021 Towards Higher Sensitivity of Mass Spectrometry: A Perspective From the Mass Analyzers *Front. Chem.* **9** 1–21

[22] Cornish T J and Bryden W A 1999 Miniature Time-of-Flight Mass Spectrometer for a Field-Portable Biodetection System *John Hopkins Apl Tech. Dig.* **20** 335–42

[23] Scheltema R A, Hauschild J, Lange O, Hornburg D, Denisov E, Damoc E, Kuehn A, Makarov A and Mann M 2014 The Q Exactive HF, a Benchtop Mass Spectrometer with a Pre-filter, High-performance Quadrupole and an Ultra-high-field Orbitrap Analyzer *Mol. Cell. Proteomics* **13** 3698–708

[24] Kelstrup C D, Jersie-Christensen R R, Batth T S, Arrey T N, Kuehn A, Kellmann M and Olsen J V 2014 Rapid and Deep Proteomes by Faster Sequencing on a Benchtop Quadrupole Ultra-High-Field Orbitrap Mass Spectrometer *J. Proteome Res.* **13** 6187–95

[25] Perry R H, Cooks R G and Noll R J 2008 Orbitrap mass spectrometry: Instrumentation, ion motion and applications *Mass Spectrom. Rev.* **27** 661–99

[26] Eliuk S and Makarov A 2015 Evolution of Orbitrap Mass Spectrometry Instrumentation *Annu. Rev. Anal. Chem.* **8** 61–80

[27] Ekman R, Silberring J, Westman-Brinkmalm A and Kraj A 2009 *Mass spectrometry Instrumentation, Interpretation, and Applications* (John Wiley & Sons, Inc)

[28] Resurreccion E P and Fong K 2022 The Integration of Metabolomics with Other Omics: Insights into Understanding Prostate Cancer *Metabolites* **12** 488

[29] Hasin Y, Seldin M and Lusis A 2017 Multi-omics approaches to disease *Genome Biol.* **18** 83

[30] Aryan Z, Szanto A, Pantazi A, Reddi T, Rheinstein C, Powers W, Wilson E, Deo R C, Chowdhury S, Salz L, Dimmock D, Nahas S, Benson W, Kingsmore S F, MacRae C A and Vuzman D 2020 Moving Genomics to Routine Care *Circ. Genomic Precis. Med.* **13** 406–16

[31] Song M, Greenbaum J, Luttrell J, Zhou W, Wu C, Shen H, Gong P, Zhang C and Deng H-W 2020 A Review of Integrative Imputation for Multi-Omics Datasets *Front. Genet.* **11** 1–15

[32] Luque de Castro M D and Quiles-Zafra R 2020 Lipidomics: An omics discipline with a key role in nutrition *Talanta* **219** 121197

[33] Han X 2016 Lipidomics for studying metabolism *Nat. Rev. Endocrinol.* **12** 668–79

[34] Holčapek M, Liebisch G and Ekroos K 2018 Lipidomic Analysis *Anal. Chem.* **90** 4249–57

[35] Ward A V, Anderson S M and Sartorius C A 2021 Advances in Analyzing the Breast Cancer Lipidome and Its Relevance to Disease Progression and Treatment *J. Mammary Gland Biol. Neoplasia* **26** 399–417

[36] Masoro E J 1977 Lipids and Lipid Metabolism *Annu. Rev. Physiol.* **39** 301–21

[37] Natesan V and Kim S 2021 Lipid Metabolism, Disorders and Therapeutic Drugs - Review *Biomol. Ther. (Seoul).* **29** 596–604

[38] Szefel J, Kruszewski W J and Sobczak E 2015 Factors Influencing the Eicosanoids Synthesis In Vivo *Biomed Res. Int.* **2015** 1–6

[39] Liakh, Pakiet, Sledzinski and Mika 2019 Modern Methods of Sample Preparation for the Analysis of Oxylipins in Biological Samples *Molecules* **24** 1639

[40] Dennis E A and Norris P C 2015 Eicosanoid storm in infection and inflammation *Nat. Rev. Immunol.* **15** 511–23

[41] Calder P C 2013 Omega-3 polyunsaturated fatty acids and inflammatory processes: nutrition or pharmacology? *Br. J. Clin. Pharmacol.* **75** 645–62

[42] Hishikawa D, Shindou H, Kobayashi S, Nakanishi H, Taguchi R and

Shimizu T 2008 Discovery of a lysophospholipid acyltransferase family essential for membrane asymmetry and diversity *Proc. Natl. Acad. Sci.* **105** 2830–5

[43] Johnson A M, Kleczko E K and Nemenoff R A 2020 Eicosanoids in Cancer: New Roles in Immunoregulation *Front. Pharmacol.* **11** 1–11

[44] Saini R K and Keum Y 2018 Omega-3 and omega-6 polyunsaturated fatty acids: Dietary sources, metabolism, and significance — A review *Life Sci.* **203** 255–67

[45] Yamaguchi A, Botta E and Holinstat M 2022 Eicosanoids in inflammation in the blood and the vessel *Front. Pharmacol.* **13** 1–17

[46] Harvey J. Weiss V T T 1979 Prostacyclin (Prostaglandin I2, PGI2) Inhibits Platelet Adhesion and Thrombus Formation on Subendothelium *Blood* **53** 244–50

[47] Gomes R N, Felipe da Costa S and Colquhoun A 2018 Eicosanoids and cancer *Clinics* **73** e530s

[48] Tassoni D, Kaur G, Weisinger R S and Sinclair A J 2008 The role of eicosanoids in the brain. *Asia Pac. J. Clin. Nutr.* **17 Suppl 1** 220–8

[49] Sun P D, Foster C E and Boyington J C 2004 Overview of Protein Structural and Functional Folds *Curr. Protoc. Protein Sci.* **35** 1–189

[50] Gladine C, Ostermann A I, Newman J W and Schebb N H 2019 MS-based targeted metabolomics of eicosanoids and other oxylipins: Analytical and inter-individual variabilities *Free Radic. Biol. Med.* **144** 72–89

[51] Tang X, Hou Y, Schwartz T W and Haeggström J Z 2022 Metabolite G-protein coupled receptor signaling: Potential regulation of eicosanoids *Biochem. Pharmacol.* **204** 115208

[52] Biringer R G 2022 A review of non-prostanoid, eicosanoid receptors: expression, characterization, regulation, and mechanism of action *J. Cell Commun. Signal.* **16** 5–46

[53] Kovarik J J, Bileck A, Hagn G, Meier-Menches S M, et al. 2023 A multi-omics based anti-inflammatory immune signature characterizes long COVID-19 syndrome *iScience* **26** 105717

[54] Andrade-Eiroa A, Canle M, Leroy-Cancellieri V and Cerdà V 2016 Solid-phase extraction of organic compounds: A critical review (Part I) *TrAC Trends Anal. Chem.* **80** 641–54

[55] Maranata G J, Surya N O and Hasanah A N 2021 Optimising factors affecting solid phase extraction performances of molecular imprinted polymer as recent sample preparation technique *Heliyon* **7** e05934

[56] Wilkins M R, Sanchez J, Gooley A A, Appel R D, Humphery-Smith I, Hochstrasser D F and Williams K L 1996 Progress with Proteome Projects: Why all Proteins Expressed by a Genome Should be

Identified and How To Do It *Biotechnol. Genet. Eng. Rev.* **13** 19–50

[57] Aslam B, Basit M, Nisar M A, Khurshid M and Rasool M H 2017 Proteomics: Technologies and Their Applications *J. Chromatogr. Sci.* **55** 182–96

[58] Cristea I M, Gaskell S J and Whetton A D 2004 Proteomics techniques and their application to hematology *Blood* **103** 3624–34

[59] Jiang L, Wang M, Lin S, et al. 2020 A Quantitative Proteome Map of the Human Body *Cell* **183** 269-283.e19

[60] Aebersold R and Mann M 2003 Mass spectrometry-based proteomics *Nature* **422** 198–207

[61] Chait B T 2006 Mass Spectrometry: Bottom-Up or Top-Down? *Science (80-.).* **314** 65–6

[62] Gao Y and Yates J R 2019 Protein Analysis by Shotgun Proteomics *Mass Spectrometry-Based Chemical Proteomics* (Wiley) pp 1–38

[63] Uhlén M, Fagerberg L, Hallström B M, et al. 2015 Tissue-based map of the human proteome *Science (80-.).* **347**

[64] Wang D, Eraslan B, Wieland T, Hallström B, Hopf T, Zolg D P, Zecha J, Asplund A, Li L, Meng C, Frejno M, Schmidt T, Schnatbaum K, Wilhelm M, Ponten F, Uhlen M, Gagneur J, Hahne H and Kuster B 2019 A deep proteome and transcriptome abundance atlas of 29 healthy human tissues *Mol. Syst. Biol.* **15** 1–16

[65] Thul P J and Lindskog C 2018 The human protein atlas: A spatial map of the human proteome *Protein Sci.* **27** 233–44

[66] Digre A and Lindskog C 2021 The Human Protein Atlas—Spatial localization of the human proteome in health and disease *Protein Sci.* **30** 218–33

[67] Human Protein atlas (https://www.proteinatlas.org/about/organization) accessed on 23.04.2023

[68] Petyuk V A, Qian W, Chin M H, Wang H, Livesay E A, Monroe M E, Adkins J N, Jaitly N, Anderson D J, Camp D G, Smith D J and Smith R D 2007 Spatial mapping of protein abundances in the mouse brain by voxelation integrated with high-throughput liquid chromatography–mass spectrometry *Genome Res.* **17** 328–36

[69] Ortiz C, Navarro J F, Jurek A, Märtin A, Lundeberg J and Meletis K 2020 Molecular atlas of the adult mouse brain *Sci. Adv.* **6** 1–14

[70] Sun B, Lorang C, Qin S, Zhang Y, Liu K, Li G, Sun Z, Francke A, Utleg A G, Hu Z, Wang K, Moritz R L and Hood L 2021 Mouse Organ-Specific Proteins and Functions *Cells* **10** 3449

[71] Tomczak K, Czerwińska P and Wiznerowicz M 2015 Review The

Cancer Genome Atlas (TCGA): an immeasurable source of knowledge *Współczesna Onkol.* **1A** 68–77

[72] Schneider C and Brash A R 2002 Lipoxygenase-catalyzed formation of R-configuration hydroperoxides *Prostaglandins Other Lipid Mediat.* **68**–**69** 291–301

[73] Alsenan S, Al-Turaiki I and Hafez A 2020 A Recurrent Neural Network model to predict blood–brain barrier permeability *Comput. Biol. Chem.* **89** 107377

[74] Beloica S, Cvijić S, Bogataj M and Parojčić J 2015 In vitro-in vivo-in silico approach in biopharmaceutical characterization of ibuprofen IR and SR tablets *Eur. J. Pharm. Sci.* **75** 151–9

[75] Ribitsch I, Baptista P M, Lange-Consiglio A, Melotti L, Patruno M, Jenner F, Schnabl-Feichter E, Dutton L C, Connolly D J, van Steenbeek F G, Dudhia J and Penning L C 2020 Large Animal Models in Regenerative Medicine and Tissue Engineering: To Do or Not to Do *Front. Bioeng. Biotechnol.* **8** 1–28

[76] Casal M and Haskins M 2006 Large animal models and gene therapy *Eur. J. Hum. Genet.* **14** 266–72

[77] Niederstaetter L, Neuditschko B, Brunmair J, Janker L, Bileck A, Del Favero G and Gerner C 2021 Eicosanoid Content in Fetal Calf Serum Accounts for Reproducibility Challenges in Cell Culture *Biomolecules* **11** 113

[78] Ribitsch I, Bileck A, Egerbacher M, Gabner S, Mayer R L, Janker L, Gerner C and Jenner F 2021 Fetal Immunomodulatory Environment Following Cartilage Injury—The Key to CARTILAGE Regeneration? *Int. J. Mol. Sci.* **22** 12969

[79] Janker L, Schuster D, Bortel P, et al. 2023 Multi-omics empowered deep phenotyping of ulcerative colitis identifies biomarker signatures reporting functional remission states *J. Crohn's Colitis* 1–16

[80] Yu G, Wang L-G, Han Y and He Q-Y 2012 clusterProfiler: an R Package for Comparing Biological Themes Among Gene Clusters *Omi. A J. Integr. Biol.* **16** 284–7

[81] Wu T, Hu E, Xu S, Chen M, Guo P, Dai Z, Feng T, Zhou L, Tang W, Zhan L, Fu X, Liu S, Bo X and Yu G 2021 clusterProfiler 4.0: A universal enrichment tool for interpreting omics data *Innov.* **2** 100141

[82] Benjamini Y and Hochberg Y 1995 Controlling The False Discovery Rate - A Practical And Powerful Approach To Multiple Testing *J. R. Stat. Soc. Ser. B* **57** 289–300

[83] Ziboh V A, Cho Y, Mani I and Xi S 2002 Biological significance of essential fatty acids/prostanoids/ lipoxygenase-derived monohydroxy fatty acids in the skin *Arch. Pharm. Res.* **25** 747–58

[84] Jenkins C M, Cedars A and Gross R W 2008 Eicosanoid signalling

pathways in the heart *Cardiovasc. Res.* **82** 240–9

[85] Matthew A. Bailey R J U 2019 Renal Physiology *Comprehensive Clinical Nephrology* (Elsevier) pp 14–28

[86] Wang T, Fu X, Chen Q, Patra J K, Wang D, Wang Z and Gai Z 2019 Arachidonic Acid Metabolism and Kidney Inflammation *Int. J. Mol. Sci.* **20** 1–28

[87] Alvarez M de L and Lorenzetti F 2021 Role of eicosanoids in liver repair, regeneration and cancer *Biochem. Pharmacol.* **192** 114732

[88] Quiroga J and Prieto J 1993 Liver Cytoprotection by Prostaglandins *Pharmacol. Ther.* **58** 67–92

[89] Cuberos H, Vallée B, Vourc'h P, Tastet J, Andres C R and Bénédetti H 2015 Roles of LIM kinases in central nervous system function and dysfunction *FEBS Lett.* **589** 3795–806

[90] Antonucci F, Corradini I, Fossati G, Tomasoni R, Menna E and Matteoli M 2016 SNAP-25, a Known Presynaptic Protein with Emerging Postsynaptic Functions *Front. Synaptic Neurosci.* **8** 1–9

[91] Nestler E J, Hyman S E and Malenka R C 2014 Chapter 4: Signal Transduction in the Brain (https://neurology.mhmedical.com/content.aspx?sectionid=72649067&bookid=1204) *Molecular Neuropharmacology: A Foundation for Clinical Neuroscience, Third Edition* (McGraw Hill) pp 1–55, accessed on 28.03.2023

[92] Shrivastava A N, Triller A and Sieghart W 2011 GABAA Receptors: Post-Synaptic Co-Localization and Cross-Talk with Other Receptors *Front. Cell. Neurosci.* **5** 1–12

[93] Drozdzik M, Drozdzik M and Oswald S 2021 Membrane Carriers and Transporters in Kidney Physiology and Disease *Biomedicines* **9** 426

[94] Motohashi H and Inui K 2013 Organic Cation Transporter OCTs (SLC22) and MATEs (SLC47) in the Human Kidney *AAPS J.* **15** 581–8

[95] Riddick D S, Ding X, Wolf C R, Porter T D, Pandey A V, Zhang Q, Gu J, Finn R D, Ronseaux S, McLaughlin L A, Henderson C J, Zou L and Flück C E 2013 NADPH–Cytochrome P450 Oxidoreductase: Roles in Physiology, Pharmacology, and Toxicology *Drug Metab. Dispos.* **41** 12–23

[96] Jetter A and Kullak-Ublick G A 2020 Drugs and hepatic transporters: A review *Pharmacol. Res.* **154** 104234

[97] Lindskog C, Linné J, Fagerberg L, Hallström B M, Sundberg C J, Lindholm M, Huss M, Kampf C, Choi H, Liem D A, Ping P, Väremo L, Mardinoglu A, Nielsen J, Larsson E, Pontén F and Uhlén M 2015 The human cardiac and skeletal muscle proteomes defined by transcriptomics and antibody-based profiling *BMC Genomics* **16** 475

[98] Wang Z, Ying Z, Bosy-Westphal A, Zhang J, Schautz B, Later W, Heymsfield S B and Müller M J 2010 Specific metabolic rates of major organs and tissues across adulthood: evaluation by mechanistic model of resting energy expenditure *Am. J. Clin. Nutr.* **92** 1369–77

[99] Jiang L, Wang M, Lin S, et al. 2020 A Quantitative Proteome Map of the Human Body *Cell* **183** 269-283.e19

[100] Houten S M, Violante S, Ventura F V and Wanders R J A 2016 The Biochemistry and Physiology of Mitochondrial Fatty Acid β-Oxidation and Its Genetic Disorders *Annu. Rev. Physiol.* **78** 23–44

[101] Vasko R 2016 Peroxisomes and Kidney Injury *Antioxid. Redox Signal.* **25** 217–31

[102] Tahri-Joutey M, Andreoletti P, Surapureddi S, Nasser B, Cherkaoui-Malki M and Latruffe N 2021 Mechanisms Mediating the Regulation of Peroxisomal Fatty Acid Beta-Oxidation by PPARα *Int. J. Mol. Sci.* **22** 8969

[103] UniProt (https://www.uniprot.org/) accessed on 24.03.2023

[104] KEGG (https://www.genome.jp/kegg/kegg2.html) accessed on 24.03.2023

[105] Sjölin K, Kultima K, Larsson A, Freyhult E, Zjukovskaja C, Alkass K and Burman J 2022 Distribution of five clinically important neuroglial proteins in the human brain *Mol. Brain* **15** 52

[106] Sjöstedt E, Fagerberg L, Hallström B M and Häggmark A 2015 Defining the Human Brain Proteome Using Transcriptomics and Antibody-Based Profiling with a Focus on the Cerebral Cortex 1–20

[107] Sjöstedt E, Zhong W, Fagerberg L, et al. 2020 An atlas of the protein-coding genes in the human, pig, and mouse brain *Science (80-.).* **367**

[108] Hilborn J and Bjursten L M 2007 A new and evolving paradigm for biocompatibility *J. Tissue Eng. Regen. Med.* **1** 110–9

[109] Hardwick J P, Eckman K, Lee Y K, Abdelmegeed M A, Esterle A, Chilian W M, Chiang J Y and Song B-J 2013 Eicosanoids in Metabolic Syndrome *Adv. Pharmacol.* vol 66 pp 157–266

[110] Breyer R C and Harris M 2008 CHAPTER 11. Arachidonic Acid Metabolites and the Kidney *Brenner and Rector's The Kidney, 8th ed.* (Saunders Elsevier)

[111] Łapczuk-Romańska J, Droździk M, Oswald S and Droździk M 2023 Kidney Drug Transporters in Pharmacotherapy *Int. J. Mol. Sci.* **24** 2856

[112] Giacomini K M, Huang S-M, Tweedie D J, et al. 2010 Membrane transporters in drug development *Nat. Rev. Drug Discov.* **9** 215–36

[113] Funk C D, Song W-C and FitzGerald G A 2009 Prostaglandins and Other Lipid Mediators in Reproductive Medicine *Yen & Jaffe's Reproductive Endocrinology* vol 4 (Elsevier) pp 121–37

[114] Choi J and Bothwell A L M 2012 The nuclear receptor PPARs as important regulators of T-cell functions and autoimmune diseases *Mol. Cells* **33** 217–22